

WARMING AND STRATIFICATION CHANGES IN
LAKE KIVU, EAST AFRICA

A THESIS

SUBMITTED TO THE FACULTY OF THE GRADUATE SCHOOL

OF THE UNIVERSITY OF MINNESOTA

BY

ARTHUR ALLEN AABERG

IN PARTIAL FULFILLMENT OF THE REQUIREMENTS

FOR THE DEGREE OF

MASTER OF SCIENCE

SERGEI KATSEV

JULY 2013

© Arthur Allen Aaberg 2013

Acknowledgements

I am grateful to my advisor, Dr. Sergei Katsev, for his guidance and support – as well as the opening he had for me to start on this project my first summer as a graduate assistant. I would also like to thank Professor Thomas C. Johnson for the discussions I had with him and for allowing me to borrow several books during the data analysis phase of my research. I'd like to thank Dr. Sean Crowe for the help he provided in the field in Rwanda, as well as the assistance of the boat crew members that helped wherever they could while providing us with transportation on Lake Kivu. I also thank Dr. Jay Austin for the discussions I've had with him and the knowledge his classes provided me with, as well as for having space to conduct lab testing in his research lab at the Large Lakes Observatory. I also thank Sergio Contreas for the encouragement he has provided me with during discussions I've had with him. I am also thankful for the discussions and support that Matt Kistner, Rozhan Zakaria, Messias Macuiane, Daniel Titze, Blair Elliott, Hari Chapagain, and the other students at the LLO and those on campus have provided me, as well as for the friendships formed in my time at UMD.

This research was funded by the UMN OIP Seed Grant, the UMD VCAA/Dean's Office grant for Research in Energy and Environment, and Sergei Katsev's start-up funds. I

am thankful to the University of Minnesota, Duluth Physics Department summer scholarship and the OIP grant for providing me with funding support for summer research and the Mylan Radulovich Graduate Fellowship provided by the Department of Physics at the University of Minnesota, Duluth.

Abstract

To investigate changes in the temperature and stratification structure in Lake Kivu, we have installed a string of temperature recorders and performed CTD casts. The obtained data have been compared to historical profiles and the heat budget for the lake was analyzed.

Lake Kivu is a meromictic lake characterized by an anomalous temperature distribution with a temperature minimum close to the base of the seasonally mixed layer. Warming rate at the depth of the temperature inversion is consistent with the historical warming rate of the surface layer of $\sim 0.14 \pm 0.02$ °C per decade. Deep waters (greater than 350 m) exhibit variability in temperature and are currently warming at a rate of $\sim 0.04 \pm 0.02$ °C per decade based on the increase in heat content since the 1970's and the increase in temperature seen in the deepest measurements between our 2011 and 2012 profiles. The monimolimnion of Lake Kivu cannot be considered to be in a steady state.

The depth of wind-induced surface mixing during the dry season varies significantly between years. Mixing to 80 m (the present depth of the temperature inversion) requires continuous winds blowing from the south at $9\text{--}10$ m s⁻¹, whereas typical wind speed maxima are around $5\text{--}6$ m s⁻¹ and capable of mixing to around 65 m depth. Occasional

stronger winds cause episodic mixing closer to the inversion which removes heat, but this does not happen on a regular basis. As the temperature inversion in recent historical profiles has been as shallow as 65 m, mixing to the inversion depth is possible during years with stronger than average winds. With heat diffusing towards the temperature inversion from both above and below, the temperature at the inversion will continue to rise, resulting in a reduced transport of heat out of the deep waters that will increase the rate at which the water column is warming.

Contents

	Page
Acknowledgements	i
Abstract	iii
Contents	v
List of Tables	ix
List of Figures	x
1 Introduction	1
1.1 Objectives of this Work	3
1.2 Hypotheses	3
2 Background	5
2.1 Lake Kivu: General Information	5
2.2 Stratification	9
2.2.1 Inversion in temperature profile	9
2.3 Components of the Heat and Water Budgets	10
2.3.1 The water budget of Lake Kivu	11

3	Methods	13
3.1	Sampling and measurements	13
3.1.1	CTD Profiles	13
3.1.2	Array of temperature recorders	17
3.2	Corrections to Temperature, Conductivity, and Pressure	18
3.2.1	Conductivity corrections	18
3.2.2	Salinity and Density Profiles	20
3.2.3	Pressure to Depth Conversion	24
3.3	Heat fluxes accros the lake surface	26
3.3.1	Heat loss due to evaporation	26
3.3.2	Long-wave Thermal Radiation Heat Fluxes	27
3.3.3	Heat Flux Due to Sensible Radiation	29
3.3.4	Solar Radiation Contributions to the Heat Budget	29
3.4	Meteorological Data	30
3.5	Dissolved gas measurements in silicone tubing	31
3.6	Simulation of a limnic eruption in lab	34
4	Results	39
4.1	Temperature distributions in the water column	39
4.1.1	Temperature profile inversion	39
4.1.2	Positions of thermoclines	40
4.2	Lateral variability in temperature distributions	41
4.2.1	Inflows	41
4.3	Temporal variability in the temperature profiles	46
4.3.1	Variability within the mixolimnion	46

4.3.2	Temperature variability in the deep waters	50
4.4	Conductivity distribution in Lake Kivu	51
4.4.1	Spatial variability in water column conductivity	53
4.4.2	Temporal variability in water column conductivity	55
4.5	Oxygen distributions in the water column	56
4.6	Gas pressure measurements with silicone tubing	57
4.6.1	Calibration of silicone tubing	57
4.6.2	Field measurements of gas pressures	59
4.7	Limnic eruptions in lab	63
5	Discussion	65
5.1	Comparisons of historical temperature distributions in the water column	65
5.1.1	Decadal scale warming at the depth of temperature inversion	73
5.2	Heat content and temperature changes in the water column	74
5.2.1	Heat content changes in the mixed layer	74
5.2.2	Heat content changes below the temperature inversion	75
5.2.3	Implications of warming	76
5.3	Warming in Lake Kivu versus other tropical lakes	77
5.4	Double Diffusion and its Variability	78
5.4.1	Variability in the depth of temperature inversion	82
5.4.2	Temperature and energy conservation requirements at and above the temperature inversion depth	85
5.5	Stability of the Water Column	88
5.6	Local weather averages and heat budget	93

5.6.1	Weather averages in Lake Kivu region	93
5.6.2	Components of the Heat Budget for Lake Kivu	94
5.7	Pycnocline movements	101
5.7.1	Historical comparisons indicate vertical movement in the boundaries of the pycnoclines	101
5.7.2	Temporal variability expected due to internal waves	102
5.8	Effects from conductivity and temperature of inflows	108
5.9	Gas Pressure Measurements in Silicone Tubing	109
5.10	Limnic eruptions in lab	112
6	Conclusions	114
	References	117

List of Tables

2.1	Water Budget Estimates for Lake Kivu	12
3.1	Profiling Location Information	14
4.1	Depths of the major pycnoclines in Lake Kivu	40
4.2	Gas Pressure Measured with Silicone Tubing	60
4.3	Summary of attempts to create a limnic eruption in lab using CO ₂ as a gas source.	64
5.1	Summary of methane measurement techniques that have been used on Lake Kivu	68
5.2	Approximate K _z values in the water column of Lake Kivu	86
5.3	Heat fluxes across the surface of Lake Kivu.	98
5.4	Monthly averages for temperatures, precipitation, and relative humidity near Lake Kivu	99

List of Figures

2.1	Bathymetric map of Lake Kivu – contour intervals of 100 m	6
3.1	Map of profiling and equipment installation on Lake Kivu	15
3.2	Sea and Sun CTD Profiler	16
3.3	Winch device used for profiling done January 2011	17
3.4	Onset U22 thermistor installed at KP1	18
3.5	Approximate Salinity Profile of Lake Kivu	22
3.6	Density Profile of Lake Kivu due to T and S	23
3.7	Installed PortLog weather station	32
3.8	Silicone Tubing Calibration Pressure Chamber	33
3.9	Bubble chamber for CO ₂ dissolution	35
3.10	Limnic eruption beaker replacement	37
3.11	Closer view of limnic eruption setup for tall tube	38
4.1	Temperature Profiles of the Kibuye Transect, 7 Jan, 2011	43
4.2	Near Shore Transect Temperature Profiles, 9 Jan, 2011	44
4.3	σ_T for Kibuye Transect	45
4.4	Master Station Temperature Profiles – Inset Zoomed to Primary Pycnocline	47
4.5	Master Station Temperature Profiles – Inset Soomed to Temperature In- version	48
4.6	Diurnal Temperature Variation in the upper 25 m of the water column .	49

4.7	2011 time series of temperatures in the upper 60 meters recorded at KP1 methane extraction plant in the northwest section of Lake Kivu using Onset HOBO U22 logging thermistors.	50
4.8	January - November 2011 temperature versus time profiles for individual Onset U22 thermistors.	51
4.9	Current profiles showing deep water temperature variability	52
4.10	κ profiles and σ_{κ} in January 2011	54
4.11	2011 and 2012 deep cast conductivity profile comparisions	56
4.12	Oxygen profiles taken January 2011 and February 2012	58
4.13	Silicone tubing sampler calibration plot	61
4.14	Overlay of pressure sampler results onto previous measurements done by Schmid et. al.	62
5.1	Historical methane concentrations	69
5.2	Historical temperature profile comparison	70
5.3	Historical temperature profiles near 250 m	71
5.4	Historical temperature profiles near temperature inversion	72
5.5	Double Diffusive staircases (175–295 m)	81
5.6	Double Diffusive staircases (295–410 m)	82
5.7	Heat flux calculation example near the temperature inversion	87
5.8	Stability of the water column in Lake Kivu	92
5.9	Wind speed and wave energies	93
5.10	Monthly temperature and precipitation averages from airports of Gisenyi, Goma, and Bukavu	95
5.11	Mean temperatures in Rwanda since the late 19 th century	96

5.12	Defining pycnocline boundaries	102
5.13	Conductivity profiles from January 2011 and interna waves	104
5.14	In-situ and temperature-adjusted conductivity comparison with historical profiles	105
5.15	In-situ and temperature-adjusted conductivity profile comparison at primary chemocline	106
5.16	In-situ and temperature corrected conductivity profile comparison in upper 100 m of water column	107
5.17	Conductivity inflow insets 2012	109

1

Introduction

The warming of the surface waters of many East African lakes over the last century (Verburg and Hecky, 2009; Rosenzweig et al., 2007) has important consequences for the lakes' physical and ecological structures, as well as the populations that rely on the lake resources. Among the East African lakes, the meromictic Lake Kivu is unique and of particular interest due to the presence of a persistent temperature inversion in its water column, as well as high concentrations of dissolved methane and carbon dioxide in the deep waters (Degens and Kulbicki, 1973; Tietze et al., 1980). The gas accumulation is both a valuable economic resource to the area and a deadly threat, evidenced by the catastrophic limnic eruptions in Cameroon at Lake Nyos in 1986 (Baxter and Kapila, 1989) and in Lake Monoun in 1984 (Sigurdsson et al., 1987). At these lakes, large quantities of CO₂ gas exsolved into the atmosphere from the deep water and killed (through asphyxiation) ~1,700 people and 3,500 livestock in the surrounding valley of Lake Nyos and 37 people in the valley surrounding Lake Monoun. Warming of Lake Kivu's water column poses several risks: warmer water can contain less dissolved gases, and

changing physical stratification may affect the mixing regime and rates of heat, nutrient, and gas transport through the water column. Quantifying and monitoring vertical heat fluxes are therefore important for the long-term stability of the lake and its gas reserves. However, accurate estimations of heat fluxes at a free surface are difficult to calculate (Calder and Neal, 1984; Lallemand et al., 1996; Staley and Jurica, 1972) due to variability in cloud cover, surface water temperature, air temperature near the surface water, wind speed, humidity, evaporation, and rainfall throughout the year. As a result, estimations of these fluxes are made based off of the regional averages, which introduces large uncertainties (Venäläinen et al., 1999). These estimates are further complicated when data is limited and significant variability exists from one year to the next in local weather (Finch and Calver, 2008). In Lake Kivu, this variability affects the depth of the inversion from one year to the next (Schmid and Wüest, 2012).

This work aims to:

quantify heat fluxes to the lake surface and the currently observed inversion depth, compare the warming rates with that of other African lakes, and estimate water column stability to determine the energy input needed to mix the water column to the temperature inversion depth. Lateral and temporal variability in the temperature and conductivity profiles are examined to quantify the changes in temperature and depths of the pycnoclines to identify possible sub-surface inflows, and gain insight into the overall water movement in the water column.

1.1 Objectives of this Work

The specific objectives of this work are:

- To quantify the long-term trends and short-term variability in the lake's heat content and physical stratification.
- To quantify the changes in temperature at key depths in the water column, including at the base of the mixolimnion, at the depth of temperature inversion, and in the deep waters below the primary chemocline.
- To estimate the heat fluxes near the depth of temperature inversion to verify previous suggestions that mixing down to the inversion occurs episodically and to constrain the heat budget for the lake.
- To estimate the heat fluxes across the free surface of the lake to gain insight into whether the heat budget of the lake is balanced.
- To investigate the spatiotemporal variability of the temperature and conductivity profiles in the lake, including in the deep water, to gain insight into the deep mixing processes and the contributions from deep heat sources.

1.2 Hypotheses

H1 : The temperature in the mixolimnion, down to the depth of temperature inversion, has been increasing over the past 40 years at a rate of 0.14 °C per decade, consistent with regional atmospheric warming. This warming of the lake surface waters

is consistent with heat transfer predominantly from the atmosphere, rather than from deep heat sources.

H2 : The deep water is warming due to a combination of increasing gas content, warm subsurface springs, geothermal heating from the volcanic basin, and reduced upward heat transport from the warming occurring at the temperature inversion depth.

H3 : Mixing to the depth of temperature inversion does not occur every year. Occasional drier and windier conditions may cause deeper mixing that can remove heat from depths near the temperature inversion, and thus can affect the rate of heat removed from the deeper waters.

2

Background

2.1 Lake Kivu: General Information

Lake Kivu is the smallest of the African Great Lakes. It lies on the Albertine Rift and has a lake surface area of approximately 2650 km² (2370 km² excluding islands) and a catchment area of approximately 7000 km². It is situated between 1°34'25" and 2°29'40" S latitude and between 28°51'4" and 29°22'38" E longitude, on the border between Rwanda and the Democratic Republic of the Congo. The only surface outflow to the lake is the Ruzizi River, which has $\sim 3.0 \text{ km}^3 \text{ yr}^{-1}$ discharge feeding into Lake Tanganyika (Schmid and Wüest, 2012; Muvundja, 2010).

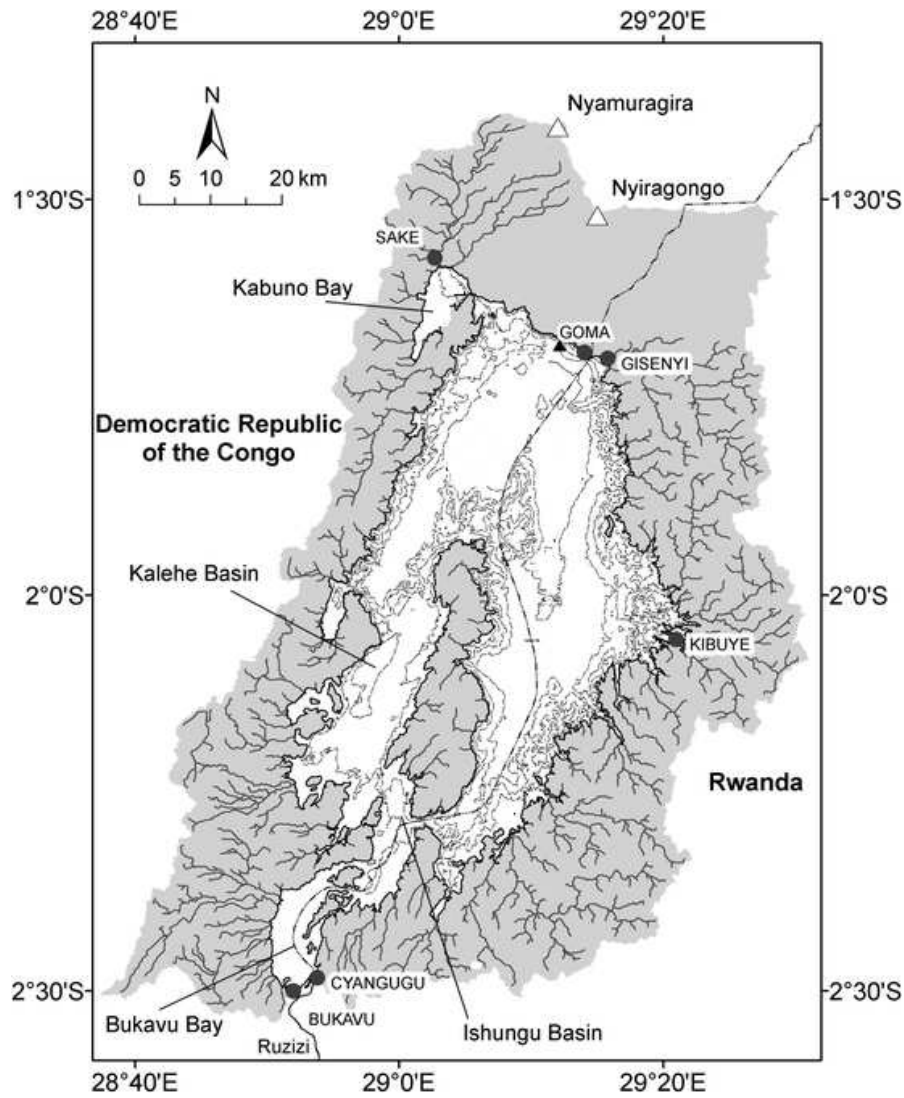


Figure 2.1: Bathymetric map of Lake Kivu showing major cities and the basins, based on Fig. 2.1 of Schmid and Wüest (2012). The contours are in 100 m intervals, and the catchment is shaded grey.

Lake Kivu differs greatly from other African Great Lakes by its volcanic origin, high altitude, and the strong and permanent stratification in its water column that is due to the physico-chemical properties of its water (Degens and Kulbicki, 1973; Schmid and Wüest,

2012; Damas, 1937). Resting at an altitude of 1463 m, Lake Kivu is located significantly higher than any other of the Albertine rift lakes; it lies between three mountain chains: the Mitumba Mountains in the west, the Rwandan dorsal in the east (Muvundja, 2010), and the Virunga Mountains to the North (Halbwachs et al., 2002). The Virunga mountains include several active volcanoes, two of which are located within 25 km of the lake shore near Goma, DRC. These two, Mt. Nyiragongo and Mt. Nyamuragira, account for nearly 40% of Africa's recorded volcanic eruptions and are still very active today.

Lake Kivu can be separated into five primary basins (Damas, 1937) and the Bay of Kabuno, the later connected to the rest of the lake via a shallow sill of approximately 11 m depth (Schmid and Wüest, 2012). The land surrounding the lake consists of steep hills and mountain sides which are eroding with landslides and seismic activity (Maongo, 2007). The lake is fed by 127 surface streams (Muvundja et al., 2009; Muvundja, 2010) and has several small surface hot spring runoff inflows. During the wet season, occasional rivers flow into the lake through the town of Bukavu on the southern end at times of high precipitation (Muvundja, 2010). Importantly, subsurface springs so far found mostly along the northern shore enter the lake at various depths, affecting the lake's water budget and stratification (Degens and Kulbicki, 1973; Schmid et al., 2005; Bergonzini, 1998).

The climate in the Kivu basin is considered tropical, with a long wet season extending from September through June – with several shorter season classifications – and a dry season from July through August. The rainiest month is April with an average of ~200 mm of precipitation to the lake surface (as measured on the North side of the lake) and ~190 mm on its watershed (Bergonzini, 1998). A short dry season in February exists

with precipitations of between 130 and 140 mm per month. In the dry season, precipitations are only around 27 mm per month on the lake surface and 25 mm per month on its watershed (Bergonzini, 1998). During the long dry season (July – September), strong winds blow from the South, which aid in mixing the surface water, as evaporation cools the water in the epilimnion down to between 40 and 60 m – and occasionally as deep as 80 m. The total rainfall estimates are between 1300 and 1500 mm per year (Bergonzini, 1998; Schmid and Wüest, 2012). The hydrology of Lake Kivu is maintained by the precipitation, since the catchment area consists of mainly small mountainous tributaries (Bergonzini, 1998; Marlier, 1954) aside from the North end which is drained through sub-aqueous inflows into the lake.

Like other African Great Lakes, Lake Kivu is vulnerable to human activities such as the increasing subsistence agricultural activities, deforestation, and urbanization. As deforestation leads to soil erosion and landslides (Jones and van der Walt, 2004) into the lake, increases in nutrient inputs to the lake have occurred (Bootsma and Hecky, 2003). Industrial activities consist mainly of two breweries and some processing of agricultural products, primarily tea, coffee, and quinine (Muvundja, 2010). Rivers and streams which drain into local lakes (including Lake Kivu) are very turbid and brown-colored due to the abundant phytoplankton and suspended organic matter; this is a result of agricultural activities and further contributes to the nutrient inputs into the lake (Lejeune and Frank, 1990).

2.2 Stratification

The lake surface water has an average temperature of 23.5°C (Sarmiento et al., 2006), varying between ~ 23.0 °C and 24.6 °C seasonally. Lake Kivu is permanently stratified without oxygen in its deeper waters (Damas, 1937; Lorke et al., 2004) and seasonal convective mixing of the surface waters extends only to about 50 m depth (Tietze et al., 1980). Below the seasonal mixing depth, several temperature gradients define the profile of the water column. At approximately 80 m depth, an inversion occurs in the temperature profile, below which the temperature increases with depth to the lake floor.

2.2.1 Inversion in temperature profile

The increase in temperature with depth in the deep water column of Lake Kivu is anomalous. Typically, due to warm water being less dense than cooler water, lakes stratify so that the temperature decreases with depth. The increase in temperature below 80 m in Lake Kivu is caused mainly by sub-aquatic flows (Degens and Kulbicki, 1973) of the volcanic basin. The stability of the water column is maintained by the increase in water salinity with depth. This chemical profile is defined by the concentrations of dissolved salts and dissolved gases that increase with depth. Concentrations of salts, primarily bicarbonates of magnesium, potassium, and calcium (Schmid et al., 2002), increase from the surface concentration of ~ 1 g l⁻¹ to ~ 6 g l⁻¹ at 450 meters depth. The dissolved gases of primary concern are carbon dioxide and methane. Methane dissolution causes a slight decrease in density (due to a negative contraction coefficient in water), whereas dissolved CO₂ increases density (Schmid et al., 2002; Wüest et al., 1996).

2.3 Components of the Heat and Water Budgets

A lake's heat budget is affected by several heating and cooling mechanisms. Being located just south of the equator means that Lake Kivu receives a near constant rate of incoming solar radiation year round above the clouds. The depth to which the photosynthetically active radiation (PAR, which is mostly visible light) penetrates is around 22 meters, at which point the light intensity is about 1% of the value at the lake surface (S. Crowe, unpublished). Liquid water gains energy (and therefore heats up) primarily through vibrational transitions caused by absorption in the mid-infrared (i.e. longwave) region of the electromagnetic spectrum. This spectral region corresponds to wavelengths between 6000 nm and 3000 nm. Since the attenuation of these wavelengths in water is much greater than PAR, heating of the surface waters directly from incoming radiation is very limited in depth, and thus any temperature increases observed deeper are a result of heat transport from the surface downward.

Both emission and absorption of thermal radiation by the lake surface are characterized by a blackbody radiative spectrum, which depends on temperature and emissivity. The Stefan-Boltzmann law states that the total energy radiated per unit surface area per unit time (also known as irradiance and radiant flux) is:

$$j_* = \epsilon \sigma T^4 \quad (2.1)$$

where $\sigma = 5.67 \cdot 10^{-8} \text{ J s}^{-1} \text{ m}^{-2} \text{ K}^{-4}$, the Stefan-Boltzmann constant, T the body's temperature in Kelvin, and ϵ is the coefficient of emissivity.

Small adjustments need to be made to the Stephan-Boltzmann law to account for the emissivity of lake water, which is only 3% different from a true blackbody. Quantifying the atmosphere's downward radiation into the lake, however, is more complicated. Variations in cloud cover, temperature, and humidity need to be considered (Lallemant et al., 1996). The coefficient of emissivity for the atmosphere varies as temperature, humidity, and pressure changes occur, whereas the lake surface remains at a constant $\varepsilon = 0.97$.

Heat is lost from a lake surface through the energy transferred by evaporation. The evaporation rate increases with wind speed (Yu, 2007). The loss of energy from the lake associated with evaporation is found through considering the energy to be the latent heat of vaporization. Other sources of heat energy include heat transfer from the surrounding land and the air immediately above the lake surface through heat conduction. The lake sediments may add heat to the water column if they are warmer than the water. Likewise, warmer water will cool down on contact with cooler sediments. Similarly, a warmer surface water will conduct heat into the atmosphere. As the warmer air rises from the lake surface, a convective process removes heat from the lake's surface. As wind blows over the lake surface, it increases heat exchange, a process typically referred to as sensible heat loss.

2.3.1 The water budget of Lake Kivu

Table 2.1 summarizes the rainwater runoffs and river flows into Lake Kivu, compiled from literature sources. Rainwater runoff into the surface was estimated to be $\sim 2.4 \text{ km}^3 \text{ yr}^{-1} \pm 10\%$ (Muvundja, 2010) with an additional $1.3 \text{ km}^3 \text{ yr}^{-1}$ input due to the sub-surface sources assumed to be primarily in the Goma-Nyiragongo region at the northern

end of the lake (Schmid et al., 2005). Temperatures of the river inflows (Muvundja et al., 2009) range between 16.5°C and ~22°C. Precipitation of ~1.4 m yr⁻¹ (Muvundja et al., 2009; Muvundja, 2010) at the lake surface (2365 km²) contributes the additional 3.3 km³ yr⁻¹. Evaporation and outflow estimates based on data of the Congolese Hydropower Company (Muvundja, 2010) from the Ruzizi dam flows and Bergonzini (1998) yield 3.6 km³ yr⁻¹ outflow. This outflow combined with the 3.4 km³ yr⁻¹ evaporation (Muvundja, 2010) account for a total loss of ~7.0 km³ yr⁻¹, leading to an approximately balanced water budget.

Table 2.1 Water budget, inflow and outflow estimates for Lake Kivu (Tietze, 2000; Kling et al., 2006; Muvundja et al., 2009).

Water Budget Source/Sink	Amount inflow/outflow
Runoff from catchment	2.4 km ³ yr ⁻¹ (18.0°C to 23.1°C)
Precipitation at surface	1.4 m yr ⁻¹ → ~3.3 km ³ yr ⁻¹
Subsurface inflows	1.3 km ³ yr ⁻¹
Total Water Input:	~ 7.0 km ³ yr ⁻¹
Evaporation	3.4 km ³ yr ⁻¹
Outflow Ruzizi	3.6 km ³ yr ⁻¹
Total Water Loss:	~ 7.0 km ³ yr ⁻¹

3

Methods

3.1 Sampling and measurements

3.1.1 CTD Profiles

Conductivity Temperature Depth (CTD) profiles were recorded in the water column of Lake Kivu in January 2011 and February 2012 at multiple locations. Times and locations of the CTD casts are summarized in Table 3.1. Figure 3.1 provides a visual of the sampling locations overlain onto a map of Lake Kivu. The locations labeled CTD3–CTD6 are referred to here as the Kibuye transect. CTD1 and CTD7 were taken at approximately the same location in the deep basin, referred to here as the Master Station (MS). Profiles labeled CTD8–CTD12 represent the 'near-shore transect'. The location labeled SF12 is where all 3 of the 9 February, 2012 profiles were taken (from the Rwandan Energy Corporations (REC) platform). A Garmin 60CSx hand-held GPS was used to record the profile locations.

Table 3.1 Table of Locations, Times, and Conditions associated with the profile names in Figure 3.1

Profile Name	Date Time	Longitude	Latitude	Conditions
CTD1 (MS*)	Jan 06, 2011 7h10	29°12' 30" E	1°46' 60" S	Calm but hazy, wind waves picked up at 14h00
CTD2	Jan 06, 2011 17h00	29°15' 25.6" E	1°45' 32.7" S	Calm
CTD3	Jan 07, 2011 7h10	29°15' 17.0" E	1°48' 19.9" S	Calm
CTD4	Jan 07, 2011 8h15	29°15' 1.9" E	1°52' 49.1" S	Calm
CTD5	Jan 07, 2011 9h30	29°16' 35.3" E	1°57' 36.1" S	Calm entering Kibuye Bay
CTD6	Jan 07, 2011 10h40	29°19' 16.4" E	2°1' 21.6" S	Calm in Kibuye Bay
CTD7 (MS*)	Jan 08, 2011 13h30	29°12' 30" E	1°46' 60" S	Master Station Deep Cast
KP1	Jan 07, 2011	29°14' 14.9" E	1°43' 29.9" S	Location of Thermistors on KP1 extraction plant
CTD8	Jan 09, 2011 16h00 - 18h00	29°12' 56.9" E	1°45' 55.4" S	Windy all day on casts from Master Station to shore
CTD9		29°14' 11.3" E	1°45' 17.8" S	
CTD10		29°14' 56.1" E	1°45' 0.2" S	
CTD11		29°15' 50.1" E	1°44' 45.5" S	
CTD12		29°16' 4.6" E	1°44' 37.6" S	
PLWS	Jan 07, 2011	29°19' 51.18" E	2°4' 20.4" S	Installation site of the weather station on the Contour Global work-site
SF12	Feb 09, 2012 9h00 - 14h00	29°14' 34.1" E	1°43' 55.9" S	REC Platform Feb. 2012 profiling loca- tion

* Profiles taken at what we considered the Master Station (MS). Drifting of the boat during profiling means the coordinates may differ slightly from those given.

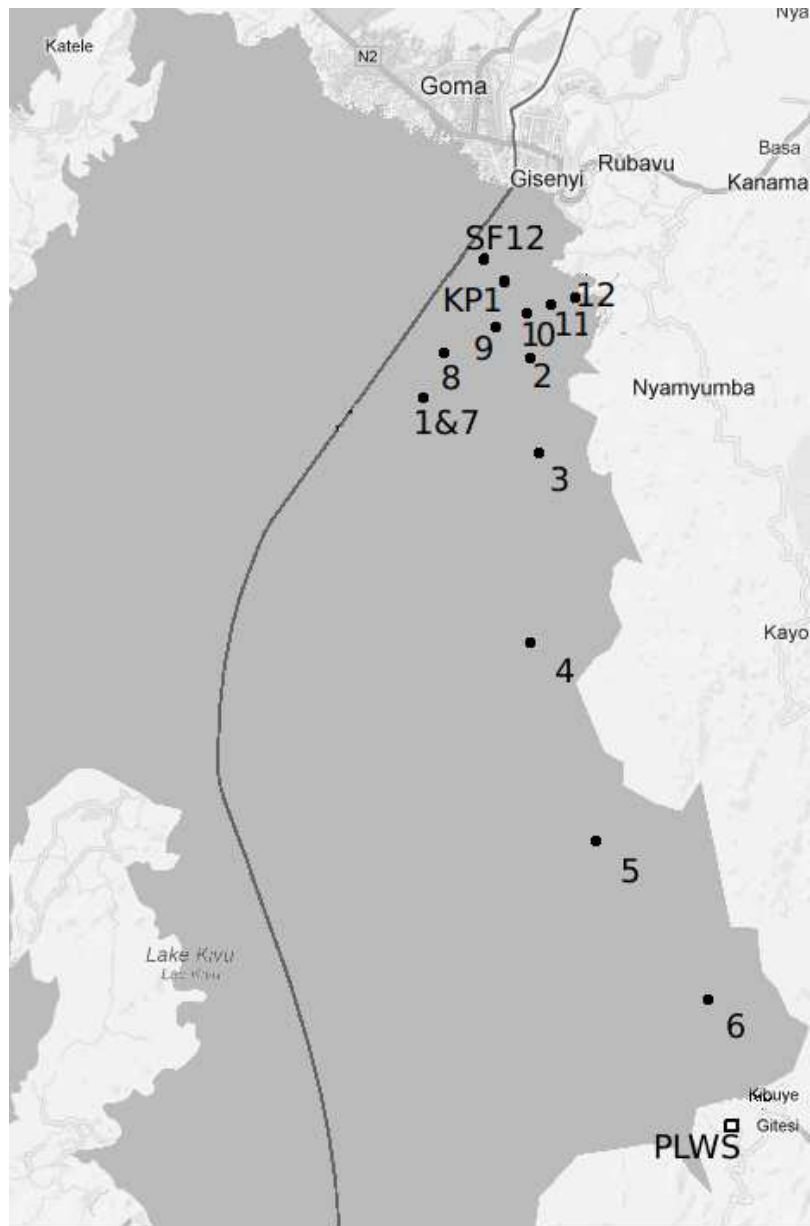


Figure 3.1: Map of the locations of the 12 CTD profiles taken in January 2011 and February 2012, and the thermistor string at the KP1 methane extraction platform in the northern part of Lake Kivu. The location of the PortLog weather station installation site is also indicated (PLWS).



Figure 3.2: The Sea and Sun CTD 90M probe used to obtain profiles of temperature, conductivity, and dissolved oxygen concentration in Lake Kivu.

Conductivity-Temperature-Depth profiles were taken using three different CTDs. Two Sea and Sun profilers (a CTD60 and CTD90M (Figure 3.2)) were utilized for most of the profiles, and one profile was obtained using an RBR XRX-420 logger. Sampling devices were attached to a winch that could either be operated with an electric motor or by hand (Figure 3.3). Galvanized steel aircraft cable with a diameter of 3/32 in. was used to attach the CTD to the winch system. Most of the profiles were taken using

the hand operated setup for the winch for better control of the rate at which the CTD was lowered. Typical rates for lowering were between 0.7 and 0.8 m s^{-1} . Depth was monitored using a Humminbird 858c series GPS/echo-sounder.



Figure 3.3: Picture of the winch used to raise and lower the CTD profiler (primarily by hand) through the water column in January 2011.

3.1.2 Array of temperature recorders

A string of Onset U22 thermistors (Figure 3.4) was installed on the KP1 methane extraction platform ($-1^{\circ}43' 56.445'' \text{ S}$, $29^{\circ}14' 34.2456'' \text{ E}$) on January 9, 2011. A total of 19 thermistors were programmed to record the water temperature at depth intervals of 3 meters between 6 and 60 meters depth every 20 minutes. The location was chosen

for the convenience of access and security of the equipment. The U22 thermistors have a resolution of 0.02 °C, making them capable of measuring the changes in temperature in the mixolimnion of Lake Kivu. The relatively low accuracy (0.2 °C) makes comparisons between individual thermistors ambiguous when their temperature differences are smaller than 0.2°C. Accordingly, corrections were made post deployment. Post deployment corrections for the 2011 season were performed by Professor Sally MacIntyre and Javier Vidal (University of California, Santa Barbara).



Figure 3.4: Example of the 19 HOBO Onset U22 temperature loggers used on the thermistor string at the KP1 methane extraction plant in the upper 60 m of the water column.

3.2 Corrections to Temperature, Conductivity, and Pressure

3.2.1 Conductivity corrections

The conductivity recorded by the Sea&Sun CTD is the in-situ conductivity measured at the in-situ temperature. Conductivity of water, like those of most substances, varies as a function of temperature, so the temperature associated with each conductivity datum is

essential to correctly compare among different profiles (Smith, 1962). Proper comparisons therefore require a common temperature for the profiles, so conductivity data are commonly adjusted to a fixed temperature. Measurements of conductivity made using the same CTD in the water column with constant – or at least nearly constant – temperature can be compared without this correction.

A common temperature-conductivity relation is for 18 °C pure water at atmospheric equilibrium, setting the standard as $1\mu\text{mho cm}^{-1}$ ($0.8\cdot 10^{-6}$ mhos depending on conditions) (Washburn, 1918; Smith, 1962). The three most commonly used temperature standards today are 18 °C, 20 °C and 25 °C. The conductivities are then referred to as κ_{18} , κ_{20} and κ_{25} , respectively. Since some available historical data were already adjusted to 20°C (Lorke et al., 2004), the temperature chosen for our profiles was 20°C. A linear adjustment of resistivity (the inverse of conductivity) is usually good enough over small enough temperature ranges, given by $R(T) = R_0(1 + \alpha(T - T_0))$. Applying this to conductivity in our profiles, we have adjusted the conductivity coefficient of resistivity, α , for water in our temperature range given by the method of Pawlowicz (2008):

$$\kappa_{20} = \frac{\kappa_T}{(1 + 0.0191(T - 20))} \quad (3.1)$$

where κ_T is the recorded in situ conductivity, $0.0191 [1/K]$ is the average value for the temperature coefficient to correct to 20°C in waters with the temperature range of interest, and T is the in-situ temperature in °C. Similar adjustments are made to correct to either 18 or 25 °C (Smith, 1962), with the only change made to Equation 3.1 the value of the temperature coefficient for the desired temperature standard.

All of our profiles were individually corrected. The average of the profiles was also

computed using Matlab and adjusted to 20 °C. A resolution for the average of 0.05 meters was chosen based on the fall rate and sampling frequency of the CTD. Results of the Sea and Sun CTDs were compared with the single cast of the RBR CTD to check for consistency.

3.2.2 Salinity and Density Profiles

Estimations of the salinity are required to calculate water density, which determines the stability of the water column. The density of the water at a given depth is determined by its composition and temperature. The density in the upper portion of the water column in Lake Kivu is governed primarily by temperature and salinity, with gasses having only minor contributions above the temperature inversion depth. This allows for calculation of the density by standard methods. The surface water of Lake Kivu (above 50 m depth) has relatively low salinity, variations in its density are primarily due to temperature. Salinity increases the density of the surface water in Lake Kivu by about 0.1 g m⁻³. Chen and Millero (1986) suggested an empirical expression for the density of water to a precision of better than 2·10⁻⁶ g cm⁻³:

$$\begin{aligned}
 \rho_0(\text{g cm}^{-3}) = & 0.9998395 + 6.7914 \cdot 10^{-5}T - 9.0894 \cdot 10^{-6}T^2 \\
 & + 1.0171 \cdot 10^{-7}T^3 - 1.2846 \cdot 10^{-9}T^4 \\
 & + 1.1592 \cdot 10^{-11}T^5 - 5.0125 \cdot 10^{-14}T^6 \\
 & + (8.181 \cdot 10^{-4} - 0.85 \cdot 10^{-6}T + 4.96 \cdot 10^{-8}T^2)S
 \end{aligned} \tag{3.2}$$

Here, T is temperature in $^{\circ}\text{C}$ and S is salinity in grams of dissolved salts per 1 kg of water. Application of Equation 3.2 is valid for waters with salinities less than about 0.6 g kg^{-1} (Chen and Millero, 1986; Wüest et al., 1996). Effects due to the compressibility of water under pressure were ignored as negligible in comparison to the uncertainty in density expected due to increasing concentrations of dissolved gasses and instrumental accuracy. The salinity profile was estimated from conductivity measurements and is shown in Figure 3.5. Multiplication by a conversion factor of $\sim 1.024 \text{ g}\cdot\text{kg}^{-1}\cdot\text{cm}\cdot\text{mS}^{-1}$ was used to calculate salinity (from κ_{20}) in the upper 250 m of the water column. This factor was derived from the first order coefficient resulting from the method of Wüest et al. (1996) for converting conductivity to salinity. The ionic concentrations of Tassi et al. (2009) were used for the calculation of the conversion factor. Below 250 m depth, the significant increase in the quantity of dissolved CO_2 results in larger proportions of carbonic acid in comparison to other dissolved substances. This increase results in a first order conversion factor of $\sim 1.096 \text{ g}\cdot\text{kg}^{-1}\cdot\text{cm}\cdot\text{mS}^{-1}$.

The density of the profile calculated due to the effects of temperature and salinity (Equation 3.2) is shown in Figure 3.6 and compared to the density profiles of Schmid et al. (2005).

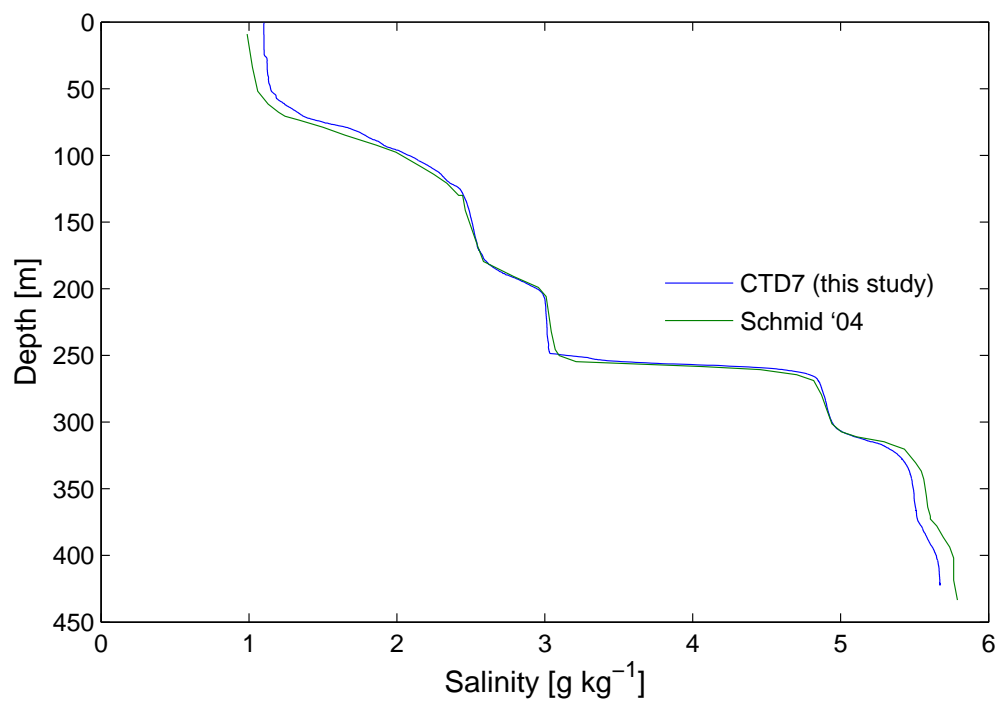


Figure 3.5: Approximate salinity of Lake Kivu based on the conductivity profile taken at the KP1 methane extraction platform. Calculated as described in section 3.2.2. A comparison with the profile of Schmid et al. (2002) is made for reference.

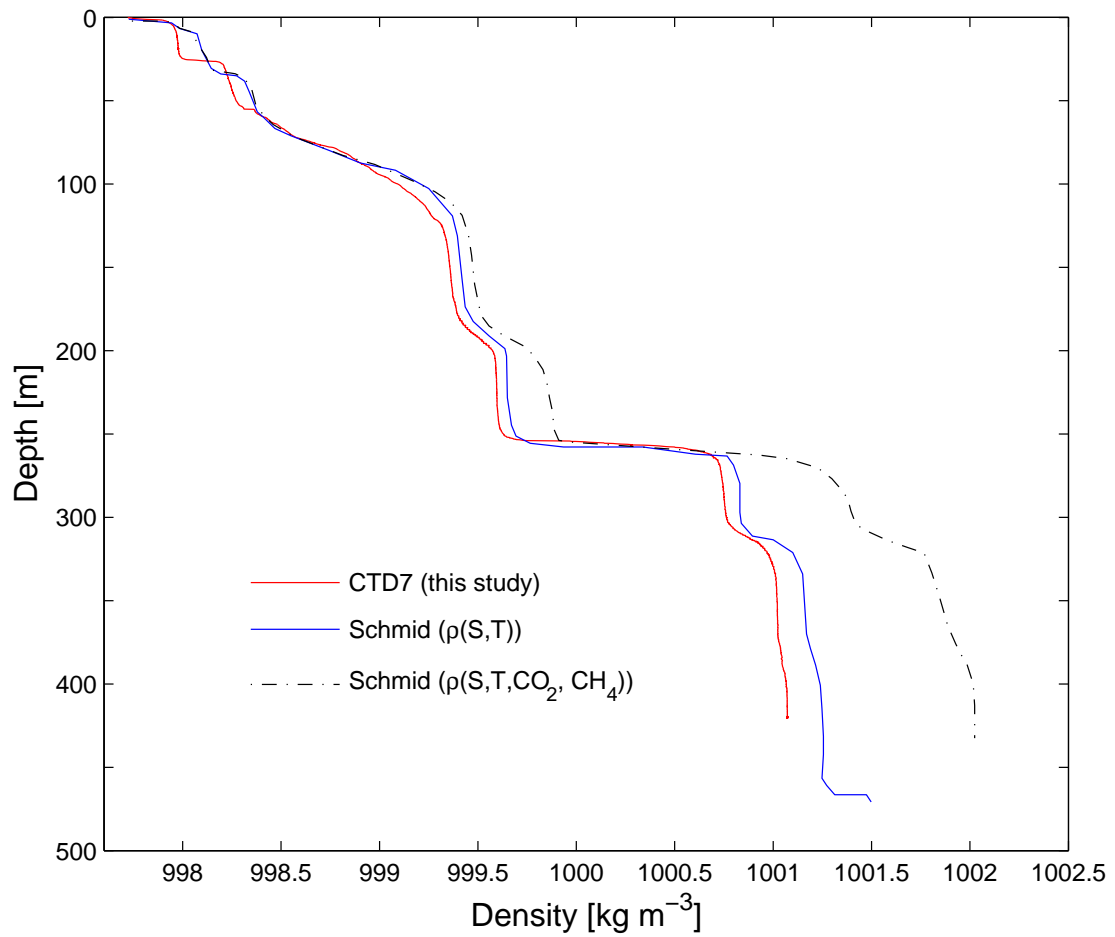


Figure 3.6: Approximate density profile in Lake Kivu calculated from the temperature and salinity profiles of CTD7. Comparisons with the profiles of Schmid et al. (2002) is made, which account for density contributions from dissolved gasses (CO₂ and CH₄).

3.2.3 Pressure to Depth Conversion

As the CTD records pressure (in dbar) rather than depth, a correction has to be made to obtain the true depth. To obtain the proper depth from the pressure measurements then requires using the hydrostatic principle with an accurate density profile:

$$P(h) = \int_0^h \rho(P, S, T, \dots) \cdot g_\phi \, dx \quad (3.3)$$

where $P(h)$ is the pressure at depth h and $\rho(P, S, T, \dots)$ is the density of the water column at depth h , dependent on Pressure, Salinity, Temperature, and other dissolved substances (such as the CO_2 and CH_4 in Kivu). The interdependency of density on pressure and pressure on density make application of Equation 3.3 difficult. However, under the range of densities in Lake Kivu of approximately 998 kg m^{-3} to 1002 kg m^{-3} (Tietze, 1978; Schmid et al., 2002), an $\sim 4 \text{ kg m}^{-3}$ difference exists between the surface waters and bottom waters. This means an $\sim 0.4\%$ maximum error may exist in reported depth by ignoring density variations. At a depth around 200 m this results in an uncertainty of $\pm 0.8 \text{ m}$, and at 400 m a value of $\pm 1.6 \text{ m}$. An additional uncertainty from the accuracy of the CTD adds another 0.1% error to the depths (that is another 0.2 m at 200 m depth), for a total of $\pm 1\text{--}2 \text{ m}$ depending on depth in the water column.

As in-situ measurements of density were not made, other methods need to be applied to obtain the depth. A common approximation used to convert pressure to depth is made using a correction factor: multiplying the pressure in dbars by 1.0197 (i.e. a 1.97% adjustment) (Fofonoff and Millard Jr., 1983). This approximation works well when the assumption of relatively low salinity (i.e. a nearly constant density of $\sim 1000 \text{ kg m}^{-3}$) and mid-latitude lakes near sea level can be made. As the water density of Lake

Kivu is not uniformly 1000 kg m^{-3} , adjustments are needed, as well as adjustments to the local gravitational field strength, g_ϕ . Variations in g_ϕ closer to the equator and at higher elevations are made by considering the Earth to be a rotating oblate ellipsoid and applying a free-air correction for elevation. The resulting expression for g is given by the 1967 Geodetic Reference System:

$$g_\phi = g_0 \left[(1 + \alpha \sin^2 \phi - \beta \sin^2 2 \cdot \phi) - \gamma \cdot h \right] \left[\frac{m}{s^2} \right] \quad (3.4)$$

where $g_0 = 9.78031846 \text{ m s}^{-2}$, $\alpha = 0.0053024$, $\beta = 0.0000058$, and $\gamma = 3.155 \times 10^{-7}$.

Applying Equation 3.4 gives a value for g at the altitude and latitude of Lake Kivu (taken to be 2°S) to be approximately 9.77 m s^{-2} . To obtain a better factor for the pressure dependent depth conversion then requires application of Equation 3.3 with the assumption of an average water column density, $\bar{\rho}$, the depth is then given by:

$$d = \frac{P [\text{dbar}] \cdot 10^4}{\bar{\rho} \cdot g_\phi} [m] \quad (3.5)$$

Applying Equation 3.5 to Lake Kivu results in a conversion factor of $\sim 2.34\%$, which was used instead of 1.97% . An additional minor correction for pressure used in oceanography is to add an additional $1.092 \cdot 10^{-6} \cdot P$ to Equation 3.5 to account for the compressibility of water (Fofonoff and Millard Jr., 1983). As the magnitude of such a correction is smaller than the expected uncertainty in depth, such a correction has not been used in calculating the depths of our profiles.

3.3 Heat fluxes accross the lake surface

Heat exchange across the free surface of a lake consists of solar radiation flux (Q_s), incoming thermal radiation from the atmosphere ($Q_{L_{in}}$), outgoing thermal radiation from the lake surface ($Q_{L_{out}}$), sensible and latent heat fluxes (Q_c and Q_e), and heat input from precipitation (Q_p). The total heat budget (Q_T) is then:

$$Q_T = Q_s + Q_{L_{in}} + Q_{L_{out}} + Q_c + Q_e + Q_p$$

An annually balanced budget would mean a seasonally averaged Q_T of 0 W m^{-2} .

3.3.1 Heat loss due to evaporation

The amount of heat removed from the lake surface by evaporation can be calculated from the specific latent heat of vaporization:

$$Q_e = L_{H_2O} \rho_{\text{surface}} \cdot V_e \quad (3.6)$$

where L_{H_2O} is the latent heat of vaporization for water, ρ is the density of surface water, and V_e is the volume of evaporated water. Quantities used for V_e are based on past estimations of the water budget (Table 2.1).

3.3.2 Long-wave Thermal Radiation Heat Fluxes

Thermal radiation energy lost from the lake surface were calculated for typical water surface temperatures of Lake Kivu using the Stephan-Boltzmann equation for gray-bodies¹:

$$Q_{L_{out}} = \varepsilon \sigma T^4 \quad (3.7)$$

where ε is the greyness coefficient (emissivity) for the emitting surface, σ is the Stephan-Boltzmann constant, $5.67 \cdot 10^{-4} \text{ W m}^2 \text{ K}^{-4}$, and T is the absolute temperature (i.e. in Kelvin) of the emitting body. Radiation is considered “long-wave” if it falls between visible light and microwaves, having a wavelength typically between 5 and 25 μm . For the long-wave radiation energy loss, ε_{H_2O} is taken to be 0.97 (Warnecke et al., 1971). This is the standard value for liquid water (Robinson and Davies, 1972; Davies et al., 1971; Muvundja, 2010).

For the thermal radiation recieved by the lake from atmospheric emissions, the emissivity coefficient, ε_{air} , is more difficult to estimate, as the atmosphere is a gas where both temperature and pressure effects are important to ε_{air} (Swinbank, 1963; Jiménez et al., 1987). The radiation in air does not come from a surface, as in a liquid or solid, but rather from gas molecules, water droplets, and aerosols at various altitudes and temperatures throughout the atmosphere above the lake surface (Staley and Jurica, 1972). The temperature for the atmosphere’s emission is taken as the temperature at approximately 2 meters above the water surface. The long-wave radiative transfer from the air to the water surface (Imberger and Patterson, 1981) is then:

¹A gray body radiates with a similar spectrum to a blackbody, but the total radiated energy is reduced by some factor of emissivity based on its composition.

$$Q_{L_{in}} = \epsilon_{air} \sigma T_{air_2}^4 \cdot (1 + 0.17\beta^2) \cdot (1 - R_t(lw)) \quad (3.8)$$

where T_{air_2} is the air temperature [K], β is the fractional cloud cover, $R_t(lw)$ is the total reflectivity of the water surface for long-wave radiation. The emissivity of the air, ϵ_{air} , is temperature dependent. It also depends on the partial pressure of the water vapor in the air. An alternative to using the vapor partial pressures under the conditions of varying humidity is to use an approximation for ϵ_{air} (Swinbank, 1963) that uses a dimensional empirical coefficient, C_ϵ , (in units of $^\circ\text{C}^{-2}$) and thus makes the emissivity of air directly proportional to temperature squared. The dimensional empirical coefficient depends on several factors, however, in practice is typically taken to be an average value for the associated range. Jacquet (1983) gives a range for C_ϵ of $0.906 \cdot 10^{-5}$ to $0.999 \cdot 10^{-5} \text{ }^\circ\text{C}^{-2}$ while Blanc (1985) gives a mean value of $0.938 \cdot 10^{-5} \text{ }^\circ\text{C}^{-2}$. In the estimates made from our data, the average value of $0.938 \cdot 10^{-5} \text{ }^\circ\text{C}^{-2}$ was used. The effective emissivity is then:

$$\epsilon_{air} = C_\epsilon T_{air_2}^2 \quad (3.9)$$

For the temperature of the air near Lake Kivu's surface, equation 3.9 results in a value of $\epsilon_{air} = \sim 0.80$ at the current average air temperatures of $19 \text{ }^\circ\text{C}$ (Schmid et al., 2012; Sarmiento et al., 2006).

3.3.3 Heat Flux Due to Sensible Radiation

The sensible heat loss caused by the air convection, wind, and heat conduction to the air from the lake surface can be found using the model of Imberger and Patterson (1981), in which heat losses are proportional to the wind speed 10 m above the water surface:

$$Q_c = C_S c_{\text{pair}} \rho_{\text{air}} u_{10\text{m}} (T_{\text{air r}} - T_{\text{water}}) \quad (3.10)$$

Here,

C_S is the stability dependent bulk coefficient of sensible heat transfer,

c_{pair} is the specific heat capacity of air at constant pressure,

ρ_{air} is the density of air – taken to be 1.2 kg m^{-3} ,

$u_{10\text{m}}$ is the wind speed at 10 m above the surface,

$T_{\text{air r}}$ is the dry bulb temperature of air at the water-air interface above the water surface,

and T_{water} is the surface water temperature.

C_S is taken to be $1.4 \cdot 10^{-3}$, and the specific heat capacity of air is approximately $1003 \text{ J kg}^{-1} \text{ K}^{-1}$ near the surface air temperatures.

3.3.4 Solar Radiation Contributions to the Heat Budget

The shortwave solar radiation heat fluxes received at the lake surface were calculated based on a running 19-year average of 24-hour mean Global Horizontal Irradiance (GHI) data available on the SolarGIS database (Sol, 2011). The values available were reported as the region averages in $\text{kWh} \cdot \text{m}^{-2}$. These values were converted to $\text{W} \cdot \text{m}^{-2}$ by simply

dividing by 24 hours. GHI accounts for the total amount of shortwave radiation received by a horizontal surface near the ground – including both direct normal irradiance and diffusive shortwave horizontal irradiance due to dispersion by clouds. Here, shortwave refers to the near infra-red, visible light, and near ultra-violet radiation region of the electromagnetic spectrum, ranging from 200 nm to 3000 nm. Incoming solar radiation is taken to be mostly in this range, as the Sun emits mostly shortwave radiation.

3.4 Meteorological Data

We installed a PortLog portable weather station on top of a storage container located on the Contour Global work site (Figure 3.7 and 3.1) to collect basic meteorological data, such as temperature and wind speed throughout these seasons. Data collected included ambient temperature, relative humidity, average and maximum wind speed, rainfall, barometric pressure, and solar radiation. The device was programmed to take measurements every 60 minutes. Unfortunately, when the storage device became completely filled with data, the data became corrupt. As a result of this failure, the wind speed data and temperature averages were obtained instead from the information available online. The information came mainly from the nearby weather observation systems based at airports away from the lake shore and higher than 10-meters above the lake surface.

3.5 Dissolved gas measurements in silicone tubing

Silicone tubing samplers were designed to measure the partial pressures of the dissolved gases in Lake Kivu. The design was based on a saturated soil sampler (Klefoth et al., 2011; Jacinthe and Dick, 1996) and the pressure measurement technique used by Evans et al. (1993) for determining the CO₂ concentrations in Lake Nyos, Cameroon. Samplers consisted of lengths of silicone tubing of outer diameters: 4 and 7 mm (Figure ??). The 4 mm OD tubing had 1 mm sidewall thickness; whereas the 7 mm OD tubing had 1.5 mm sidewall thickness. The ends of the tubing were cleaned with isopropanol and allowed to air dry. Once dried, one end was plugged with fresh silicone and allowed to cure. The other end was then capped with a luer 3-way stopcock that permitted a syringe to be connected to collect the accumulated gases. The samplers were tested in lab using a pressure chamber and a CO₂ source. The CO₂ pressure in the chamber was controlled at the gas cylinder's pressure regulator valve and verified by the pressure gauge installed on the chamber (Figure 3.8). The samplers were submerged in water within the chamber and the water allowed to saturate with the gas at known pressure via gentle shaking of the chamber every few minutes to dissolve the CO₂ gas into the water. The silicone walls of the tubing allowed the gas to diffuse inside until the gas phase inside the tubing was in equilibrium with the dissolved gas in the ambient water.



Figure 3.7: PortLog portable weather station installed near Kibuye, Rwanda.

Figure 3.8: Pressure chamber and gauge used in testing the silicone tubing gas pressure samplers.

Deployment of the samplers in Lake Kivu was performed by attaching the silicone tubes to a 3.5 mm nylon cord with a quick release loop. Additionally, a zip tie was looped through the samplers at each loop to secure the tubing to the cord while ensuring that the connection was not tight enough to result in compression of the tubing as gases expanded during retrieval. The luer locks were tied shut to prevent their opening while being lifted back up through the water column. Syringes were installed on the threaded port to the luer locks and the locks opened as soon as possible once on deck to allow the pressure from the expanded gas inside the tube to force the syringe plunger out. Once the syringes had expanded completely their plunger displacements were recorded. Samples of the gas were also taken in septum capped vials for analysis.

Initial deployment in Lake Kivu consisted of four tubes deployed at 60 m depth for one-half hours on January 5, 2011. Upon recovery, it was found that not enough gas had diffused into the tubing to be measurable with a 20 ml syringe. On January 6, the tubing was deployed for 2.5 hours (8h40 to 11h10) at 70 m depth. Unfortunately, the valves had opened up while being lifted through the water column and the captured gas escaped. The tubes were redeployed at 11h25 at 80 meters but had to be recovered shortly afterwards due to high wind, and no gas was collected. On January 8, tubes were deployed at depths of 80 meters, 110 meters and 140 meters, with three replicate tubes at each depth. Again, strong winds prevented lengthy deployment (13h55 to 14h20) and high drag angle meant the tubes were not as deep in the water as measured by the cord length. The reported depth has been corrected for this error as best as possible. Not enough gas was

collected to push the syringe plungers out for measurements. Nevertheless, hissing was heard, indicating both that gas was being released from the tubing, and that the tubes were deep enough to allow the dissolved gas to diffuse and accumulate inside. Finally, on January 9, the tubings were deployed for 35 minutes. Despite the wind, the average rope angle allowed for estimation of the deployment depths at 122 meters, 130 meters, and 138 meters. Physically measurable quantities of gas were obtained from the tubing upon recovery.

3.6 Simulation of a limnic eruption in lab

Several approaches were used to simulate the limnic eruption process on a small scale. A large beaker was filled three-fourths full with tap water at 20 °C. The bottom fourth of the beaker was slowly filled through polyethylene tubing with water at 6 °C, which was enriched with CO₂ in a bubble-chamber (Figure 3.9) immersed in an ice bath. A syringe with a long narrow needle was then filled with near boiling water, which was injected into the cold bottom waters in an attempt to stimulate an eruption by gas exsolution. In separate experiments, the cold CO₂-rich water was made saline to increase the density gradient. Additionally, several trials used surface water at 75 °C for the same purpose.



Figure 3.9: Image of the bubble chamber created to dissolve CO₂ into the water prior to drip-feeding the water into the lower layer of the beaker or the narrow tube which replaced the beaker

In a separate set of experiments, the 25-cm tall beaker and the bubble chamber were replaced by an 80-cm tall narrow plastic tube (see figure 3.10). The cylindrical water column could be capped to slightly increase the pressure for better CO₂ dissolution. A tightly fitting closed-cell foam cap was fit to the tube to maintain an increased pressure as water was fed into the bottom of the column. Large quantities of salt were used in the CO₂ rich water to increase the density gradient. After several trials with this system, a modification was made whereby, once the CO₂ siphon was started, the cool water could be fed by gravity through a small hole in the bottom of the cylinder without having to pass through the warm upper water (see figure 3.11). Various eruption triggers to bring CO₂ out of solution were tried that included injecting boiling water into the lowest water layer, initially through a small hole in the CO₂ water supply line and then by carefully removing the supply line and replacing it with a hot water inflow. In a different approach based on the diet-coke menthos reaction, salt, sand, and sugar substitutes were mixed

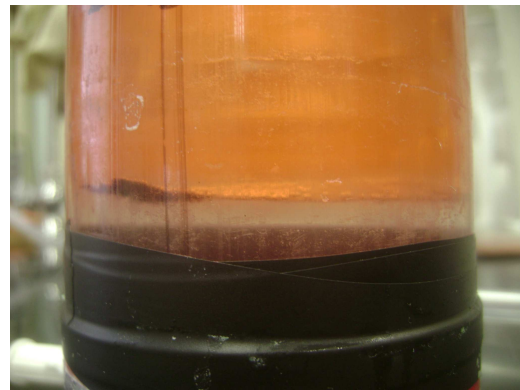
in a beaker with water and left to dry. Once dry, the mixture was broken up into small conglomerate chunks that were subsequently dropped into the water column.



Figure 3.10: View of the bottom half of the tall narrower tube used to replace the beaker initially used in attempts to create a small scale limnic eruption.



(a)



(b)

Figure 3.11: View of the bottom inflow created in the tall tube of figure 3.10 before (a) and after (b) the cool salty CO_2 water was carefully injected underneath the high column of warm tap water. In the lower left of the chamber is the injection point where polypropylene tubing entered through a hole and was pierced by a syringe to inject the near boiling tap water was to attempt a limnic eruption within the tube.

4

Results

4.1 Temperature distributions in the water column

Profiles of temperature obtained from the CTD casts in January 2011 are shown in Figures 4.1 – 4.5. Figures 4.4 and 4.5 correspond to the Master Station, Figure 4.1 corresponds to the long transect to Kibuye, and Figure 4.2 to the short transect between the Master Station and the shore (see Figure 3.1).

4.1.1 Temperature profile inversion

All profiles show the inversion in the temperature profile at around 78 meters depth. Between the surface and 78 m depth, the temperature decreases with depth, following a typical pattern in stratified lakes. Below 78 m, the temperature increases.

4.1.2 Positions of thermoclines

Temperature variations below 78 m depth indicate a step-like stratification: regions of strong temperature gradients are inter-spaced with regions of weak gradients. Our profiles do not extend all the way to the lake floor; however, a gradual temperature increase is assumed to continue past the deepest temperature measurement (26.01 °C at 417.9 m) in the profile of CTD7 (deepest) to the lake floor. The first strong gradient, between ~ 170 and 202 m, is referred to here as the upper thermocline. The temperature increases gradually down to a depth of ~ 250 m, at which depth the largest change (sharpest gradient) exists at the primary thermocline, having an ~ 1.0 °C temperature increase occur over ~ 12 m (down to 262 m depth). Another gradual increase occurs down to 300 m, followed by the second strongest gradient at the lower thermocline with ~ 0.5 °C increase from 301 to 331 m depth. A small thermocline below the lower thermocline of 0.23 °C increase exists between 368.5 and 403 m depth.

The positions of the thermoclines coincide with the salinity (density) gradients. Their positions are summarized in Table 4.1.

Table 4.1 Depths of the major pycnoclines in Lake Kivu

Pycnocline	Depth m	Temperature Change °C	Temperature Gradient °C m ⁻¹
Upper	170–202	0.4	0.0125
Primary	250–262	1.0	0.083
Lower	301–331	0.5	0.017
Deep	368–403	0.23	0.007

4.2 Lateral variability in temperature distributions

Small lateral variations exist in the temperature profiles when compared across the lake. Lateral variability in the depth region between the seasonal thermocline ($\sim 35\text{-}40$ m depth) and the temperature inversion depth is on the order of 0.01 °C (Figure 4.3), whereas in the region between the inversion and 120 m depth it is on the order of 0.005 °C. Between 120 m and the upper pycnocline, profiles taken at different locations can vary by ~ 0.01 °C. This variability is determined based on the standard deviation of the Kibuye transect temperature profiles (Figure 4.3), and likely can be considered as a measure of the natural variability in the lake.

4.2.1 Inflows

The profiles taken at the Master Station (CTD1 and CTD7 in 2011) and at the REC platform (SF12 and Oct12 in 2012) show several prominent negative excursion in temperature. One of these negative excursions appears near 90 m depth. Another negative excursion in temperature appears in CTD1, CTD7, and CTD8 (the closest profile on the Near Shore transect to the MS) and the 2012 profiles at the upper boundary of the primary pycnocline (at ~ 248 m). Negative excursions that appear in only the profiles taken at the REC platform in 2012 appear at 160 m, 170 m, and 284 m in February and at 125 m, 165 m, 170 m, 230 m, 294 m, and 298 m in October (Figure 4.9). These features do not appear in the other CTD profiles; however, the near shore transect profiles do not go into the deeper waters to observe the negative excursions in temperature that were detected in the 2012 profiles. Most of these negative excursions are assumed to be due to subsurface inflows near these depths. However, the signal at 90 m is related to the

Kibuye Power 1 (KP1) re-injection plume, as the re-injection depth of KP1 is ~ 90 -95 m, which produces a plume from ~ 93 to 109 m as it disperses to its isopycnal depth (Pasche et al., 2010).

The temperature of the signal at 248 m cooled by 0.085 °C between January 2011 and February 2012, and warmed by 0.022 °C by early October 2012. However, as the 2011 and 2012 profiling locations differ, and because the other profiling locations do not show these features, the variation in the temperature of the 248 m inflow are assumed due to changes in the plume's temperature as it moves across the lake in the process of settling to its isopycnal depth. The less prominent negative excursion in temperature appearing in the temperature profile from CTD7 near 170 m depth appears in both the February and October 2012 profiles as well; however, instead a single excursion as in CTD7, it appears as two separate excursions (at 163 and 170 m). These two inflows likely combine to form a larger single plume further from the source, as CTD7 is further from the shoreline.

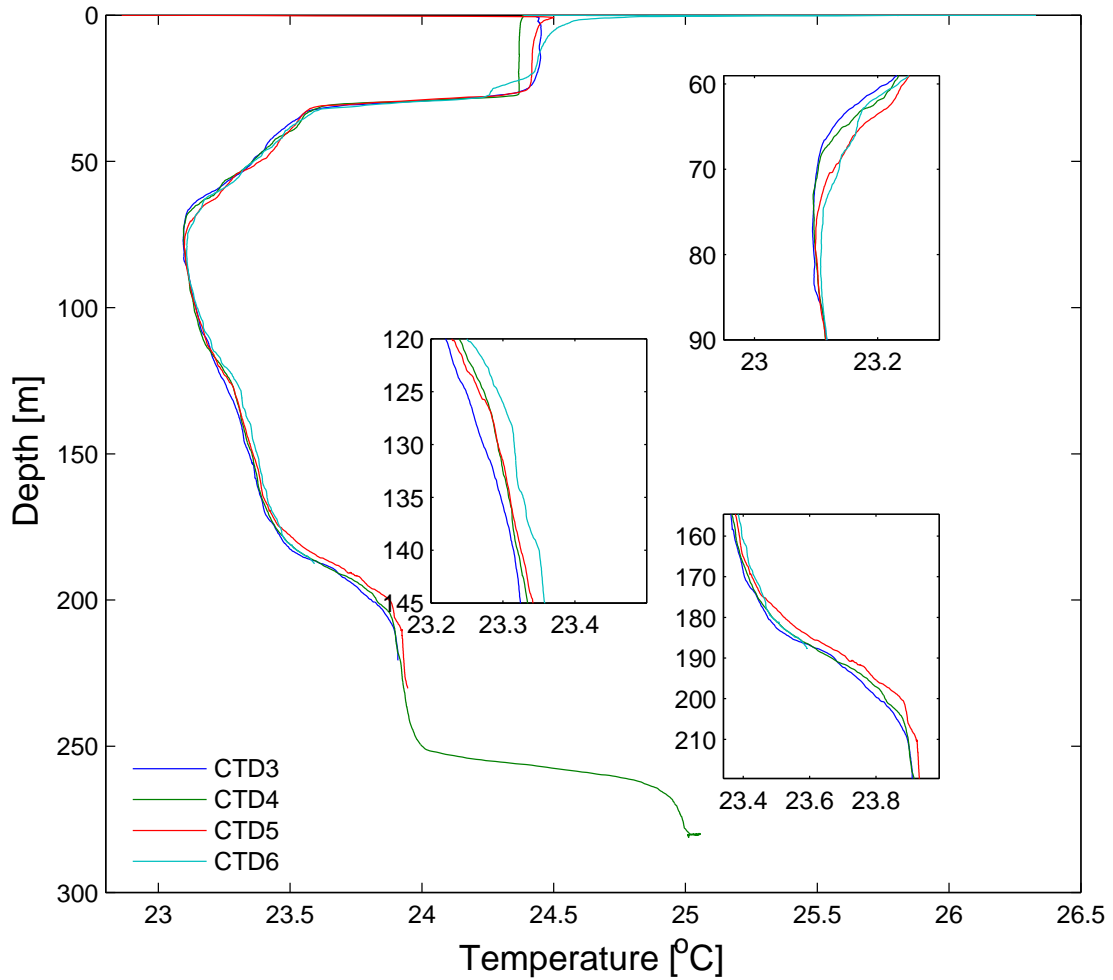


Figure 4.1: Temperature profiles taken during the morning of 7 January, 2011 on the transect to Kibuye (CTD3-CTD6) (Figure 3.1). The insets zoom in on the regions where larger variability is seen.

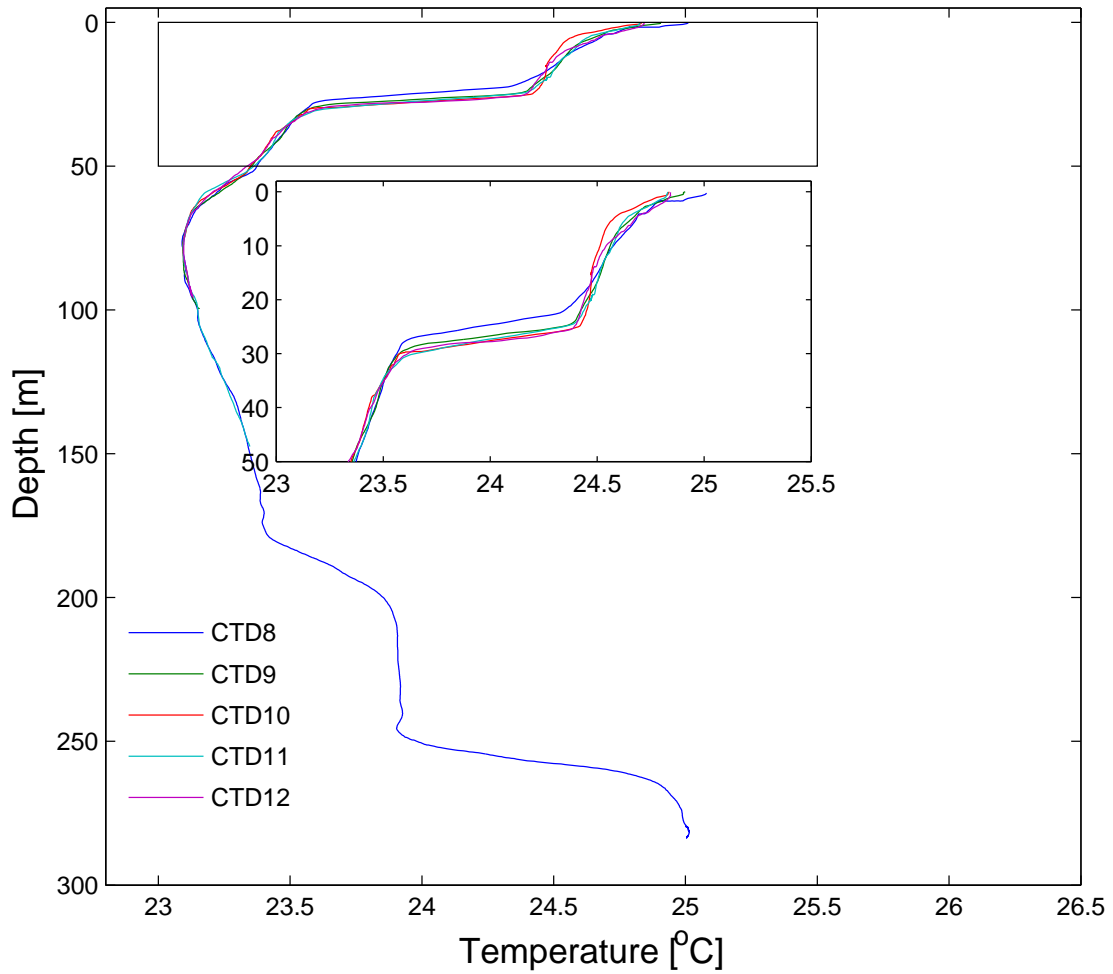


Figure 4.2: Temperature profiles measured on January 9, 2011 between 16h00 and 18h00 on a transect from the Master Station towards shore. Weather conditions were windy and overcast all day.

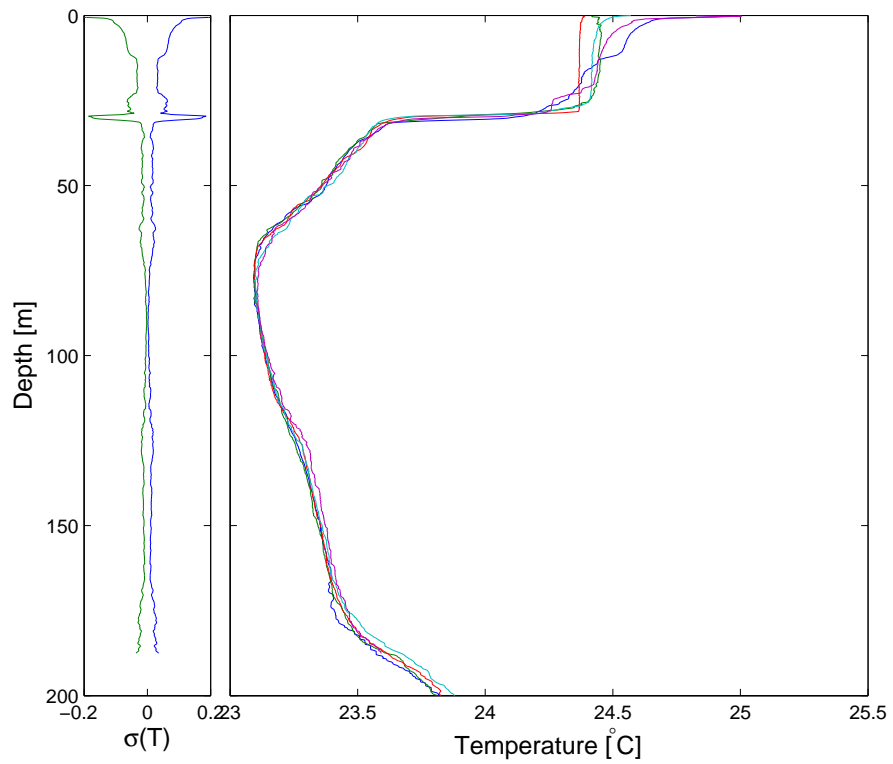


Figure 4.3: Standard deviation for temperature at a given depth, calculated from the profiles of the Kibuye Transect, 7 January, 2011.

4.3 Temporal variability in the temperature profiles

4.3.1 Variability within the mixolimnion

Diurnal temperature variations in the uppermost 20–25 meters of the water column caused by the daytime absorption of solar radiation and nighttime wind and cooling can be seen in Figure 4.6, where CTD1 corresponds to the morning of January 6, CTD2 to the early evening of January 6, CTD3–CTD6 were taken the following morning, and CTD7 the next afternoon. The temperature profile obtained from CTD1 reveals a temporary thermocline at ~13 m depth. Analysis of the temperature of the upper 25 m of the water column from CTD2 reveals warming of the waters and the formation of another temporary thermocline near 8 m depth between the morning cast of CTD1 and the evening cast of CTD2. Temperature profiles obtained from CTD3 and CTD4 show that winds overnight on January 6 mixed the water column to 25 m depth, destroying the two temporary thermoclines. Calm conditions over the course of January 7 and 8 caused warming of the waters in the upper 12 m of the water column and the formation of another temporary thermocline is seen deepening as time progressed through January 8 (CTD7 at the Master Station). Diurnal variation is also seen in Figure 4.8 in the plot of temperatures obtained from the thermistors nearest the surface.

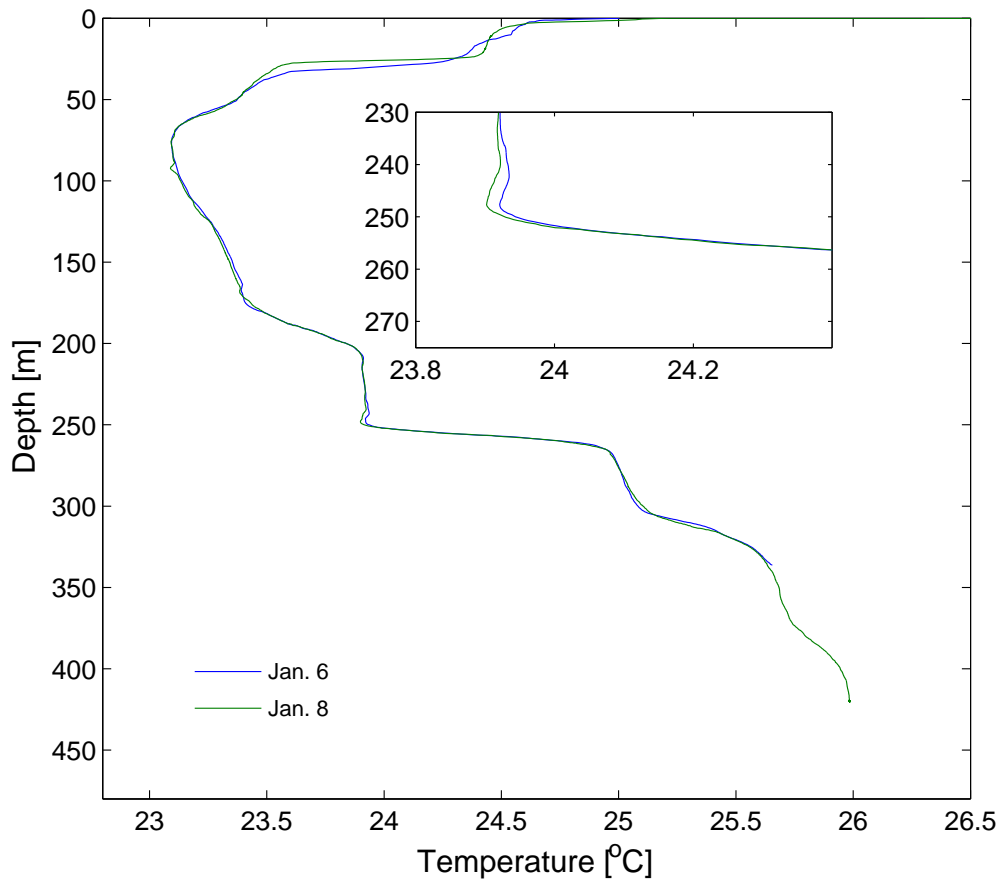


Figure 4.4: Temperature profiles taken during late morning on 6 January 2011 and early afternoon on 8 January 2011 at the Master Station. The inset zooms in on the region near the top of the primary pycnocline.

On a seasonal time scale, the temperature time series recorded by the moored array of temperature recorders are shown in Figures 4.7 and 4.8. Figure 4.8 shows the individual thermistor temperature profiles, which reveal the year-round warming of waters within 20 m of the current inversion depth, while Figure 4.7 shows the corrected 2011 temperature-depth contour series. The thermistors' data only cover the upper 60 m of the water column for most of the year 2011, from mid-January to late November. The

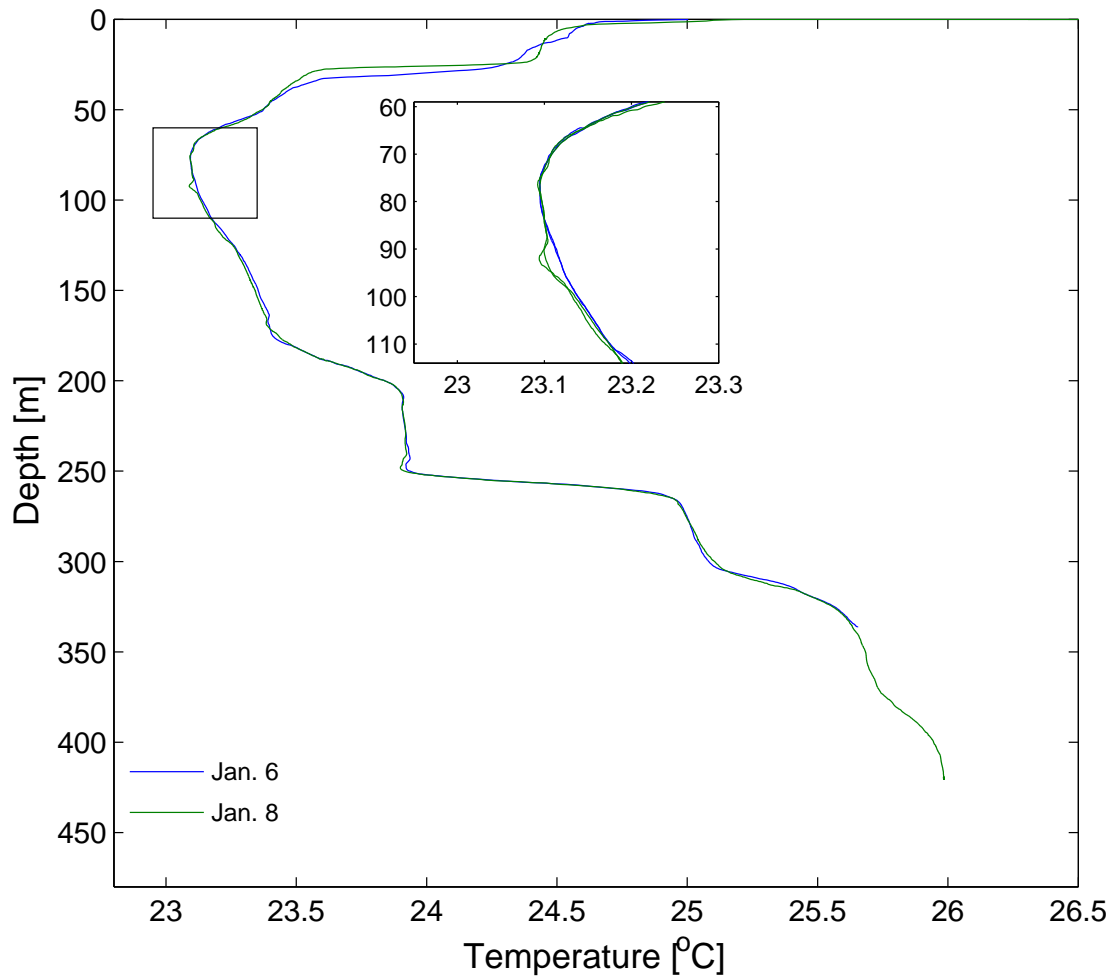


Figure 4.5: Temperature profiles taken during late morning on 6 January 2011 and early afternoon on 8 January 2011 at the Master Station. The inset zooms in on the region surrounding the temperature profile inversion.

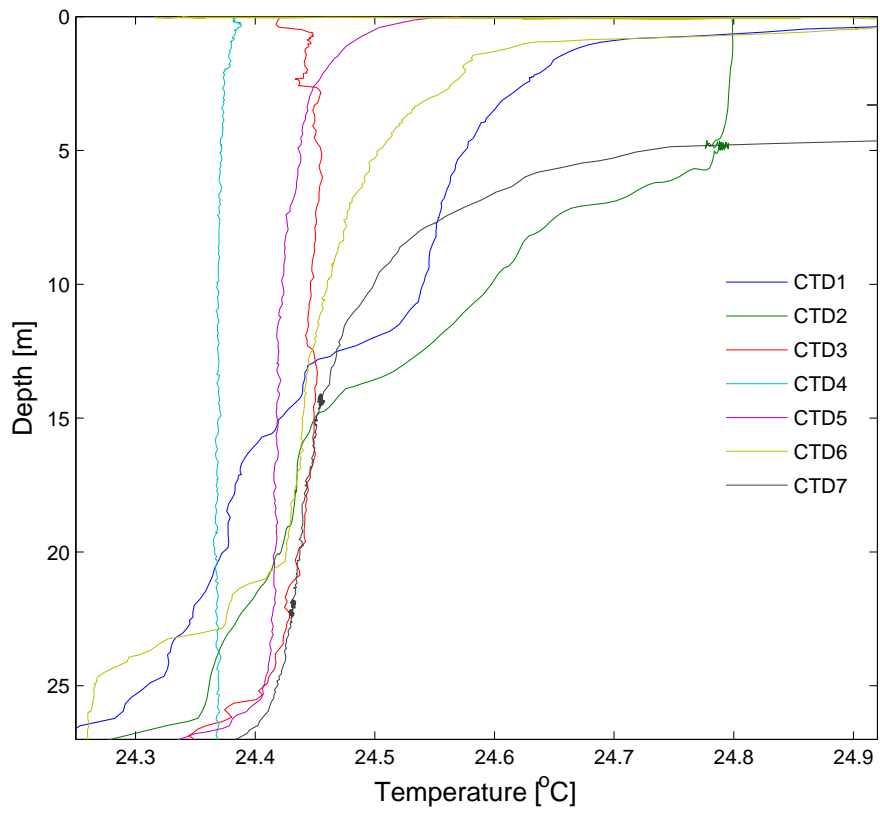


Figure 4.6: Comparison of CTD profiles in the uppermost 25 meters of the water column over a three-day period. Variation in temperature due to surface weather patterns is evident over short time periods.

results show that the temperatures in the mixolimnion became homogenized down to about 45-50 meters near the end of the dry season in late August. Several shallower mixing events occurred in April and October of 2011 that mixed the water column down to the 35 m seasonal thermocline. All mixing events were shallower than the depth of the temperature inversion, which in January 2011 was at 78.3 ± 0.97 m at 23.08 °C (Figures 4.1, 4.2, and 4.3).

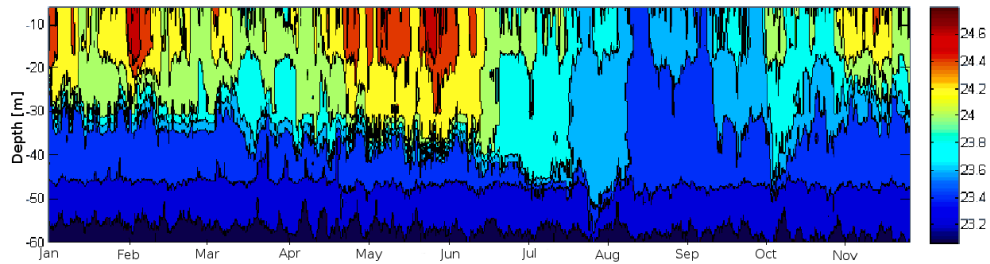


Figure 4.7: 2011 time series of temperatures in the upper 60 meters recorded at KP1 methane extraction plant in the northwest section of Lake Kivu using Onset HOBO U22 logging thermistors.

4.3.2 Temperature variability in the deep waters

Comparison of the deep profiles taken in January 2011 (CTD1 and CTD7) and those in 2012 at the end of the dry season (early October) and during the wet season (early February) reveal small variations in the temperature of deep waters (Figure 4.9). The region at 285 m depth (between the lower and primary pycnoclines) cooled by 0.041 °C from January 2011 to February 2012, and subsequently warmed by 0.018 °C by October 2012. This variability is likely due to differences in the location of the sampling, as the January 2011 Master Station profile was at a different station than the 2012 profiles, and the 2012 profiles revealed inflows in this region that were not present at

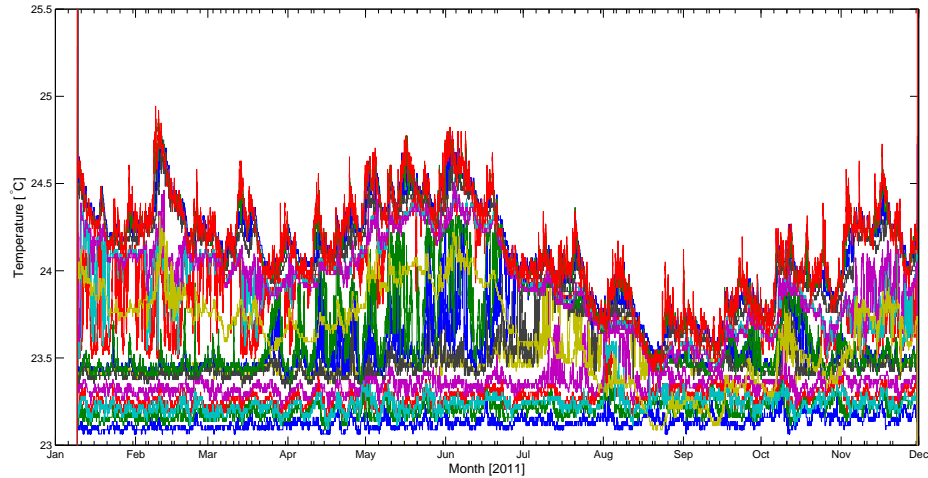


Figure 4.8: January - November 2011 temperature versus time profiles for individual Onset U22 thermistors.

the Master Station. Comparisons of temperature profiles below 340 m reveal a similar warming trend of $0.0067\text{ }^{\circ}\text{C}$ near 355 meters (see inset of Figure 4.9) from January 2011 to February 2012. Between February and September 2012, warming at the same depth was $\sim 0.049\text{ }^{\circ}\text{C}$, equivalent to $0.0065\text{ }^{\circ}\text{C}$ when the same rate is extrapolated to a one year time span. Based on comparisons of CTD7 and the February 2012 temperature profiles, depth variations on the order of 2.5 to 3 meters exists in the primary pycnocline.

4.4 Conductivity distribution in Lake Kivu

Conductivity measurements made in January 2011 are shown in Figure 4.11. All the profiles show a nearly constant conductivity between the surface and about 45 – 50 m depth, below which the conductivity increases. All profiles show a significant increase

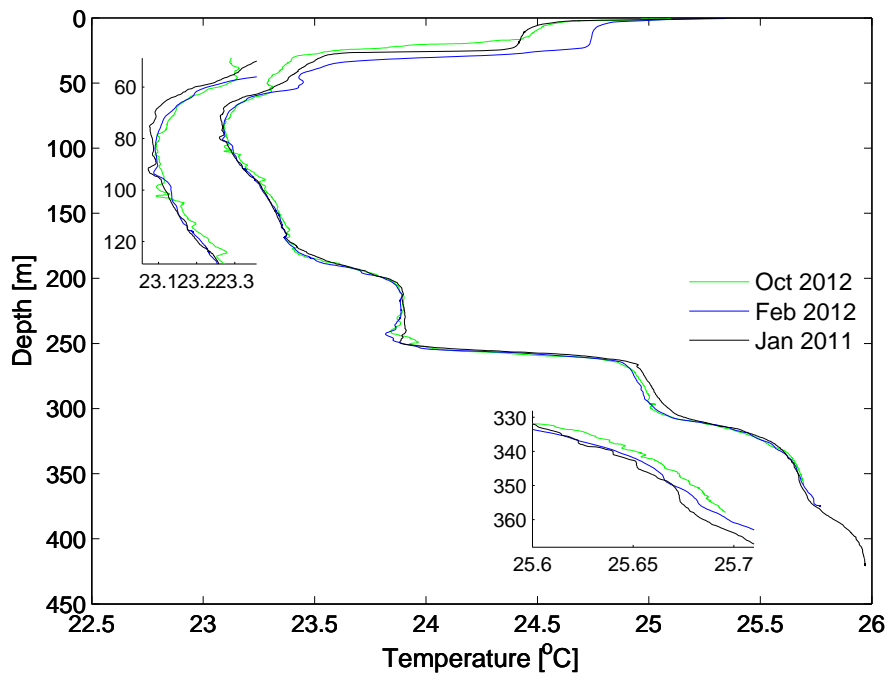


Figure 4.9: Temperature profiles showing variability over the course of one and a half years from the Master Station CTD7 (January 2011) and the REC platform in February 2012 and October 2012. Insets zoom in on the region near 350 m depth and the temperature inversion near 80 m depth.

in conductivity (1.17 mS cm^{-1} to 1.20 mS cm^{-1}) between 55 m and 125 m, defining the uppermost permanent density gradient in Lake Kivu. A smaller change from 2.70 mS cm^{-1} to 3.12 mS cm^{-1} , occurs at the upper chemocline (Table 4.1). The largest increase (3.21 mS cm^{-1} to 4.78 mS cm^{-1}) occurs at the primary chemocline (250 m depth). An increase in conductivity from 4.99 mS cm^{-1} to 5.45 mS cm^{-1} occurs at the lower chemocline. Between these regions of sharp conductivity gradients (the pycnoclines), conductivity continually increases with depth, but at a much slower rate.

4.4.1 Spatial variability in water column conductivity

Small lateral variations exist in the conductivity profiles. The largest deviations occur along the strong gradients (Table 4.1), based on the standard deviation of all the January 2011 profiles (Figure 4.10). At the upper boundary of the primary chemocline, conductivity at a given depth varies by $\sim 0.1 \text{ mS cm}^{-1}$. The upper chemocline had a deviation of $\sim 0.04 \text{ mS cm}^{-1}$, and the lower $\sim 0.05 \text{ mS cm}^{-1}$. However, the deviation in the lower chemocline is based on only two deep profiles (CTD1 and CTD7). In regions between pycnoclines, variations of conductivity are less than 0.01 mS cm^{-1} , which is on the order of the accuracy of the conductivity probe and thus considered as a minimal natural variability of the water (possibly due to the effects of temperature on the measurement device). Deviations near the depth of the temperature inversion were on the order of 0.04 mS cm^{-1} , similar to the deviations in the upper chemocline. As the regions of larger variability correspond to the depths of the pycnoclines, as did the variability in temperature, the variability in the conductivity is assumed due to internal

waves. Variability in conductivity between near shore profiles versus offshore profiles near the depths of sub-surface inflows is assumed due to the respective plumes mixing into the water.

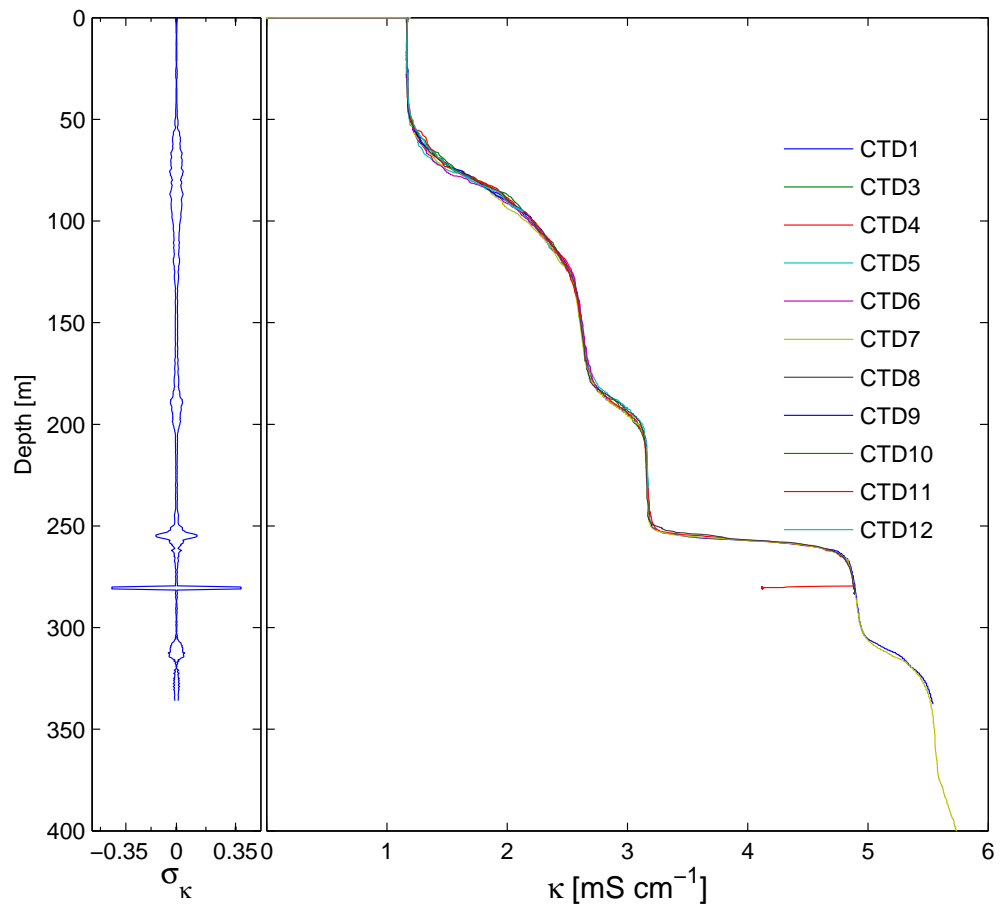


Figure 4.10: Standard deviation for conductivity at a given depth, calculated from all January 2011 profiles.

4.4.2 Temporal variability in water column conductivity

Comparison of the January 2011 and February 2012 profiles (Figure 4.11) indicates that conductivity profiles exhibited minor variability from one year to the next in the upper 170 m. Increases in conductivity were on the order of at least 0.025 mS cm^{-1} through most of the water column. This observed increase is likely due to instrumental differences, as the February 2012 profiles were obtained with a different model probe using the same style sensor. However, a decrease in conductivity on the order of 0.005 mS cm^{-1} appears above the seasonal thermocline, as well as between the lower boundary of the primary chemocline and upper boundary of the lower chemocline ($\sim 268 \text{ m}$ to 301 m depth). These slight decreases are likely due to a combination of internal waves, slight differences in location, and the effects of sub-surface inflows near the shoreline which are more evident in profiles from the REC platform than the Master Station (see Section 4.2.1). The larger differences between the February 2012 and January 2011 conductivity profiles that appear in the left panel of Figure 4.11 at depths between ~ 50 and 120 m , in the primary chemocline ($250\text{--}262 \text{ m}$), and within the lower chemocline (from $308\text{--}320$) are assumed due to the effects of internal waves.

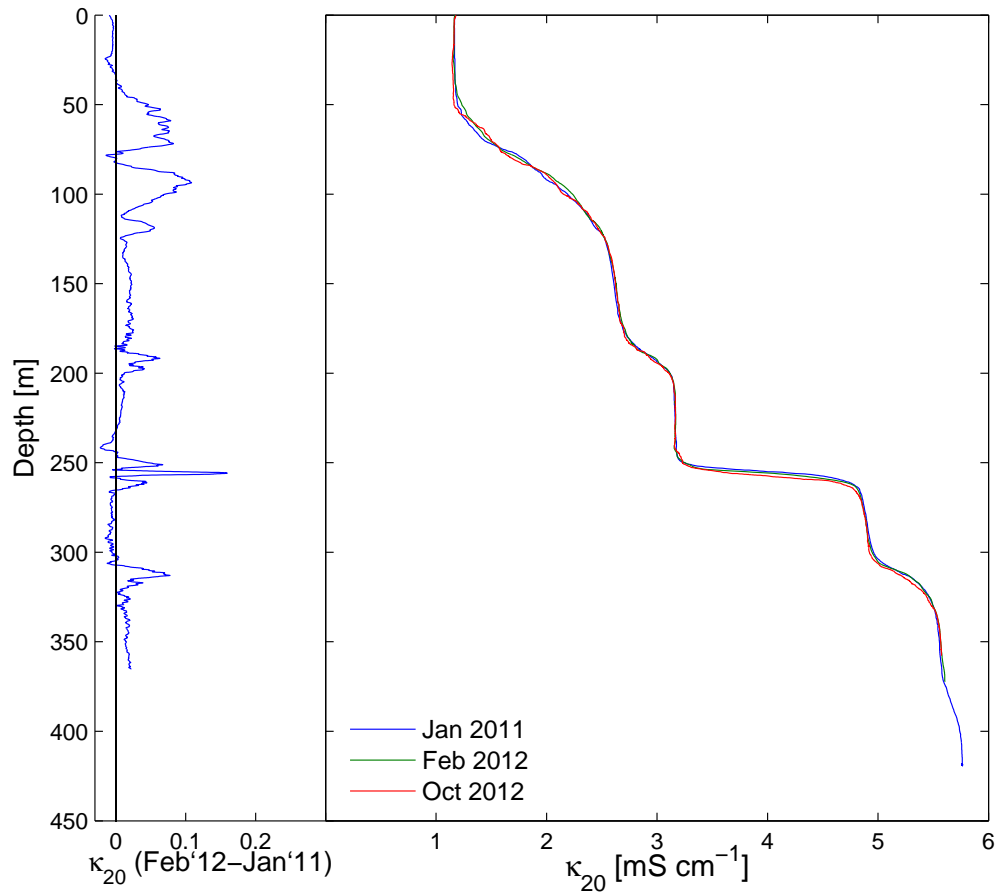


Figure 4.11: Conductivity profiles measured at the Master Station on January 8, 2011 and at the REC platform on February 9, 2012 and October, 2012. The left panel shows the difference between the February 2012 and the January 2011 profiles.

4.5 Oxygen distributions in the water column

Oxygen profiles measured in January 2011 and February 2012 are shown in Figure 4.12. Due to the reaction of hydrogen sulfide with the oxygen sensor, the signals increase

below the depth where H_2S is first present (~ 150 m). Apparent lack of saturation in waters 30 m and shallower in February 2012 is caused by a combination of warmer surface water than in January 2011 and a poorly calibrated sensor on a different CTD. Oxygen penetration depth was approximately 50 m in January 2011 (i.e. at the upper boundary of the mixed layer). Due to the poorly calibrated sensor used to obtain the February 2012 oxygen profile, the measurement never reaches zero saturation, but saturation depth was taken to be the minimum reading at ~ 67 m depth. The oxygen profiles have a strong gradient (an oxycline) at the depth of the seasonal thermocline (~ 30 – 35 m in January 2011). Lack of agreement in the depths of the oxycline between the two January profiles is due to a combination of internal waves and the CTD being lowered at different rates during the profiling cast, resulting in a lag in oxygen readings.

4.6 Gas pressure measurements with silicone tubing

4.6.1 Calibration of silicone tubing

Gas expansion volumes obtained from the silicone tube samplers in calibration experiments in the pressure chamber and the associated chamber pressure (and estimated CO_2 concentrations in the water) are summarized in Figure 4.13.

The graph indicates a roughly linear relationship between the volume of CO_2 expanded from tubing into the connected syringes and the concentration of CO_2 in the water, in agreement with an isothermal expansion of the gas within the tubing. Differences in the expansion measured versus that predicted by a true isothermal expansion are due to the friction in the stiffness of the syringe plunger. The linear relationship of

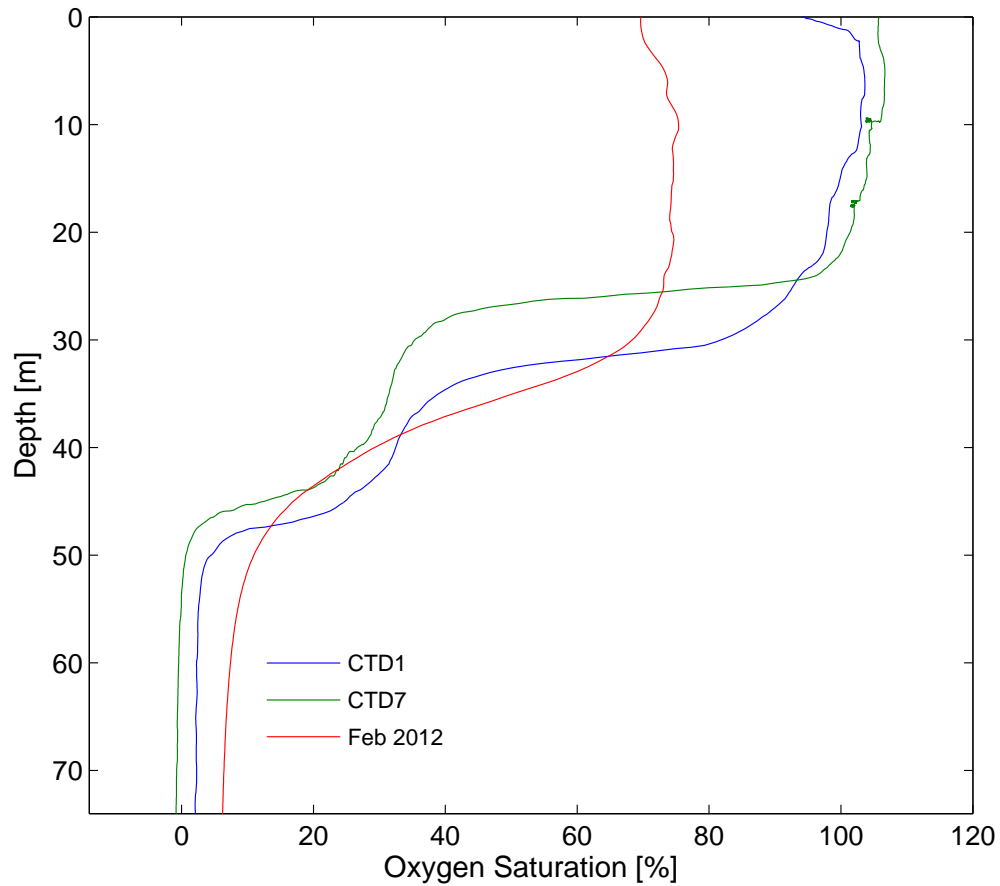


Figure 4.12: Oxygen profiles from the Master Station (January 2011) and from the KP1 platform (February 2012).

volume to CO₂ concentration for the wider diameter samplers yields the approximations:

$$\text{Concentration of CO}_2 \left[\frac{\text{mol}}{\text{L}} \right] = 0.0139 \cdot V - 0.0577 \frac{\text{mol}}{\text{L}}$$

$$\text{Partial CO}_2 \text{ pressure [dbar]} = 0.497 \cdot V - 2.056 \text{dbar}$$

where V is the measured volume expanded into the syringes and the $0.1176 \text{ mol L}^{-1}$ correction is related to the volume of the tubing filled at atmospheric pressure.

4.6.2 Field measurements of gas pressures

Measurements of gas pressures in Lake Kivu were made using a limited number of calibrated samplers (built before the calibration experiments done in lab) and several more were constructed in the field. As limited number of calibrated syringes were available at the time of measurements, additional syringes of a different size were also used. Their plungers could respond slightly different to gas pressures than in calibrated syringes; an uncertainty in the gas volumes measured in them is estimated to be ± 5 mL. Calibrated devices were used at two of the three sampling depths.

There was one successful deployment, for 35 minutes, as described above (Section 3.5). Wind and boat drift resulted in an uncertainty of $\sim 30\%$ in the deployment depth due to the angle of the deployment cord. Estimates of the partial gas pressures based on the calibration data for the tubing are listed in Table 4.2.

Table 4.2 Gas pressures in Lake Kivu from 35 minute silicone subing deployment on 9 January, 2011

Approximate Depth m	Estimated Pressure		Syringe Volumes
	dbar	MPa	mL
122	-0.81 ± 20	-0.0018	2.5, 2.5, 2.6
130	1.03 ± 18	0.010	5.5, 6.2, 7
138	7.39 ± 18	0.074	17.5, 18, 22

Figure 4.14 shows these pressures overlain onto the partial pressures calculated in Schmid et al. (2002).

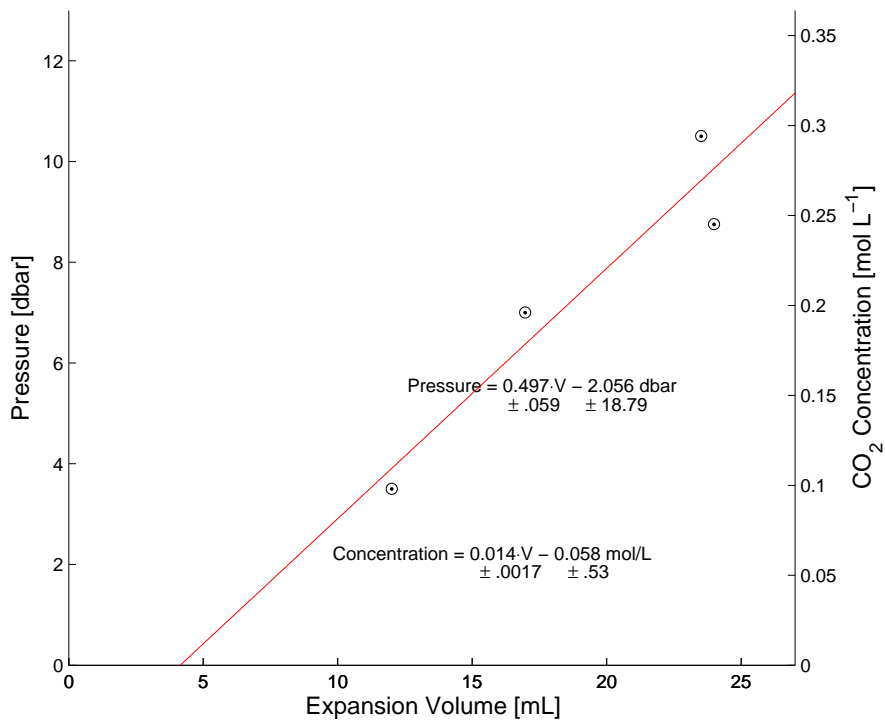


Figure 4.13: Calibration of 4 mm ID/7 mm OD silicone tubes from in pressure chamber with CO₂ saturated water. The vertical axes show gas pressure above the water and the estimated molar concentrations of CO₂ in the water.

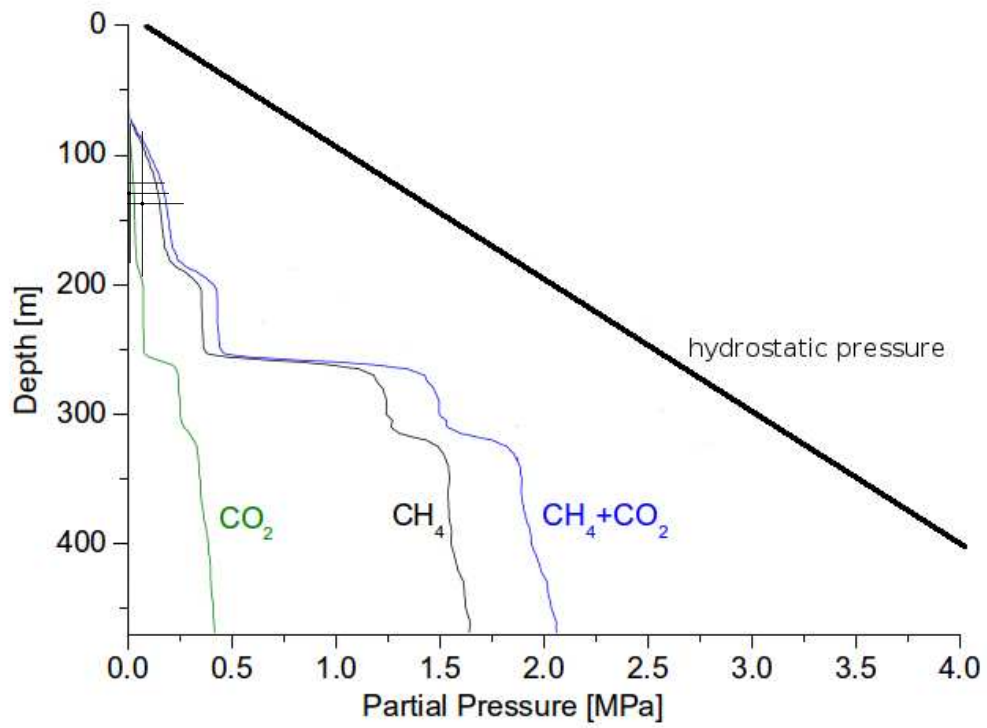


Figure 4.14: Fitting of the silicone tube estimated pressures onto the partial pressures of Figure 5 produced by Schmid et al. (2002).

4.7 Limnic eruptions in lab

Attempts to simulate a limnic eruption in lab were unsuccessful. Bubbles produced by all approaches were limited in size and quantity, and no sustained exsolution was achieved. The setup which had bubbles sustained the longest consisted of having small pieces of a conglomerate of sand, salt, aspartame, and saccharine (which were obtained by allowing water to evaporate from a solution of these constituents to form a solid conglomerate) to provide bubble nucleation surface. Data for the concentrations of solutes used for each water layer in the experimental setup can be found in Table 4.3.

Table 4.3 Summary of attempts to create a limnic eruption in lab using CO₂ as a gas source.

Salt Water	Tap Water	Trigger	Reaction Results
0.87L @ 7 °C	1.76 L @ 40 °C	Injection of near boiling water	Minor Bubbles at injection end of needle
2.2 L with 14.7g NaCl/L, 1.8g Aspartame, 0.5g Saccharine	2.5 L @ 8 °C	Injection of near boiling water	Minor Bubbling from needle tip again
2 L with 45 g/L NaCl, 3 g Aspartame, 0.8g Saccharine	2.7 L @10 °C	Injection of near boiling water	Minor Bubbling from needle tip again
2.1 L with 40g/L NaCl, 3g Aspartame, 0.8g Saccharine	2.6 L @10 °C	Salt, sand, and false-sugar conglomerate dropped in from surface	Continued bubbles (small) for several minutes off of the particulate pieces. No eruption event
Several other similar trials were made, varying quantities of salt, aspartame, and sand in the conglomerates and dissolved in the water, all with the same general results of minor bubbling.			

5

Discussion

5.1 Comparisons of historical temperature distributions in the water column

Temperatures throughout the water column in Lake Kivu have risen since initial investigations in the 1930's and 1970's. The current temperature profiles (Figure 4.9) are compared against the available historical profiles in Figures 5.2 and 5.4. Temperatures near the depth of the temperature inversion have risen by approximately 1 °C since the 1930's, and by 0.5 °C since the 1970's (i.e. $\sim 0.14^{\circ}\text{C}$ per decade). A single temperature measurement in the deep water near 370 m depth in the 1930's (Damas, 1937) suggests warming in the deep monimolimnion on the order of 0.7 to 0.8 °C. The early temperature measurements, however, may not be accurate due to the techniques used. Warming rate based on a comparison with Tietze (1978) is on the order of 0.15 °C since the 1970's (i.e. 0.04°C per decade). At the upper boundary of the primary thermocline (~ 250 m),

warming since the 1970's is on the order of 0.25 °C.

Possible causes for the warming trend include: increasing air temperatures, increasing humidity (i.e. a decrease in evaporative cooling), decreasing wind speed, changes in the flow rate or temperature of subsurface inflows, and increasing concentrations of gases. Heating contributions from gases may result from exothermic methanogenic processes as microbes convert CO₂ gas into methane and from the heat of dissolution. To verify this possibility accurate methods for measuring the concentrations of dissolved gas in the deep water are needed. The accuracy of historical measurements thus may be a significant factor in the calculations (see Table 5.1 for previous measurement techniques and Figure 5.1 for available concentrations from these measurements). Measurements of dissolved methane increases between the 1970's and early 2000's are suggested to be around 15% in waters below 250 m Pasche et al. (2011), which is ~3mmol/l. Deuser et al. (1973) gives the heat release from CH₄ formation to be 60 kcal/mol. With a 3 mmol/l increase in concentration, an estimated increase in temperature since the 1970's would then be ~0.18 °C. The formation of other gases (i.e. CO₂) also have heat released as part of the interactions involved in the methanogenic processes occurring, and these additional heat releases may be enough to account for the increase in temperature in waters below 250 m.

Increases in net heat fluxes across the lake surface should result in warming of the seasonally mixed layer. The existence of an inversion in temperature suggests that the warming caused by changes in heat fluxes across the lake surface will affect primarily the waters down to 80 meters depth, as below this depth heat would have to diffuse against the temperature gradient. Below the depth of temperature inversion, warming may be affected by the surface warming due to a resulting reduction in upward heat

fluxes, as well as by flow rates, temperature, and composition of subsurface inflows.

Table 5.1 Summary of methane measurement techniques that have been used on Lake Kivu

Reference	Year	Method	Accuracy
Schmid/Halbwachs	2003	Polyethylene tubing to lake surface to separate the gas & water phases of sampled water. Flow rates were measured with a GA2000 infrared gas analyzer.	Quotted at ~4%
Schmid/Halbwachs	2004	Capsun METS methane sensor taking measurements every 0.5sec during descent	2-5% error based on calibration of 0.4mmol/L stated by manufacturer
Schmitz and Kufferath Deuser	1971 1973	Gas chromatography was used on shipboard and on samples brought to surface and kept at in-situ pressure until analysis in lab	Not Stated Not Stated
McAullife	1971	Fixed samples with HgCl ₂ and used gas chromatography on tightly closed 150ml bottles. Only very shallow depths were measured using this method after already measuring O ₂ concentrations	
Pasche	2009	Niskin Bottles were capped with a balloon to prevent out-gassing losses due to expansion. However, references of methane concentrations from Schmid '05 are reported.	
Tassi	2009	Segments of Rislun Tubing were connected together to reach the desired depth. At the top, a three way valve attached to a syringe, pump, and sample bottle (tapped with Teflon valves). Water was retrieved "fast" enough to keep the gas that exsolved mixed with the water in the sample bottle "without" loss due to the narrow tubing diameter.	

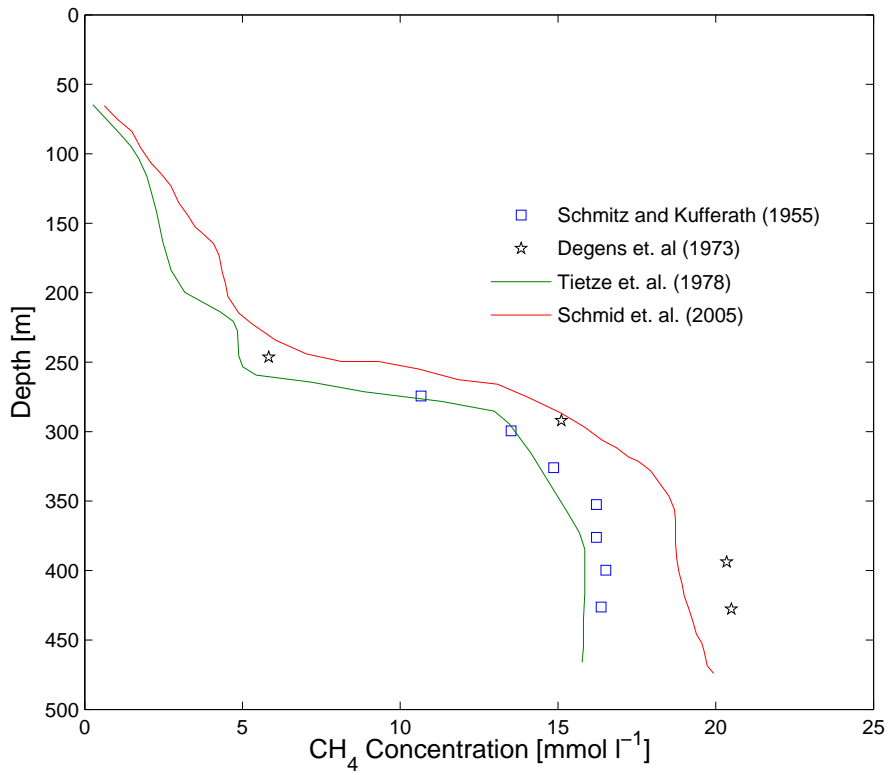


Figure 5.1: Methane concentrations as reported by Schmitz and Kufferath (1955), Degens et. al. (1973), Tietze et. al. (1978), and Schmid et. al. (2005). Methods used to obtain these concentrations are described in Table 5.1.

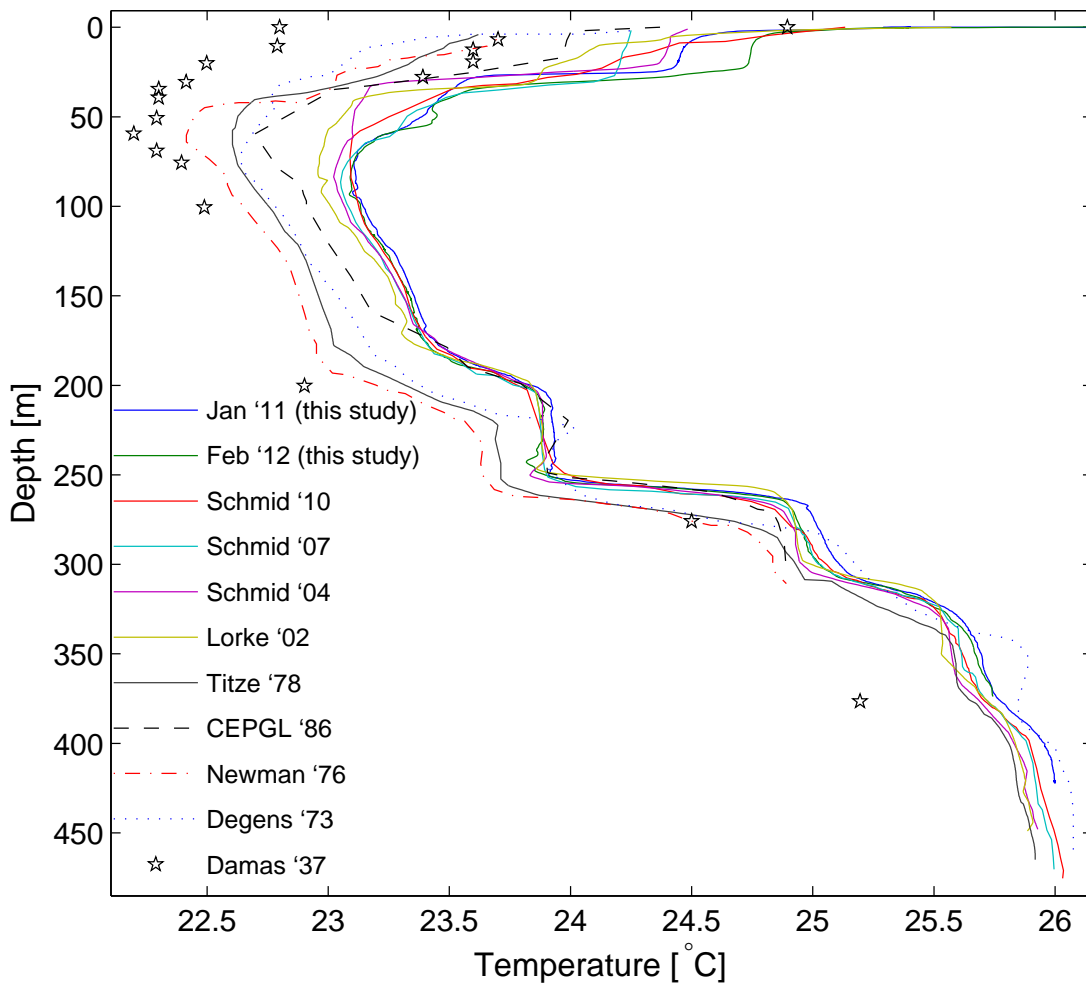


Figure 5.2: Comparison of temperature profiles in Lake Kivu taken in 1935 (Damas, 1937) using a reversing thermometer, 1971 (Degens and Kulbicki, 1973), between 1973 and 1975 (Tietze, 1978; Tietze et al., 1980), 1976 (Newman, 1976), 1986 (Tuttle et al., 1990), February 2002 on the northwestern end of the lake (Lorke et al., 2004), 2004 and 2007 (Schmid et al., 2010, 2012) with those taken in 2011 and 2012 (this study). Historical data were obtained by digitizing published plots, as the original data were unavailable. Small uncertainties in depths can result from slight differences in pressure-to-depth conversion methods, internal waves, and digitization uncertainties.

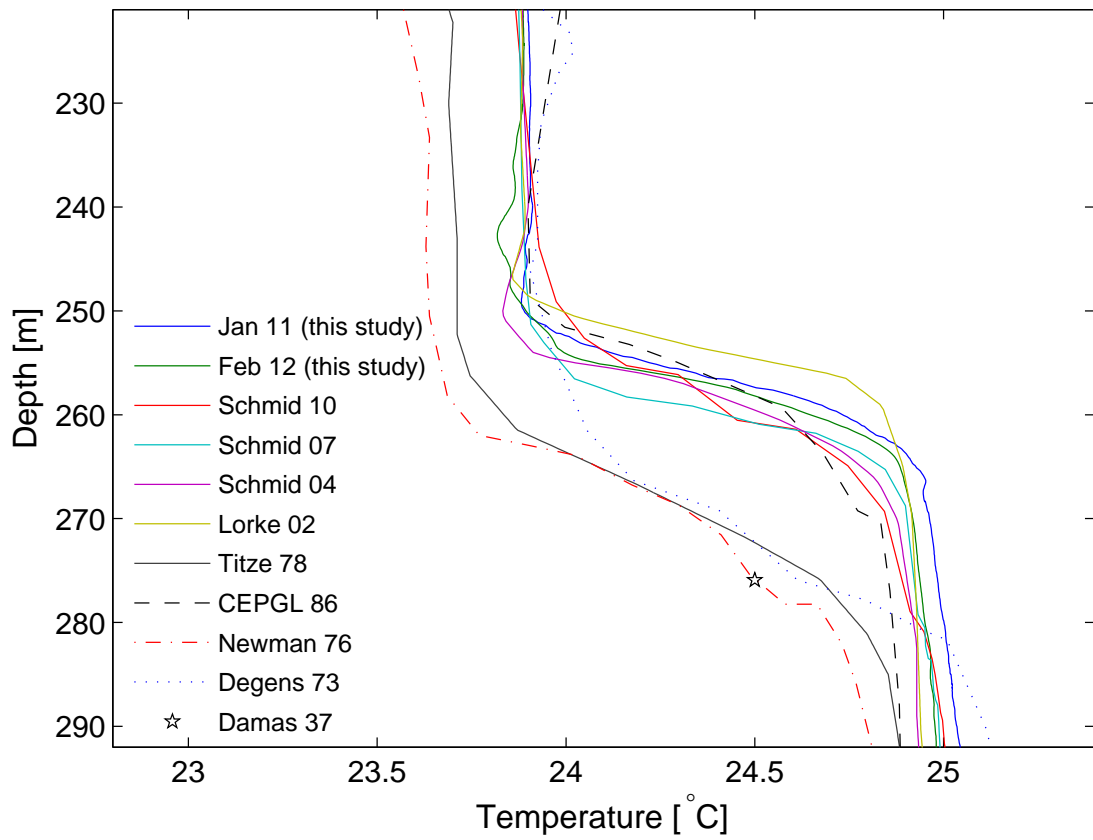


Figure 5.3: Zoomed in view of the temperature profiles from Figure 5.2 near the primary chemocline around 260 meters depth.

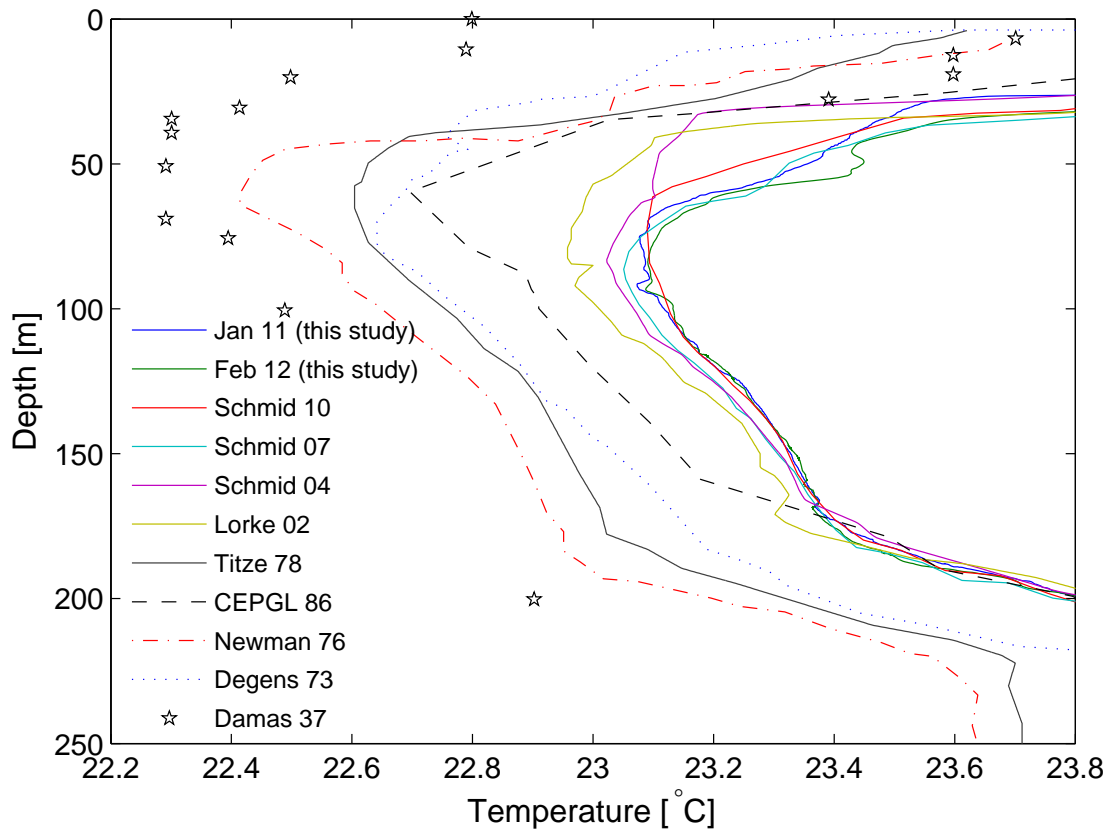


Figure 5.4: Zoomed in view of the temperature profiles from Figure 5.2 near the temperature inversion.

5.1.1 Decadal scale warming at the depth of temperature inversion

With heat diffusing towards the temperature inversion both downward from the surface and upwards from the deep waters, conservation of energy implies that the waters at the temperature inversion depth should be warming. The temperature at the depth of the temperature inversion has been steadily increasing since at least the 1970's, as can be seen by examining the historical temperature profile comparisons of Figure 5.4. Without a regular mixing to the depth of the temperature inversion, which would remove heat episodically, and without a heat sink at the temperature inversion (e.g. cold subsurface inflow), the influx of heat will cause the water column to warm at the temperature inversion. As accurate complete profiles are only available back to 1974, the rate of warming is only estimated by making comparisons with these data. Doing so suggests a rate of $0.14\text{ }^{\circ}\text{C}$ per decade at the temperature inversion depth (not a set depth below the surface). Comparisons with the more recent historical profiles (Lorke et al., 2004; Schmid et al., 2002) indicate approximately the same rate.

Although our string of thermistors at the KP1 extraction platform did not go as deep as the temperature inversion, the deepest thermistors reveal a warming trend in the water below the depth of seasonal mixing during the deployment period. The warming rate 20 m above the temperature inversion (at a depth of 58 m) is on the order of $0.078\text{ }^{\circ}\text{C yr}^{-1}$, based on a linear regression fit. As this is close to the depth of seasonal mixing, the warming rate there is expected to be larger than that of the temperature inversion's warming rate. With seasonal mixing and cooling of the mixolimnion causing the temperature to be "reset" episodically, a continuous warming at the base of the mixed layer (\sim

50 m depth) is not observed on the scale of decades, but the rate of warming throughout the year (prior to mixing) matches well with that of average decadal warming observed for the air temperature near the lake surface. This similarity to air warming rates differs from large lakes at higher latitudes in the United States. For example, Lake Superior, Lake Michigan, and Lake Huron exhibit a summer warming rate of nearly twice that of the atmospheric warming rate (Austin and Colman, 2007). Further evidence for a long-term warming trend can be seen in the flattening of the temperature profile near the temperature inversion. Flattening is to be expected as temperatures rise at the temperature inversion faster than regions slightly deeper than the temperature inversion.

5.2 Heat content and temperature changes in the water column

5.2.1 Heat content changes in the mixed layer

Heat content calculations in the water column indicate that only small changes in heat fluxes are necessary to cause the increase in temperature observed in the upper 80 m. Net changes in heat fluxes to a parcel of water can be calculated from the observed changes in the heat content of that parcel. Calculations of heat content were performed on the temperature profile from 2002 (Schmid et al., 2002) and our February 2012 temperature profile from SF12. The heat content difference from the surface down to 78 m was found to be $\sim 108 \text{ MJ m}^{-2}$, which required a surface input heat flux absorption of only $\sim 0.35 \text{ W m}^{-2}$. As the time over which this change in heat content occurred overlaps with

times of seasonal mixings to various depths above the temperature inversion, this change in heat content only accounts for the overall gain due to an imbalance of heat fluxes. The required 0.35 W m^{-2} is therefore representative of the average heat flux imbalance between 2002 and 2012. Accurate estimates of the seasonal heat fluxes during the time between mixing events are not possible with our data, as the profiles we have taken also correspond to times over which a surface mixing event occurred. As the 0.35 W m^{-2} estimated from the differences in heat content between the February 2002 profile and the February 2012 profile is close to the reported absorption of heat fluxes (0.4 W m^{-2}) in other East-African lakes (Verburg and Hecky, 2009), the heat flux Lake Kivu receives at the surface averaged over the seasons is likely $< 0.5 \text{ W m}^{-2}$.

5.2.2 Heat content changes below the temperature inversion

Heat fluxes between the depth of temperature inversion and the upper pycnocline have remained nearly unchanged between the 1970's and present. The approximate heat content change between the 1970's profile and 2002 profile was 83 MJ m^{-2} between 95 and 165 m depth. Between 2002 and 2011, the change in the same depth range was $\sim 29 \text{ MJ m}^{-2}$. Both of these changes correspond to a required net heat flux of 0.1022 W m^{-2} . This flux corresponds to a warming rate of approximately $0.11 \text{ }^\circ\text{C}$ per decade. The constancy of this number between the two time periods suggests that the warming rate in the region of the water column between 95 and 165 m has been nearly constant over the last 37 years. This suggests that the subsurface inflows must have had nearly unchanged flow rates and nearly constant temperatures. Other heat fluxes (e.g. upward diffusion from deeper water) also must have been nearly unchanged.

Increases in temperature have occurred in the deep monimolimnion as well, although they were small in comparison to the warming observed in the surface waters. The deepest heat content changes that can be calculated from our profiles (below the lower pycnocline from 370 m down to 400 m) for comparison with historical heat content suggest a significant difference in the required heat flux to cause the changes observed during the two time periods. From 370 to 400 m, change in heat content from the 1970's to 2002 was 6.7 MJ m^{-2} , equivalent to a net heat flux of $\sim 0.0081 \text{ W m}^{-2}$ (i.e. $0.02 \text{ }^\circ\text{C}$ per decade). From 2002 to 2011, however, this depth region had a change in heat content of 10.2 MJ m^{-2} , nearly twice the total heat gain that happened from the 1970's to 2002, equivalent to a heat flux of $\sim 0.0324 \text{ W m}^{-2}$ and a warming rate of $0.08 \text{ }^\circ\text{C}$ per decade. The deepest temperature profiles obtained in January 2011, February 2012, and October 2012 (Figure 4.9) suggest a warming rate at a nearby depth of 355 m to be $0.065 \text{ }^\circ\text{C}$ per decade. Inaccuracies in the calculations of the lake heat contents (especially for the deep water) between the 1970's and 2002 may be due to variability in early deep temperature profiles, digitization errors of these data, and internal waves.

5.2.3 Implications of warming

For a lake where the temperature is the dominant factor in determining the water density, and therefore stratification, an increase in surface temperature would strengthen the stratification and result in a more stable water column less prone to mixing. In the case of Lake Kivu, however, the reverse temperature gradient may actually lead to a decrease in the stability of the lower layers of the lake. Processes causing warming in the

deep waters are therefore important. Though changes in the deepest portion of the water column are small, they indicate active energy transfer processes. In a steady state, the temperature in a deep monimolimnion cannot change without local sources of heating or changes in mixing intensity. Temperature profiles in the deep water of Lake Matano, for example, exhibit a constant temperature within one one-hundredth of a degree, e.g. instrumental accuracy, over the course of decades (Katsev et al., 2010). Lake Kivu's deep water temperatures, on the other hand, vary significantly (Figures 5.2 and 4.9). Variability exists both temporally over years and laterally, as evident in comparisons of near-shore temperatures and those further from shore, which show variability due to localized inflows dispersing into the water column horizontally over several kilometers (Figure 4.1). This variability indicates that Lake Kivu is not in a steady state. Rather, it experiences water movements and heat fluxes, possibly in response to localized heating on the lake floor. This results in convection of the deep water, meaning the mixing intensity in the deep water cannot be assumed close to molecular diffusion, as the convective processes would facilitate mixing.

5.3 Warming in Lake Kivu versus other tropical lakes

Warming rates in Lake Kivu surface waters (at the base of the mixolimnion near 50 m depth) since the mid-1970s are on the order of 0.20 °C per decade, greater than the rates reported in other East African Great Lakes over the last century. In Lake Tanganyika, warming rates at a depth of 50 m are ~ 0.1 °C per decade (Verburg and Hecky, 2009) and in Lake Malawi warming rates between 10 and 50 m depth are ~ 0.13 °C per decade

(Vollmer et al., 2005). The rates near 50 m depth in lakes Tanganyika and Malawi correspond to the warming rate closer to the current temperature inversion depth in Lake Kivu (~ 0.14 °C per decade), near 80 m. In Lake Malawi, warming rates at 100 m depth (the base of the mixed layer) are only 0.06 ± 0.02 °C per decade. This depth in Lake Kivu is warming at a greater rate (0.1 °C per decade). In the deep waters between 300 and 400 m, warming rates for Lake Kivu (0.04 ± 0.02 °C per decade) are the same as warming rates reported in Lake Tanganyika ($0.04 - 0.06$ °C per decade in between 1975 and 2000) by Verburg and Hecky (2009). However, Lake Malawi is warming at a rate of 0.12 °C per decade near 300 m depth (Vollmer et al., 2005).

5.4 Double Diffusion and its Variability

The opposing effects of Lake Kivu's temperature and salinity on the density gradient allow for double-diffusion (Newman, 1976; Schmid et al., 2010). Increasing temperature with depth destabilizes stratification, whereas increasing salinity and dissolved CO₂ makes it more stable. As the molecular diffusion of heat and dissolved substances differ, local instabilities cause the formation of a thin, less salty warm layer below a thin cooler layer. As the warm layer rises it mixes with the cooler layer to cause a sharpening of the interface between the layers and a reduction in the density gradient to a nearly homogenous layer. As this small-scale mixing occurs between several different layers, a stair-case structure results that is observed in the conductivity and temperature profiles. These stair-case structures are observed in Lake Kivu over most of the water column

below the temperature inversion, first appearing around 105 m; they are shown in Figures 5.5 and 5.6. The only zones where they are not observed are in the region of the strong primary pycnocline gradient (250–262 m) (also found by Schmid et al. (2010)), a region from 387 m to 393 m where a weak gradient zone exists, and where cool sub-surface inflows enter the lake near the northern shoreline above the upper pycnocline (170–202 m). The upper pycnocline (170–202 m) and the lower pycnocline (306–325 m) do support distinct stair-case structures. Since our profiles are limited to ~ 400 m, the existence of double diffusive steps at deeper depths is unknown.

Comparisons among the January 2011 profiles and the February 2012 profiles reveal variability in the double diffusion structures at several depths. The January 2011 profiles show minor variability, primarily in step thickness, over short time periods, so larger differences are expected to exist between the 2011 and 2012 profiles as heat and salt are transported vertically upward through the staircases. Near 186 m depth, the 2012 profile lacks the double diffusive steps seen in 2011. The steps between 175 m and 190 m (within the upper pycnocline) became narrower, had reduced temperature gradients, and the total number of steps declined between January 2011 and February 2012. This suggests regional mixing, possibly caused by sub-surface inflows closer to the shoreline. Just above the primary pycnocline between 235 and 255 m, the staircases are absent, which is assumed due to the sub-surface inflows which reach their isopycnal depth and spread out laterally in this depth region (Figure 5.2). Between 295 m and 305 m, steps have become weaker and fewer well defined steps exist. Steps that exist in the 2011 profiles between 316 m and 318 m disappeared in February 2012. Between 336 m and 340 m, the staircases vary in strength between profiles. Variations on a shorter time scale exist at both the same location and laterally across the lake, showing small scale

changes in the stair-case structures. For instance, comparisons between the two Master Station profiles (CTD1 and CTD7) reveal both the development of new steps (286 m and 290 m) and the loss of steps (at 307 m and 313 m).

The variability seen in the steps suggest active processes in the water column, which may indicate minor convection in regions. Variability is also an indication that the steps may only be intermittent, forming and disappearing at various locations as heat and dissolved substances are transported through the water column. As the water column is not in a steady state, some assumptions made in modeling of the water column by past reports (Schmid et al., 2005) may not be accurate.

As the steps are observed over years throughout different seasons in the same depth regions, large scale turbulent mixing is assumed to be minimal in the regions where double-diffusive staircases are observed. If turbulence was not minimal, these small-scale staircases would be destroyed and continuous observation of them over longer time periods would not be possible. Turbulent mixing within the individual small-scale staircases is significantly enhanced compared to within a system which has the same temperature and salinity gradients but over a more continuous, smooth transition ?. This results due to the well mixed small-scale staircases, and thus works toward maintaining the overall stratification of the water column, as diapycnal transport between the strong gradients at the staircase boundaries will be nearly molecular for both heat and salts (Schmid et al., 2010). With molecular transport of heat being on the order of 100 times that of both salts and gases (Denny, 1993; ?), the double-diffusive staircases help maintain the stratification of the water column by removing the destabilizing aspect (the heat) of the water column toward the surface faster than the stabilizing salts. On the other hand, above the region of these staircases, mixing is dominated by turbulent

diffusivity.

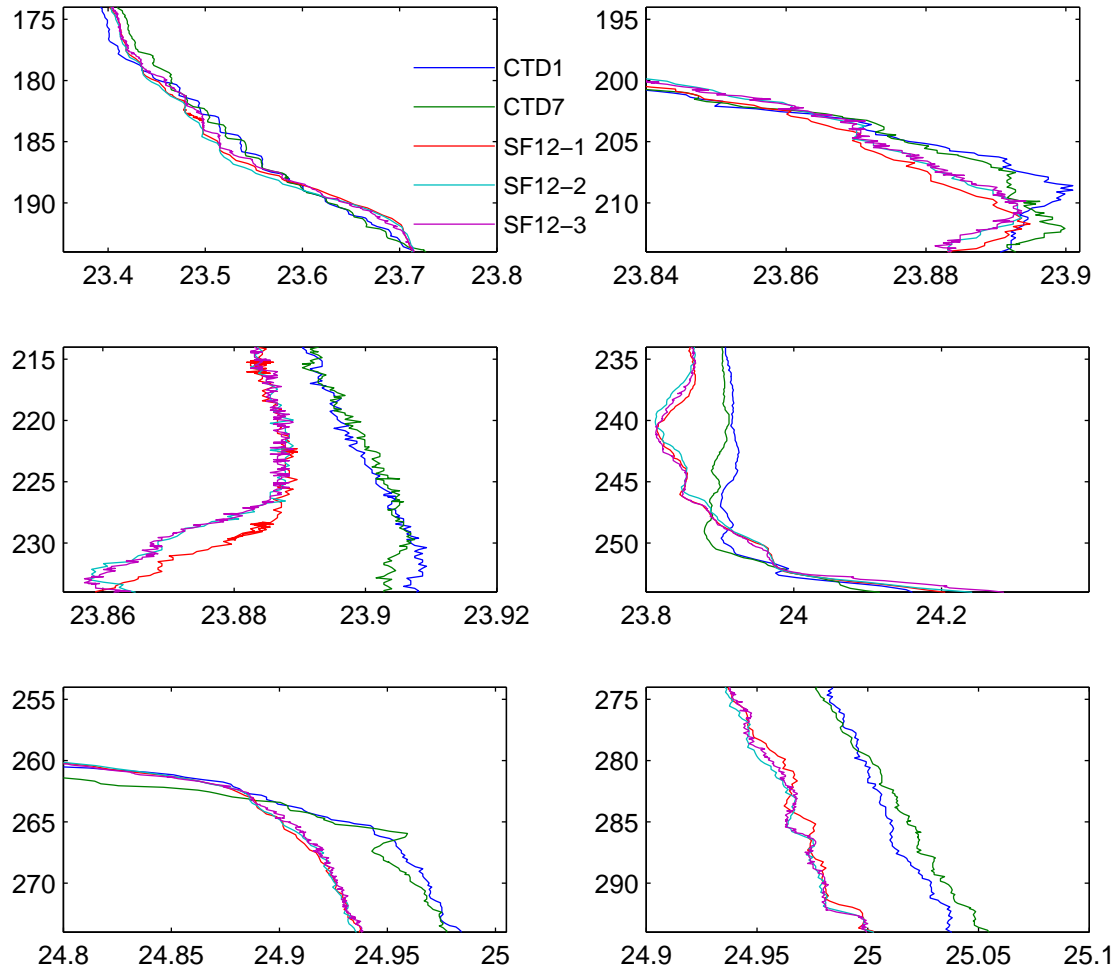


Figure 5.5: Double Diffusive steps seen in Lake Kivu in January 2011. Between profiles it is clear that small variations exist in the location of the steps. Also, the steps appear to both strengthen and weaken to the point of disappearing over time.

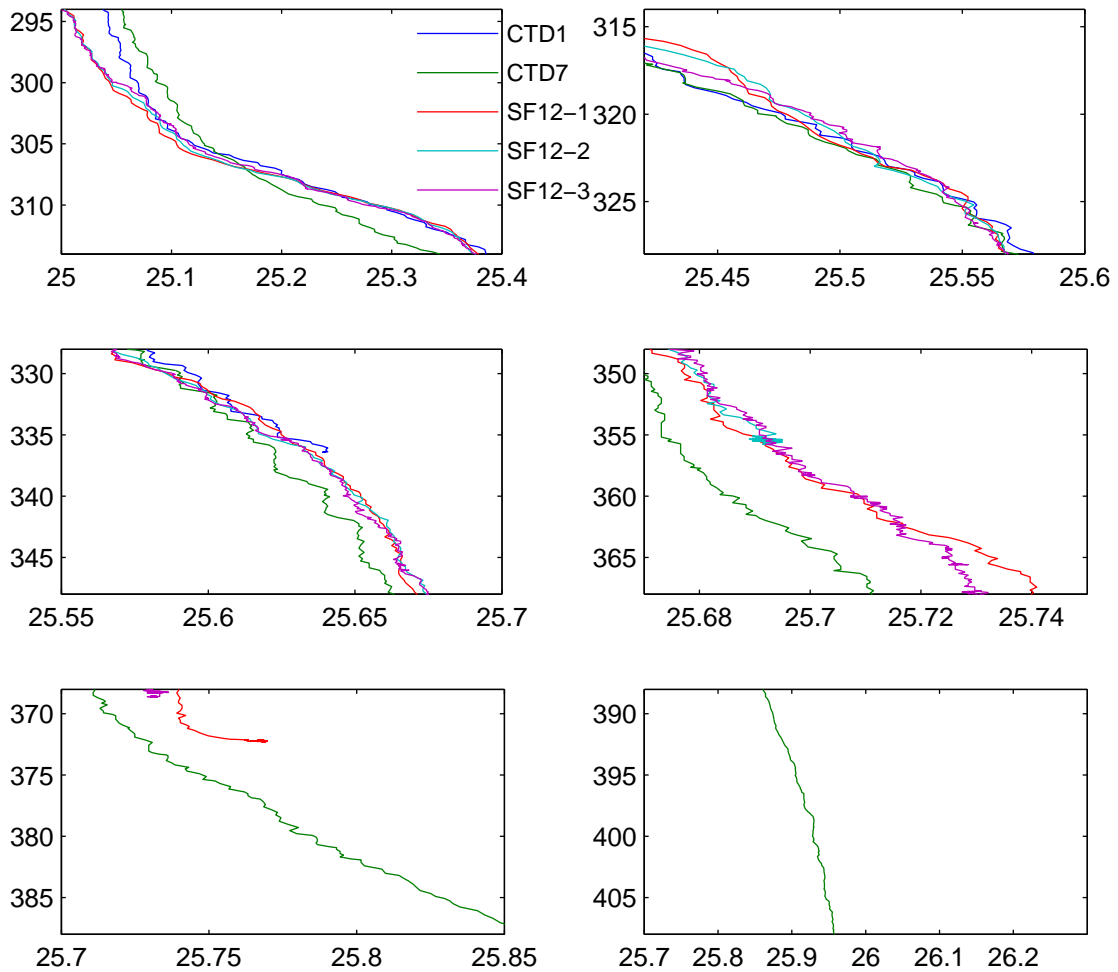


Figure 5.6: Same as in previous figure over a different range of depths

5.4.1 Variability in the depth of temperature inversion

The depth of the temperature inversion increases with time (Figure 5.4). In January 2011, this depth was 78.3 ± 0.97 m, approximately the same depth as in February 2002 (Lorke et al., 2004), but shallower than in figure 2 of Schmid et al. (2002), which indicates the depth to be 84.2 m in February of 2004. In February 2012, the temperature

inversion deepened to $82.6 \text{ m} \pm 1.1 \text{ m}$. These depths are significantly greater than in the historical profiles available from the 1970's (Tietze, 1978; Newman, 1976) and the 1930's (Damas, 1937), where the depth of the temperature inversion was over 20 m shallower, between 53 m and 57 m, near the present-day mixing depth. Schmid and Wüest (2012) note similar trends in the depth of the temperature inversion in their 2002–2007 profiles; they observed that between 2002 and 2007 a deepening of the temperature inversion occurred, which shallowed in 2008 to around 65 meters (i.e. within the possible mixing zone).

The seasonal variation in the depth of the temperature inversion is due to vertical changes in its depth, not an effect of internal waves. The magnitudes of internal waves in our profiles were on the order of 1–2 meters near the temperature inversion in both the January 2011 profiles and the February 2012 profiles. The changes in the temperature inversion depth are significantly greater than this. The significantly greater changes in the depth of temperature inversion observed thus require changes to the heat fluxes to the temperature inversion. Downward heat fluxes to the temperature inversion are caused by variability in the seasonal mixing depth, which is affected primarily by meteorological conditions during the dry season. During years with shallower mixing events, the surface waters warm more than waters near the temperature inversion. This causes a strengthening of the temperature gradient above the temperature inversion, resulting in an increase in the downward diffusion of heat and an apparent deepening of the temperature inversion. A gradual downward shift in the depth of the temperature minimum results as deeper water temperatures match those at slightly shallower depths (i.e. the depth of the previous minimum). On the other hand, during years with stronger winds and clearer skies (i.e. less downward atmospheric radiation that results in less warming

of surface waters), a reduction in downward heat flux occurs and a deep mixing event may be likely. This results in a shallowing of the temperature inversion depth as warming of the waters at the temperature minimum is dominated by upward fluxes of heat. Shallowing of the temperature inversion may be of greater magnitude if winds are able to cause a deeper mixing event to occur (i.e. to below the base of the mixed surface waters of approximately 55 m), as some excess heat at the depth of mixing will be removed to the surface. As this heat is removed, further cooling will result, reducing downward fluxes toward the temperature inversion. Mixing to depths below 55 m requires enough surface input energy by the wind to overcome the high stability of the water column caused by the large salinity gradient beginning at 55 m; this energy is discussed further in section 5.5. From comparisons of historical and current temperature profiles (Figure ??), clear variation in the depth of the temperature inversion up to more than 20 m can occur from one year to another year; however, changes during this study appear closer to 5–10 m.

If variability in surface warming rates and episodic deep mixing events were not the cause of the variability in the temperature inversion's depth, a heat sink (e.g. cool inflow) would have to exist at the temperature minimum depth to account for the the temperature inversion. As the isopycnal depth of such a sink would not be likely to vary significantly, a more constant depth of the temperature inversion would be observed. Analysis of our temperature profiles near the shoreline does not indicate the presence of subsurface inflows near the temperature inversion depth; detailed profiling done by Schmid et al. (2010) did not detect such an inflow either. Differences in the depth of various pycnoclines and the temperature inversion between locations where profiles are

taken across the lake may exist due to a combination of seiches and internal waves. However, observed variability in depths indicate only minor variability (over days) due to the location of sampling (Figure 4.1).

As the depth of the temperature inversion has deepened since the 1970's, mixing to the depth of temperature inversion is more difficult. This results in less heat being removed from the water column and the possibility that the warming rates throughout the water column could accelerate.

5.4.2 Temperature and energy conservation requirements at and above the temperature inversion depth

As energy conservation indicates that the temperature at the inversion depth must be increasing, the expected rate of warming due to the present-day heat fluxes can be calculated. In the region near the temperature inversion, vertical heat transport rates can be assumed to be primarily due to turbulent diffusion. The values of turbulent eddy diffusivity, K_z , used to estimate the dry-season mixing near the inversion were found by linear interpolation of the coefficients listed in Table 5.2. The heat flux (Φ_H) at a given depth was then determined from Fick's first law of diffusion:

$$\Phi_H = -K_z \frac{\partial T}{\partial Z} c_w \rho_w$$

where T is the temperature profile smoothed to a 0.5 m resolution, c_w , the specific heat of water, taken to be $4181 \text{ J kg}^{-1} \text{ K}^{-1}$ at the average density of the water column in the region near the temperature inversion ($\rho_w = 998.5 \text{ kg m}^{-3}$). The warming rate was then

found from Fick's second law as:

$$\frac{\partial T}{\partial t} = -\frac{1}{\rho c_w} \frac{\partial \Phi_H}{\partial Z}$$

The inversion depth in any given profile was taken as the depth where the flux crossed 0 W m^{-2} . An example of this calculation performed on the temperature profile CTD7 is shown in Figure 5.7. The average value for the expected warming rate computed with this method for all of the January 2011 and February 2012 profiles yielded the heat gain rate at the temperature inversion of $0.0018 \text{ W m}^{-3}\text{s}^{-1}$. This rate over the course of 1 year yields a 0.014°C rise in temperature, or equivalently the 0.14°C per decade, which matches the warming rate seen from temperature profiles. The agreement suggests the absence of a cool inflow at the depth of the temperature inversion, in agreement with the lack of evidence for inflows from near-shore profiles.

Table 5.2 Kz-values used to calculate heat fluxes required for energy conservation in Lake Kivu, based on Table 2 of Pasche et al. (2009).

Depth [m]	$k_z [\text{m}^2\text{s}^{-1}]$
60	$1.8 \cdot 10^{-6}$
110	$0.2 \cdot 10^{-6}$
115	$1.3 \cdot 10^{-7}$
155	$4.9 \cdot 10^{-8}$
255	$1.6 \cdot 10^{-8}$
261	$1.4 \cdot 10^{-8}$
270	$5.2 \cdot 10^{-8}$
440	$1.0 \cdot 10^{-8}$

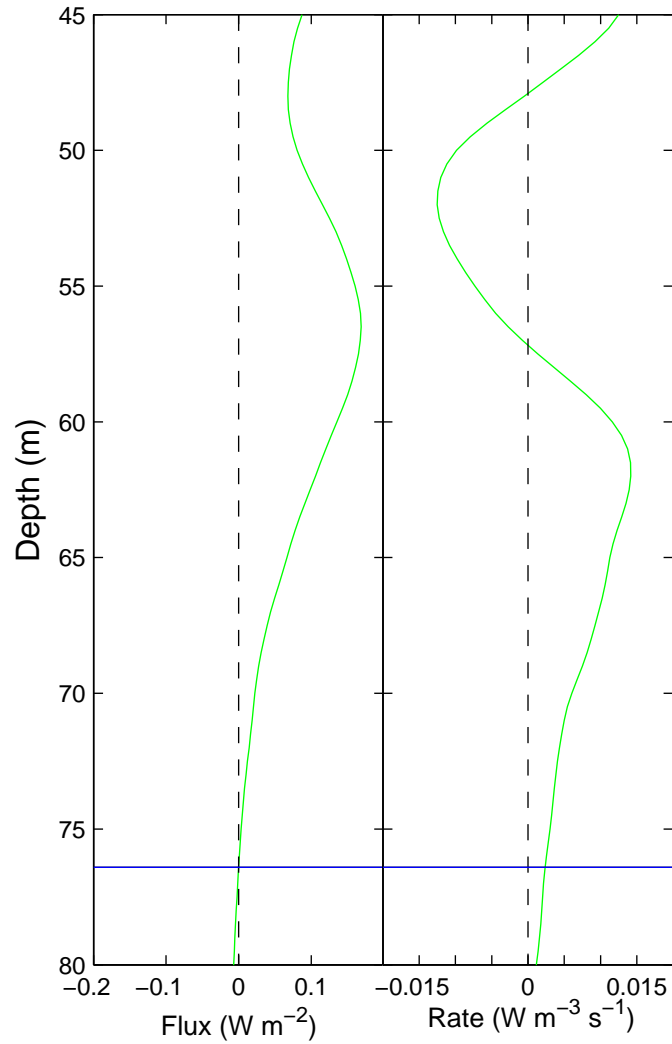


Figure 5.7: An example of the heat flux calculation performed to determine the expected warming rate based on the temperature profile of CTD7. The horizontal line (at 76.4 m) shows the depth at which the heat flux crossed zero (and the associated heat gain rate) which corresponds to the depth the temperature inversion.

5.5 Stability of the Water Column

Stability as a physical quantity characterizes the resistance of the water column to mixing. It can be defined as the energy required to homogenize the water column to a given depth (Wetzel and Likens, 2000; Hutchinson, 1975), which effectively requires the center of gravity to be raised:

$$S = \frac{1}{A_0} \int_{z_0}^{z_m} A_z (z - z_g) \cdot (\rho_z - \rho_m) dx \quad (5.1)$$

where A_0 is the surface area of the lake, z_0 is the lake surface height, z_m is the maximum mixing depth, $z_g = \frac{1}{V} \int_{z_0}^{z_m} z \cdot A_z dx$ is the center of gravity depth, and $\rho_m = \frac{1}{V} \int_{z_0}^{z_m} \rho_z \cdot A_z dx$ is the density when mixed, with ρ_z the density at depth z dependent on other factors (see section 3.2.2).

Energy input to the lake surface to cause mixing was assumed to be due to winds, which produce waves that impart energy into the water column and facilitate mixing. Potential depths of wind mixing were determined based on the wave heights relationship to wind speeds. Wave height allows for estimates of energy contained in the wave. The energy contained in waves was assumed to be equally split into potential and kinetic energy (Phillips, 1977). Estimates of necessary wind speeds to create the required wave height magnitudes were made using an approximation from the Institution of Civil Engineers (1996):

$$H_s = \frac{U F^{0.5}}{1760} \quad (5.2)$$

where H_s is the significant wave height in meters that the mixing energies are associated with, U is the continuous wind speed in m s^{-1} , and F is the uninterrupted fetch.

Equation 5.2 is plotted with associated wave energies in Figure ?? in meters. This approximation to available mixing energy was then used to determine the mixing depth based on the stability energy (Equation 5.1).

Calculations using Equation 5.1 and CTD profiles CTD1, CTD7, and Feb12 show that in Lake Kivu winds are able to mix the water column to a depth of around 50 m (Figure 5.8). Consistent with the results of typical wind speeds during the dry season, mixing extended to 50 – 55 m (Figure 4.7). Homogenizing to 50 m requires an input of $\sim 0.9 \text{ kJ m}^{-2}$ from the wind (which corresponds to wave heights of 0.65 m; this also corresponds to sustained winds of $\sim 5 \text{ m s}^{-1}$). However, mixing down to the seasonal thermocline between 30 m and 40 m depth only requires 0.46 kJ m^{-2} , equivalent to an average wave height of 0.3 m. Once homogenized down to 35 m, the energy required to homogenize deeper is reduced significantly. Energy inputs required to mix to 60 m, 80 m, and 90 m in January 2011 were 1.48 kJ m^{-2} , 3.78 kJ m^{-2} , and 5.90 kJ m^{-2} . Mixing energies requirements once the upper 35 m was already homogenized by mid-June to July at these same depths were 0.23 kJ m^{-2} , 1.83 kJ m^{-2} , and 3.57 kJ m^{-2} , respectively. The corresponding wave heights and sustained wind speeds to produce these mixing energies are 0.17 m ($\sim 2 \text{ m s}^{-1}$), 1.10 m ($\sim 8 \text{ m s}^{-1}$), and 2.15 m ($\sim 15 \text{ m s}^{-1}$), respectively. Using Equation 5.2 to calculate approximate wave heights suggests sustained winds on the order of $9\text{--}10 \text{ m s}^{-1}$ would be required for mixing to depths of 80 m. Analysis of wind records available online (MundoManz, 2006–2013) confirm such winds are possible, occurring occasionally, but not often. Typical wind speed maxima are on the order of $5\text{--}6 \text{ m s}^{-1}$, which are capable of producing waves on the order of 0.8 to 1 meter when blowing for several hours. Winds at $9\text{--}10 \text{ m s}^{-1}$ may cause mixing to near 80 m, as an event that Schmid and Wüest (2012) suggested for 2007. To mix to a depth below 80

meters, however, requires very strong winds (greater than $\sim 15 \text{ m s}^{-1}$) to blow continuously for an extended period of time. The significant increase in energy required for mixing to deeper depths is due to the large salinity gradient occurring between 55 m and 120 m. Based on the available wind data, mixing to depths around 90 m is not expected to occur regularly, although such deep mixing cannot be excluded. To further quantify whether episodic mixing to depths of 80 – 90 m is possible during the dry season requires monitoring the weather patterns on the lake surface, as Lake Kivu is located in a valley surrounded by several mountain chains that may limit the wind speeds. Currently available weather stations are located several kilometers away from the lake shore at airports of higher elevation and the data from those stations was used as an assumption for the potential mixing depths.

In the case where winds are not capable of mixing the water column to the temperature inversion, the depth of the temperature inversion can still rise. This can happen if the surface waters mix to the depth of the first salinity gradient and remain mixed to that depth for an extended period due to winds and cooler temperatures. In this case, the water below the temperature inversion will warm from the upward heat fluxes below. As this warming happens, the temperature inversion will appear to shift upward due to the waters below warming while the waters above remaining nearly unchanged. Dry seasons with higher wind speeds likely cause greater shifts in the depth of the temperature inversion to shallower waters, while years with average wind speeds during the dry season likely cause a deepening of the temperature inversion due to the increased downward heat fluxes. Higher downward heat fluxes will cause waters above the temperature inversion to warm more than waters below, causing a downward shift in the location of the temperature inversion. A combination of episodic mixing due to winds, increased

downward heat fluxes since the 1970's, and upward heat fluxes cause the current movement of the temperature inversion between ~65 m and 85 m depth.

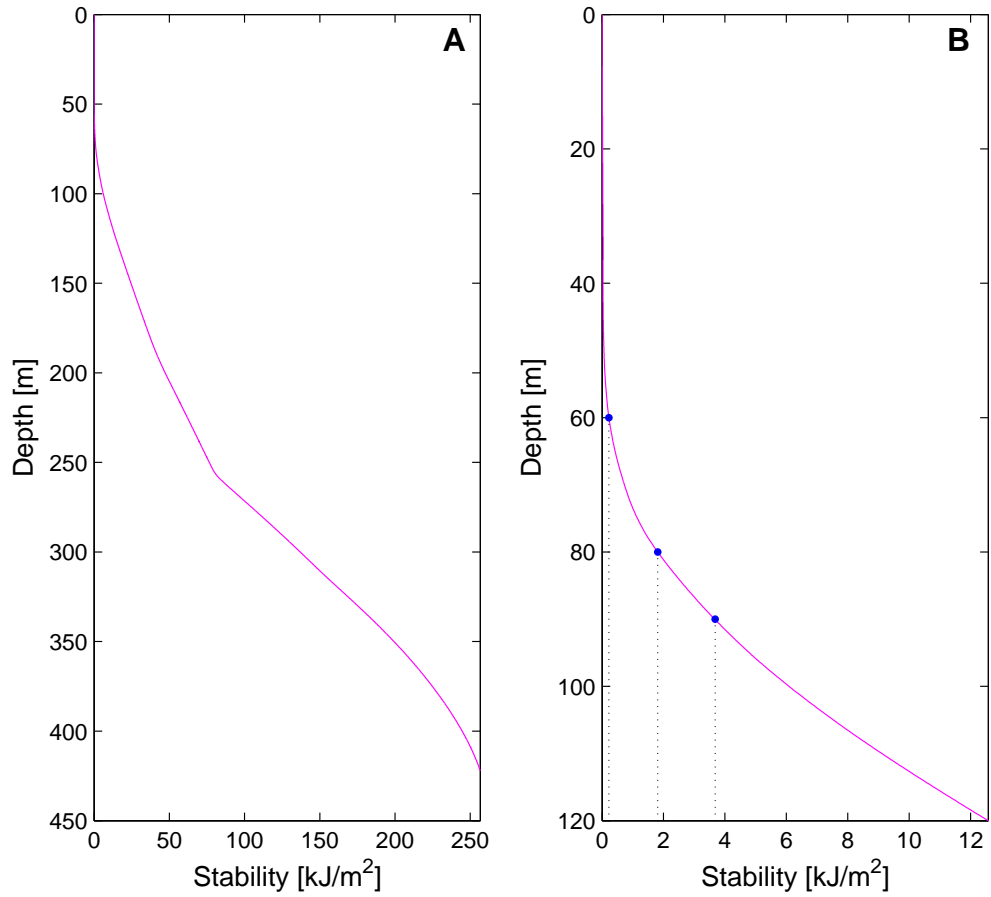


Figure 5.8: Stability (Equation 5.1), i.e. the energy input at the lake surface required to mix the water column to a given depth. Marked points are at 60 m, 80 m, and 90 m as references for proposed mixing depths from historical observations. Panel A shows the entire lake's required mixing energy based on an adjustment to profile CTD7 where the surface 35 m has been homogenized (i.e. representative of early dry season mixing). Panel B zooms in on the upper 120 m of Panel A.

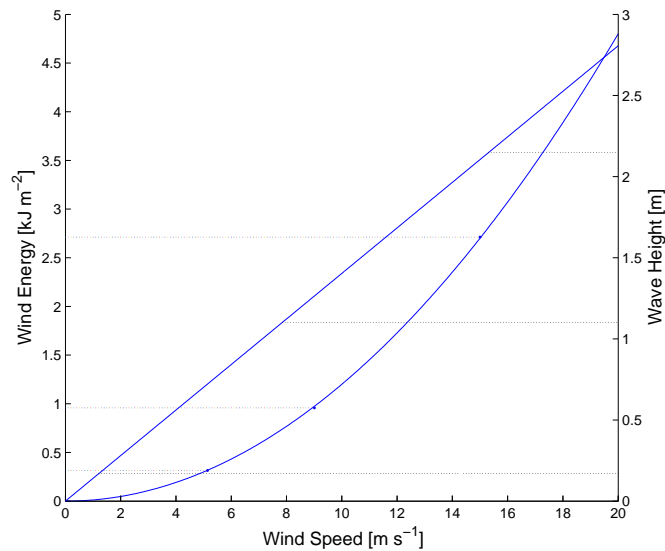


Figure 5.9: Wave height (Equation 5.2) produced by a given wind speed and the associated energy that can cause mixing of the water column. The dotted lines on the energy axis (left) correspond to the typical wind speeds in the region. The dotted lines on the wave height axis (right) correspond to the energies necessary to mix to 60, 80, and 90 m depth as found in Figure 5.8.

5.6 Local weather averages and heat budget

5.6.1 Weather averages in Lake Kivu region

Weather variability results in seasonal patterns to the depth of mixing from the surface down to between 50 m and the temperature inversion depth. Monthly averages of temperature, maximum temperature, minimum temperature, relative humidity, and average rainfall in the cities of Gisenyi(Goma) and Bukavu are listed in Table 5.4. Figure 19 shows the average maximum and minimum temperature, as well as average precipitation

by month in Gisenyi(Goma) and Bukavu. The monthly averages are over a 3 year period for all but the precipitation data for Bukavu, which is averaged over a 5 year period. These data suggest an average air temperature of ~ 19 °C during the year, in agreement with Borges 2006. Calculations using 19 °C for the surface air temperature were used to calculate an effective emissivity of the atmosphere in the heat budget calculations below. A global project effort by Berkeley Earth compiled the surface temperature data (Figure 5.11), which indicate approximately a 1 °C rise in temperature in Rwanda between the early 1970's and 2010. The data show the rate of air temperature increase from the early 1900's to the 1970's was lower than the rate of increase that has been observed since the 1970's. This suggests that increases in the surface water temperatures of Kivu may be greater between the 1970's and today than between the earliest measurements in the 1930's and the 1970's. As a result of the increased downward heat flux, a deepening of the stable depth for the temperature inversion may have occurred.

5.6.2 Components of the Heat Budget for Lake Kivu

The combination of heat gains and losses at the surface of Lake Kivu results in a relatively balanced net flux of $\sim 9 \pm 35$ W m⁻² (Table 5.3). Heat gains come primarily from the downward solar radiation and longwave atmospheric radiation, but minor additions also come from catchment runoff water, precipitation directly to the surface, and heat conduction to/from the sediments. Solar radiation contributes between 1900 kWh m⁻² and 2100 kWh m⁻² as a daily 24-hour average (Sol, 2011), which corresponds to values of 217 W m⁻² and 240 W m⁻². These being typical upper and lower bounds measured

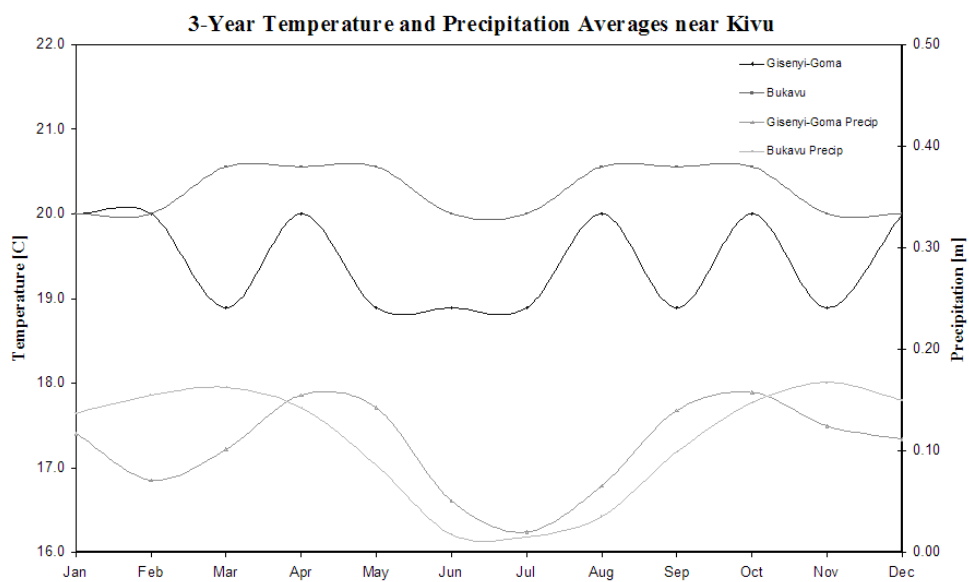


Figure 5.10: Monthly temperature and precipitation averages compiled over a 3 year period near the major cities of Gisenyi/Goma and Bukavu. Note the monthly precipitation average for Bukavu is over a 5 year period. The precipitation is the monthly total averages for that month, whereas the temperature is the average daily temperature for the entire month. These data were obtained from a compilation of various weather reporting websites (Online (2012); MundoManz (2006–2013)). The Gisenyi and Goma data are likely from the same station due to the proximity of the cities to one another.

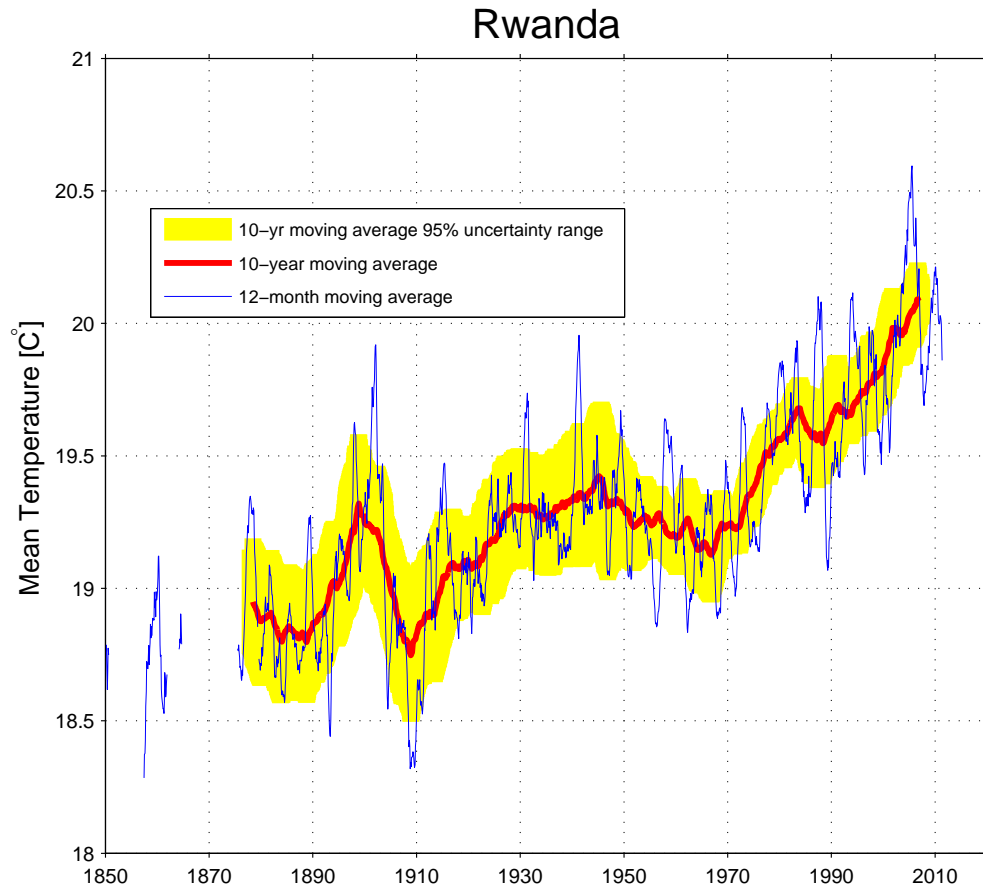


Figure 5.11: Plot of Berkeley Earth's effort to collect and determine century warming trends using available temperature data from various literature and operating weather collection sites.

in the Kivu region with variations due to cloud cover during the day. Only minor variability in solar radiation will exist over the course of the year as the latitude of Lake Kivu is only 2° south of the equator. These values account for the night time by using a 24-hour averaging. For the calculation of total heat income, we used the mid-range value of $228.5 \text{ W m}^{-2} \pm \sim 10 \text{ W m}^{-2}$. Contributions from atmospheric radiation based on current temperatures amounts to $\sim 327 \text{ W m}^{-2}$ (Equation 3.8). Temperature variations over the course of the year result in fluctuations in the the atmospheric radiation flux of $\sim \pm 5 \text{ W m}^{-2}$. Losses of heat consist of the lake surface's outgoing longwave radiation, sensible heat loss, evaporation, and cooler surface inflow streams and rainfall. Losses due to sensible radiation will vary with the season and wind speeds, having larger values during times of higher wind speeds. The values reported, however, are based on average wind speed during the year rather than during specific seasons. Calculations of sensible radiation losses made using equation 3.10 are between 5 W m^{-2} and 10 W m^{-2} . Losses due to the blackbody radiation from the lake surface are on the order of 430 W m^{-2} (Equation 3.7). Evaporative cooling (Equation 3.6) compensates for the majority of the remaining flux, having an effect of about -112 W m^{-2} . Combining these losses and gains suggest a positive flux of approximately $\sim 9 \text{ W m}^{-2}$, with a rather large uncertainty due to the variability in each of the contributing components. Due to the large range, a balanced budget is possible. These results are summarized in Table 5.3.

The advective inputs into and out of the lake surface contribute minimally to the heat budget in comparison to the other sources. The inputs consist of riverine inflows directly into the surface water of the lake and subsurface groundwater inflows which settle at various isopycnal depths based on their composition and temperature. The effect of outside stream inputs into a lake may vary depending on the inflow rates and the temperature

Table 5.3 Heat fluxes across the surface of Lake Kivu.

Heat Source	Value (W m^{-2})	Uncertainty
Energy Gain from Solar Radiation*	228.5	± 10
Energy Lost to Evaporation	-111.5	± 12.2
Blackbody Loss from lake surface	-427	± 4.7
Blackbody gain from atmosphere	327	± 5
Energy Loss from Sensible Radiation**	-7	± 2.5
Energy Loss to precipitation and runoff	-1.4	± 0.68
Totals:	~ 8.6	$\pm \sim 35$

* Based on an average Solar Radiation of SolarGIS online data

** Based on wind speeds of 1.5 m/s and 3 m/s respectively

of these inflows. Similarly, groundwater inflows may affect the heat budget of a lake if the temperature of the inflows is different than that of the water at the depth where the inflow enters. Based on the typical surface inflows into Lake Kivu as quantified by Muvundja et al. (2009), calculation of the heat budget contribution shows the effect of these surface streams is minimal (both under the assumption that all streams are at the minimum and maximum measured stream temperature). Sampling done at 127 of the in-flowing streams in the Bukavu and Kalehe basins (Muvundja et al., 2009) yielded a temperature range for the surface inflows between 18.0 ± 0.8 and 22.4 ± 2.6 °C, having an average value of 20.5 °C (Muvundja et al., 2009). Calculations using these extremums for the river inflow effects on the heat budget (equation 3.6) yield -0.81 W m^{-2} and -0.23 W m^{-2} under the assumption of a 23 °C surface water temperature. Similarly, rainfall contributions to the heat budget (Equation 3.6) yield $\sim -0.9 \text{ W m}^{-2}$ under the assumption that the rain water is at the average air temperature (19 – 20°C).

Average	Unit	Year	Jan	Feb	Mar	Apr	May	Jun	Jul	Aug	Sep	Oct	Nov	Dec
Temperature (3 yrs.)	°C	18.9	20.0	20.0	18.9	20.0	18.9	18.9	18.9	20.0	18.9	20.0	18.9	20.0
Bukavu		20.6	20.0	20.0	20.6	20.6	20.6	20.0	20.0	20.6	20.6	20.6	20.0	20.0
Goma		18.9	20.0	20.0	18.9	20.0	18.9	18.9	18.9	20.0	18.9	20.0	18.9	20.0
High temperature (3 yrs.)	°C	25.6	25.6	25.6	25.6	25.0	25.0	25.0	25.6	25.6	25.6	25.6	25.0	25.6
Bukavu		25.6	25.6	25.6	25.6	25.6	25.6	25.6	26.7	27.8	26.7	26.7	25.0	25.6
Goma		25.6	25.6	25.6	25.6	25.0	25.0	25.0	25.6	25.6	25.6	25.6	25.0	25.6
Low temperature (3 yrs.)	°C	13.9	13.9	15.0	11.7	15.0	13.9	13.9	12.8	13.9	13.9	13.9	13.9	13.9
Bukavu		15.0	15.0	15.0	15.6	15.6	15.6	13.9	13.9	13.9	15.0	15.6	15.0	15.0
Goma		13.9	13.9	15.0	11.7	15.0	13.9	13.9	12.8	13.9	13.9	13.9	13.9	13.9
Relative humidity (3 yrs.)	%	70	70	71	72	76	74	68	63	61	68	67	73	71
Bukavu		76	77	79	82	83	81	76	64	60	70	75	84	81
Goma		70	70	71	72	76	74	68	63	61	68	67	73	71
Precipitation (5 yrs.)	m	1.26	0.12	0.07	0.10	0.15	0.14	0.05	0.02	0.07	0.14	0.16	0.12	0.11
Bukavu (20 yr.avg)		1.31	0.14	0.15	0.16	0.14	0.09	0.02	0.02	0.04	0.10	0.15	0.17	0.15
Goma		1.26	0.12	0.07	0.10	0.15	0.14	0.05	0.02	0.07	0.14	0.16	0.12	0.11
Dew point (3 yrs.)	°C	13.9	13.9	15.0	13.9	15.6	15.0	12.8	11.7	11.7	13.9	13.9	13.9	13.9
Bukavu		15.6	15.6	15.6	16.7	16.7	16.7	15.0	11.7	11.7	15.0	15.6	16.7	16.7
Goma		13.9	13.9	15.0	13.9	15.6	15.0	12.8	11.7	11.7	13.9	13.9	13.9	13.9

Table 5.4 Monthly averages of temperature (°C), maximum and minimum temperature (°C), Rainfall (m), and Relative Humidity (%) in the lakeshore cities of Gisenyi/Goma and Bukavu. These data were obtained and compiled from various online weather reporting sources, some with slightly varying data. Much of the available Goma, DRC and Gisenyi, Rwanda data appear to be taken from the same station likely due to the proximity of the two cities to each other.

We estimate the increase in downward atmospheric blackbody radiation caused by the increasing air temperatures at $\sim 6.7 \text{ W m}^{-2}$ since the mid-1970's. Using the coefficient for emissivity of C_e of $0.937 \cdot 10^{-5} \text{ }^\circ\text{C}^{-2}$ (Blanc, 1985) in Equation 3.9 results in an emissivity of $\varepsilon = 0.794$ for near-surface air temperatures. The Stefan-Boltzmann law (Equation 3.8) with this emissivity gives the atmospheric long-wave heat flux into the lake of 320.4 W m^{-2} . Typical estimates for regional air temperature increases in East Africa are between 0.8 and $1.6 \text{ }^\circ\text{C}$ (Verburg and Hecky, 2009) since the 1970's. For a $1 \text{ }^\circ\text{C}$ air temperature increase, the emissivity coefficient is 0.800 , and the irradiance is 327.0 W m^{-2} . The 6.7 W m^{-2} increase in irradiance for one degree increase in air temperature is close to the estimated excess heat flux across the lake surface (Table 5.3). The excess flux of energy into the lake must be reflected in the lake temperature above the temperature inversion. Higher wind speeds and less rain may limit the warming via episodic mixing events, increased evaporative cooling, and higher sensible heat losses.

Often heat budget analyses neglect the effects of heat exchanges with the lake floor, heating/cooling due to chemical and biological processes, and kinetic energy dissipation, assuming their effects small (on the order of errors in other factors (Saur and Anderson, 1956)). For Lake Kivu, however, the effects of the heating from within and below are not negligible, as indicated by the warming in the deep water discussed in section 5.1 and seen in Figure 5.2.

5.7 Pycnocline movements

5.7.1 Historical comparisons indicate vertical movement in the boundaries of the pycnoclines

Comparison of the 2011 and 2012 temperature and conductivity profiles with the 1970's data indicates a shift in the vertical position of the pycnoclines (Table 4.1). Figure 5.14 indicates that below 225 m the lower pycnocline boundaries rose resulting in thinner pycnoclines and a strengthening of the density gradient due to the now thinner pycnoclines.

The change since the 1970's is significant. Figures 5.2 and 5.3 show the temperature profile comparisons, while Figure 5.15 shows the conductivity comparisons, both indicating the same changes in the depths of the pycnocline boundaries. Movements of the primary pycnocline's upper boundary is on the order of 4–5 meters and lower boundary close to 24 meters between the 1974 profile and 2011. Differences from the 2002 profiles of Lorke et al. (2004) indicates a rise of 2–3 m. The lower boundary of the lower pycnocline (~ 331 m) has risen by ~ 17 meters, with only small movements in the upper boundary. The 2–3 m differences seen between the 2002 depths and our current measurements are likely accounted for by internal waves. The density gradient at the upper pycnocline has remained unchanged compared to the 1970's profiles, despite the overall rise of the pycnocline. These boundaries have been classified based on the intersection of lines drawn tangent to the profile of conductivity at the middle of the gradient with lines drawn tangent to the steepest gradient in the mixed regions above and below the respective pycnocline (see example in Figure 5.12). Data of Tietze (1978) reveal the

upper pycnocline centered at 200 m depth with an upper boundary at 179 m and a lower boundary at 219 m for a thickness of 40 m. Our January 2011 data show the thickness of this pycnocline to be 39 m, i.e. virtually unchanged given the internal wave magnitudes at this depth range. The boundaries for this upper pycnocline are now at 202 m and 163 m, 17 m shallower and 16 m shallower, respectively, than in the 1970s. Small digitizing errors may lead to 2 to 3 m uncertainty in these changes.

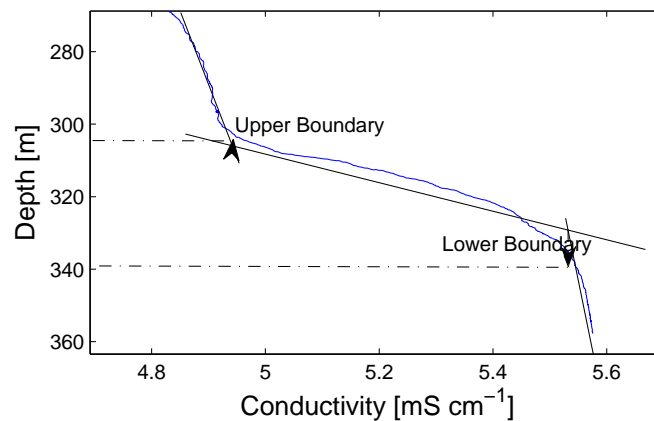


Figure 5.12: Example of the calculation for the boundaries of the pycnocline upper and lower boundaries

5.7.2 Temporal variability expected due to internal waves

Differences among the January 2011 conductivity profiles are ~ 0.01 mS cm⁻¹ in most of the the water column across the lake (Figure 4.10). Differences of 0.04–0.05 mS cm⁻¹ are observable at the major pycnoclines. The CTD conductivity sensor has an accuracy of 0.01 mS cm⁻¹ with a resolution of 0.002 mS cm⁻¹, indicating that the conductivity profile of the water column is laterally homogenized (i.e. deviations on the order of instrumental accuracy).

Variations near the pycnoclines (insets in Figure 5.13) suggest internal waves with amplitudes on the order of 2.5 to 3 m in the upper and primary pycnoclines. Near the depth of temperature inversion, the vertical variability suggests internal waves on the order of 1 to 2 m. As the lower pycnocline appears only in a single profile, internal waves there cannot be quantified. In the region at the base of the mixolimnion (i.e. 50 m depth), conductivity variations suggest internal waves on the order of 3 m.

The magnitude of internal waves vary with depth. Internal wave magnitudes are greater in waters near the primary pycnocline than near the upper pycnocline and surface. A baroclinic system explains this difference As Lake Kivu is split into multiple layers of different densities, separated by pycnoclines, waves are expected to be present at the pycnoclines. The solution to the governing equations of motion for a system with just two layers and a free surface has several special cases (Socolofsky and Jirka, 2004). With the densities at the boundary of two layers being nearly equal, Boussinesq waves can result, traveling much slower than surface waves due to the small difference in density between the two fluids. The two main solutions are the external mode and the internal mode. (Socolofsky and Jirka, 2004). The external mode has larger waves at the surface of the upper layer and the two layers travel in phase with each other as if unstratified. In the internal mode, the lower layer is out of phase with the surface layer, resulting in larger waves between the internal surfaces than at the free surface. The baroclinic mode in Lake Kivu can explain why the deeper boundary layers have larger internal waves. The magnitude of these waves may be smaller than in a simple two-layer system due to the water column having several layers, each introducing and additional adjustment to the phase and magnitude of waves at the pycnoclines.

Comparison of 2011 and 2012 conductivity profiles (Figure 4.11) reveals differences

on the order of 0.02 mS cm^{-1} over most of the water column. This is greater than the standard deviation observed laterally over the northern end of the lake and larger than the instrumental accuracy. As the January 2011 and February 2012 profiles were obtained with a different model CTD of the same manufacturer, this difference of 0.02 mS cm^{-1} likely reflects imperfect calibration of the CTDs rather than a real long-term trend for the conductivity profile.

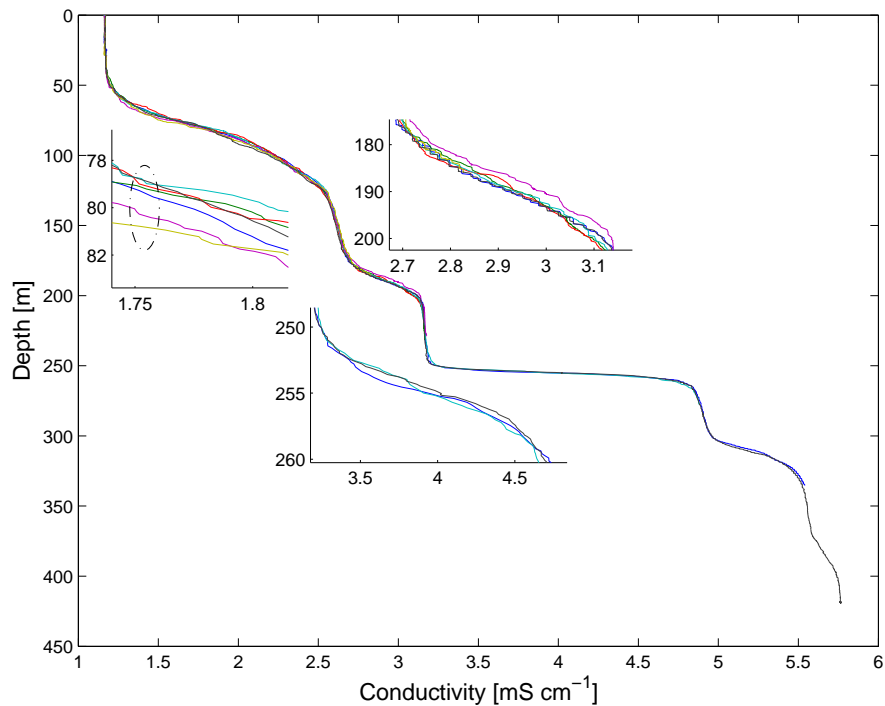


Figure 5.13: Conductivity profiles from January 2011 along the Kibuye transect and the Master Station. Insets zoom in on the regions of the upper and primary pycnocline and the temperature inversion depth (circled region) to better see the magnitude of internal waves.

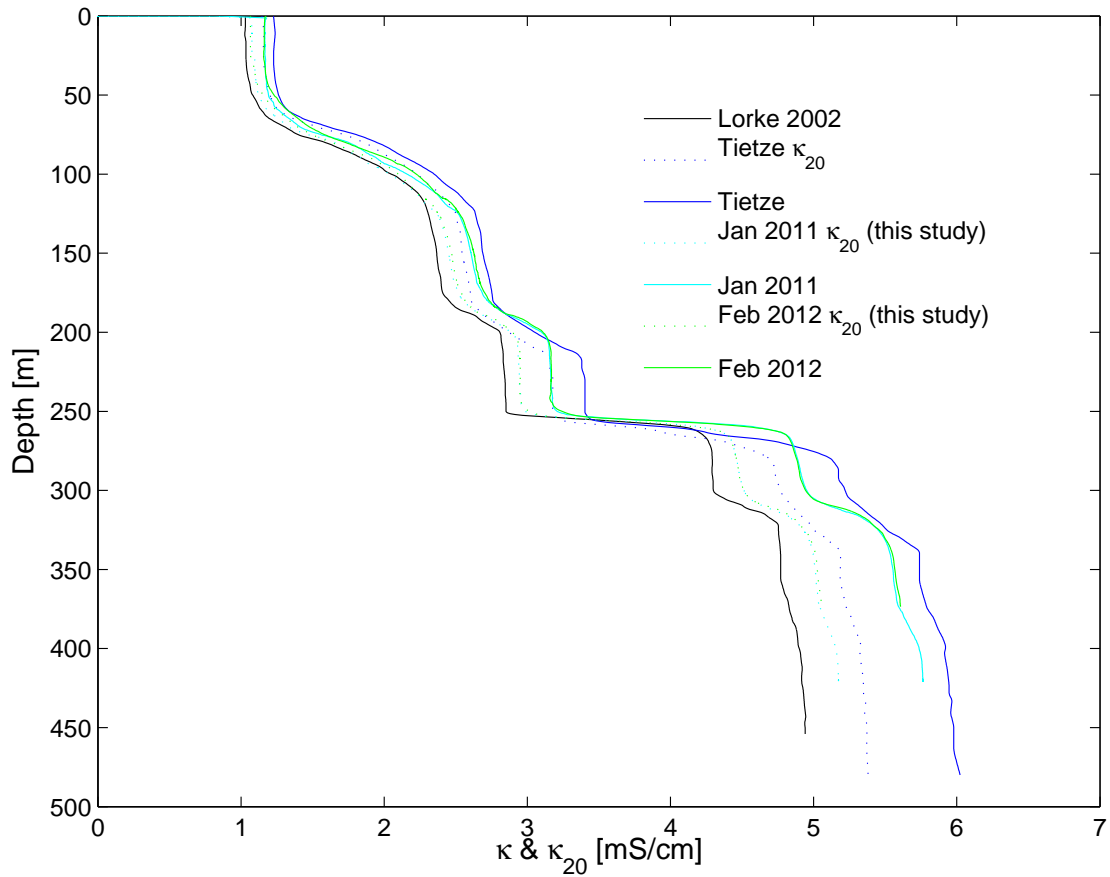


Figure 5.14: Comparison of in-situ and temperature-adjusted conductivity averages measured between 1973 and 1975 (Tietze (1978)), 2002 (Lorke et al. (2004)), January of 2011 and February of 2012. Small errors in depth on the order of 3 to 4 meters may exist due to digitizing errors of the historical profiles (1973-5 and 2002).

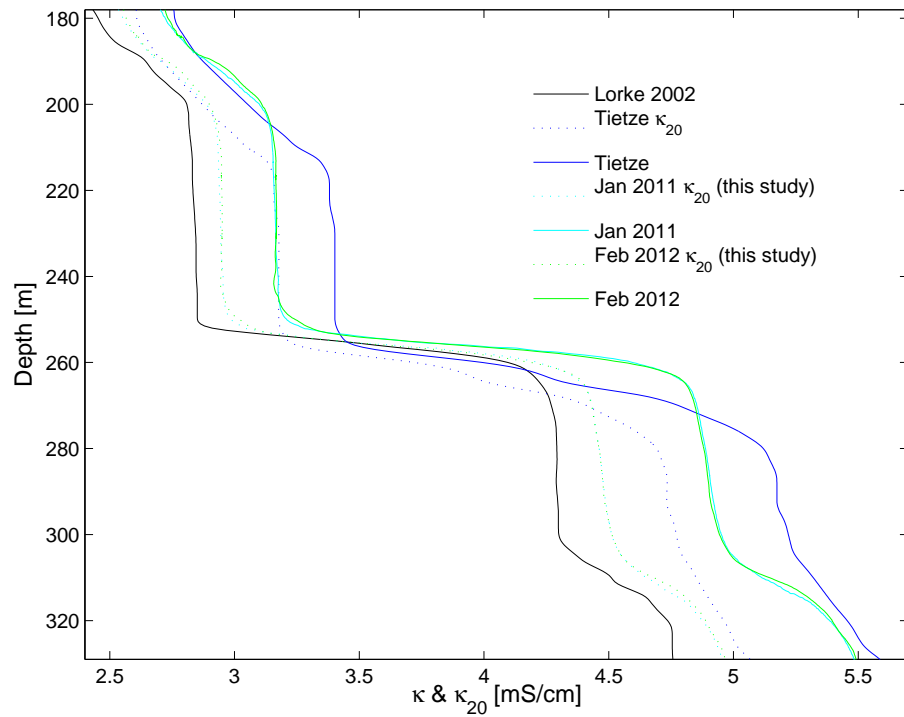


Figure 5.15: In-situ conductivity and temperature-corrected conductivity near the primary chemocline as measured between 1973 and 1975 (Tietze (1978)), 2002 (Lorke et al. (2004)), and in January 2011 and February 2012.

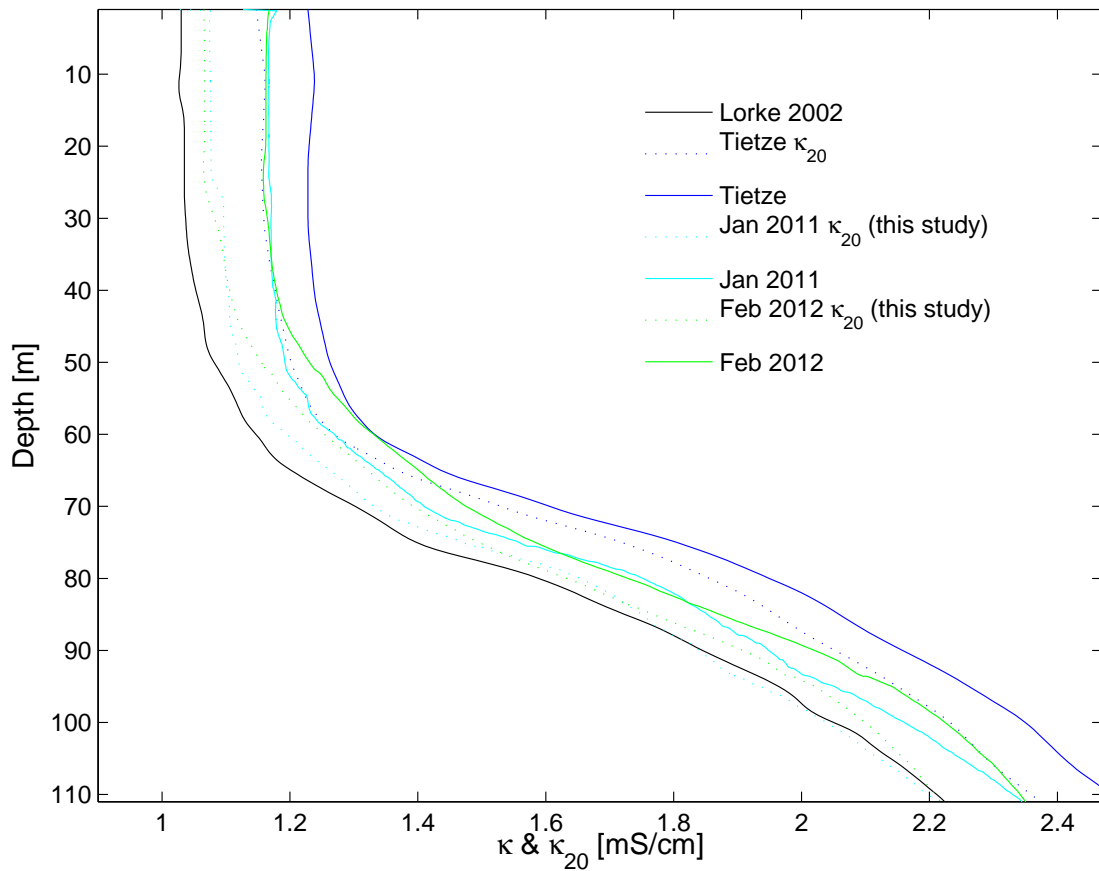


Figure 5.16: In-situ conductivity and temperature-corrected conductivity in the upper 100 meters of the water column measured between 1973 and 1975 (Tietze (1978)), 2002 (Lorke et al. (2004)), and January 2011 and February 2012.

5.8 Effects from conductivity and temperature of inflows

Subsurface inflows help to maintain the depths of the upper boundaries of the primary and lower pycnoclines in the water column. Conductivity and temperature profiles reveal the depths of subsurface inflows as mentioned in the results. As the signal from these inflows weakened as distance from the REC platform increased, the inflows are assumed to be localized primarily on the northern shore, as also found by Schmid et al. (2005). The inflows have excursions towards both lower temperature and lower conductivity (Figure 5.17). The negative excursions suggest the inflows are of less salinity than the lake water. The inflows that compose the signal at ~ 248 are the source for the negative excursion in temperature at the upper boundary of the primary pycnocline. As the inflow is also of lower conductivity than the lake water, it works to maintain the upper boundary of the primary pycnocline and leads to a strengthening of the gradient as the lower boundary with waters of higher conductivity rises due to inflows below the primary pycnocline. The inflows between the lower and primary pycnoclines (between 262 and 300 m) work in a similar way to maintain the upper boundary of the lower pycnocline (at a depth of about 301 m) and strengthen the gradient. Ascent of the upper pycnocline's boundaries discussed in section 5.7.1 may be due to inflows between the upper and primary pycnocline (i.e. inflows from $\sim 200 - 250$ m), which push the entire water column above that depth upwards. As the thickness of this pycnocline has remained unchanged, no significant inflows are expected to settle at their isopycnal depth near the boundaries of the pycnocline, unlike the primary and lower pycnocline. As the inflows are important for maintaining the current stratification of the water column, changes in the inflow properties may alter the location of the major pycnoclines and

therefore the stability of the water column.

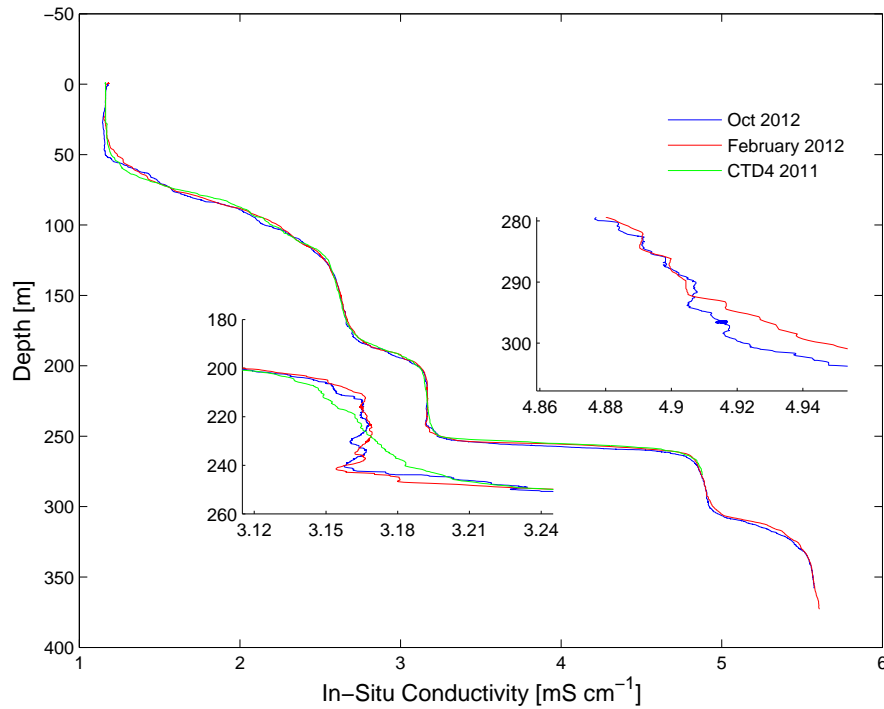


Figure 5.17: Conductivity profiles taken in February and October of 2012 from the REC platform. Insets zoom in on the negative excursions due to inflows near the upper boundaries of pycnoclines.

5.9 Gas Pressure Measurements in Silicone Tubing

Calibration plots (Figure 4.13) show that expansion volumes from silicone tubing samplers after thirty-five minutes of deployment in Lake Kivu correspond to partial gas pressures of ~ -0.81 dbar, ~ 1.03 dbar, and ~ 7.39 dbar at depths of 122 m, 130 m, and 138 m, respectively. These estimates are based on the extrapolation of the calibration conditions to the greater hydro-static pressures in Lake Kivu.

To determine accuracy of these estimates would require further testing of the samplers for known concentrations of CO₂ in the pressure chamber. Furthermore, the short deployment time in the lake was likely not long enough for the concentrations of gas in the tubes to reach equilibrium with partial pressures in the water, hence the low and even negative concentrations found. The flux of different gases through a membrane varies based on the coefficient of solubility and diffusion for the gas-membrane combination (Zhang and Cloud, 2006). For a silicone membrane, the diffusion coefficient for CO₂ and CH₄ are similar, however, the solubility of CO₂ is much higher than the solubility of CH₄ in silicone rubber (Zhang and Cloud, 2006). This means the concentration of CO₂ gas molecules in the silicone rubber is higher, leading to concentrations of CO₂ coming to equilibrium on the inside and outside of the samplers in a shorter period of time than for CH₄. Based on the overlay in Figure 4.14, the samplers may have had enough time for the CO₂ to come to equilibrium, as the estimated partial gas pressures are near the pressures of CO₂ shown in the figure of Schmid et al. (2005). However, the partial gas pressures due to CH₄ are 4 – 5 times that of CO₂ at the depths the silicone tubing samplers were deployed. As CH₄ requires more time for concentrations inside and outside the silicone samplers to reach equilibrium, and as the pressures found during the deployment time are close to the CO₂ pressures reported by Schmid et al. (2005), a longer deployment time is required to make accurate measurements of the partial gas pressure in the lake.

As the measurement of the obtained volumes depended on the stiffness of the syringes' plungers, an uncertainty in the obtained volume is estimated on the order of ~ 4 – 5 mL. This is based on the minor variability in the stiffness's between syringes of the same model used for calibration in lab. As a limited number of syringes of the same

model were available during field work, further uncertainty in the obtained volumes at 138 m depth may exist due to the uncalibrated syringes used on those samplers.

The pressure data in Figure 4.14 are within error of the concentrations measured by Schmid et al. (2005) for the depths sampled. Given these results under the windy conditions and waves the samplers were deployed during, it may be possible to develop this method as a useful gas-pressure measurement tool. As only four good pressure-volume calibrations points were obtained for the larger tubing used in Lake Kivu (Figure 4.13), the reported pressures have a large uncertainty (Table 4.2). A better set of calibration data is possible by making certain the water in the pressure chamber is saturated, and by replacing the water between trials. Furthermore, creating a finer resolution for pressures-volume measurements for calibration, along with a consistent deployment time in the pressure chamber would result in a better calibration data set. Use of the same syringe for all measurements, rather than different syringes on each tube, would also reduce variations in obtained volumes. A more reliable approach, however, would be to adapt a sensitive pressure gauge and connector piece on the tubing to replace the syringe and and luer stop-cocks. This would improve the consistency between tubing samplers and eliminate the problems that arise in the variations of syringe manufacturing. The method used on Lake Nyos to measure the partial gas pressure of CO₂ in the water at depth involved use of a pressure gauge connected to a long tube which connected to a series of silicone tubes placed at depth (Evans et al., 1993). Evans measurement required several hours for the gas pressures inside the tubing to be in equilibrium with the dissolved gas pressure, and the surface pressure measurement required an adjustment to match the pressure in the tubing at depth because of the weight of the gas in the long column.

5.10 Limnic eruptions in lab

Lack of pressure to dissolve significant quantities of CO₂ into the water was the primary issue with creating a small-scale limnic eruption. Pressure at depth in the water column of lakes where significant amounts of gases are dissolved are several atmospheres greater than the pressure either the large beaker or the plastic cylinder used in lab without a secured cap. During tubing calibration and development, the pressure chamber allowed significantly greater pressures in comparison to previous attempts with small scale eruption simulations. When pressure was relieved from the pressure chamber, bubbles formed and appeared as if a rolling boil of hot water was occurring until the partial gas pressure had dropped far enough to remain stable at atmospheric pressure. Once this exsolution of gases had happened, smaller bubbles continued to form and rise, just as in a carbonated beverage sitting in a glass, and similar to other trials in the limnic eruption tests described in section 4.7.

Keeping the gas in the layers of the water may also be an issue for shallow setups, as the diffusion of gas through the water column may be enough to dilute the concentrated CO₂ water being “piped” into the bottom of the water column and minor mixing between the warm upper water and incoming water .setup could be developed to pressurize the water column and effectively create a deeper layer of gas-rich water under a fresh warm water that remained well separated, one could potentially quickly drop the pressure to simulate a large disturbance in the water column and cause gaseous outbursts – the sort of behavior seen in shaken up soda bottle that are opened quickly, or that seen when the pressure chamber was opened.

The method of injecting hot water through the surface is not a reasonable approach,

as the narrow tube to the bottom allows the water to be cooled by surrounding water as it travels to the injection point. Further, the pressure forcing the water out of the syringe into the deep water caused a visually significant disturbance of the interface. This disturbance resulted in more mixing than desired or than would result from simply having a large quantity of hot water suddenly heat up the cool water. Also, the heat transfer required to heat the CO₂ water up enough to lose its gas-holding capacity is far greater than a small injection of hot water can provide under the pressures available in lab. As a result, the amount of gas able to remain dissolved in the water changed very little at low pressures used, and therefore provided very little exsolution of the dissolved gases in the short, non-violent bubbling periods.

6

Conclusions

- The temperature of Lake Kivu has risen throughout the entire water column since at least the mid-1970's.
- The temperature at the base of the mixolimnion at ~ 50 meters depth has risen by 0.75 °C since the 1970's (i.e. ~ 0.20 °C per decade). This rise in temperature is larger than that in other tropical lakes in the East African Rift system reported from 1993–2005: Lakes Malawi and Tanganyika having warmed by ~ 0.13 °C per decade in the surface waters near 50 meters depth.
- Temperature at the depth of the temperature inversion has risen since the mid-1970's by 0.5 °C. The average rate of the temperature increase is ~ 0.14 °C per decade. This matches the rate calculated based on the heat fluxes to the inversion (sec 5.1.1; 0.4 W m^{-2}). The warming rate matches that in surface waters in other tropical lakes. Occasional episodic mixing to the depth of the temperature inversion may occur, which would homogenize the temperature of the water column to

the inversion.

Warming from the atmosphere is the primary cause of warming down to the depth of the temperature inversion, with minor contributions from the upward flux of heat in the deep waters. As the warming rate matches the rate calculated from present-day vertical heat fluxes, there may not be a cool inflow near the temperature inversion depth. Waters in this depth region are therefore a good integrator of the heat fluxes received from both above and below.

- The warming rate observed above the temperature inversion at the base of the mixed layer (~ 50 m) in 2011 was 0.078 °C per year, based on the linear fit of the data recorded by the deepest two thermistors installed below the KP1 methane extraction platform. With episodic mixing to this depth, the effective warming rate indicated by comparisons of historical temperature profiles is ~ 0.20 °C per decade.
- Movement of the pycnocline boundaries (Table 4.1) has occurred. The upper pycnocline (currently 170 m – 202 m) has risen by ~ 16 meters and remained the same thickness as in the 1970's. The main pycnocline has been strengthened, with the upper boundary rising minimally and the lower boundary having risen ~ 24 meters from 286 meters to 262 meters. The lower pycnocline has similarly been strengthened with the upper boundary remaining relatively stationary (with perhaps 5 meters rise) while the lower boundary has risen ~ 17 meters.
- Lake Kivu cannot be considered to be in a steady state due to both upward motion of major pycnocline boundaries and increasing temperatures throughout the water

column.

Bibliography

<http://solargis.info/imaps>, June 2011.

- J. A. Austin and S. M. Colman. Lake superior summer water temperatures are increasing more rapidly than regional air temperatures: A positive ice-albedo feedback. *Geophysical Research Letters*, 34, March 2007. doi: 10.1029/2006GL029021.
- P.J. Baxter and M. Kapila. Acute health impacts of the gas release at Lake Nyos, Cameroon, 1986. *Journal of Volcanology and Geothermal Research*, 39:265–275, 1989.
- L. Bergonzini. Bilans hydriques des lacs du rift Est-Africain (lacs Kivu, Tanganyika, Rukwa et Nyassa). In *Série Sciences Géologiques*, volume 103, page 183pp. Musée Royal de l'Afrique Centrale, Tervuren (Belgique), 1998.
- T.V. Blanc. Variation of bulk-derived surface flux, stability, and roughness results due to the use of different transfer coefficient schemes. *Journal of Physical Oceanography*, 15:650–669, 1985.
- H. A. Bootsma and R. E. Hecky. A comparative introduction to the biology and limnology of the African Great Lakes. *Journal of Great Lakes Research*, 29:3–18, 2003.
- I. R. Calder and C. Neal. Evaporation from saline lakes: a combination equation approach. *Hydrological Sciences Journal*, 29(1):89–97, 1984. doi: 10.1080/02626668409490924. URL <http://www.tandfonline.com/doi/abs/10.1080/02626668409490924>.
- Chen-Tung A. Chen and Frank J. Millero. Precise thermodynamic properties for natural waters covering only the limnological range. *Limnol. Oceanogr.*, 31:657–662, 1986.
- H. Damas. Quelques caractères écologiques de trois lacs équatoriaux: Kivu, Edouard, Ndalaga. *Annales de la Société Royale Zoologique de Belgique*, 68:121–135, 1937.

- J.A. Davies, P.J. Robinson, and M. Nunez. Field determinations of surface emissivity and temperature for Lake Ontario. *Journal of Applied Meteorology*, 10:811–819, August 1971.
- E. T. Degens and G. Kulbicki. Hydrothermal Origin of Metals in some East-African Rift Lakes. *Miner. Depos.*, 8:388–404, 1973.
- Mark W. Denny. In *Air and Water: The Biology and Physics of Life's Media*. Princeton University Press, 1993. ISBN 0691087342.
- W.G. Deuser, E.T. Degens, and G.T. Harvey. Methane in Lake Kivu: new data bearing on its origins. *Science*, 181:51–53, 1973.
- W.C. Evans, G.W. Kling, M.L. Tuttle, G. Tanyileke, and L.D. White. Gas Buildup in Lake Nyos, Cameroon: The recharge process and its consequences. *Applied Geochemistry*, 8:207–221, 1993.
- J. Finch and A. Calver. Methods for the quantification of evaporation from lakes. Technical report, World Meteorological Organization, CEH Wallingford, Wallingford, Oxfordshire OX10 8BB, UK, October 2008. prepared for: Commission for Hydrology.
- N.P. Fofonoff and R.C. Millard Jr. Algorithms for computation of fundamental properties of seawater. *Unesco Tech. Paper in Mar. Sci.*, 44:58pp., 1983.
- M. Halbwachs, K. Tietze, A. Lorke, and C. Mudaheranwa. Investigations in Lake Kivu (East Central Africa) after the Nyiragongo Eruption of January 2002, Specific study of the impact of the sub-water lava inflow on the lake stability. Technical report, European Community, ECHO; Solidarités, Aide Humanitaire d'Urgence, March 2002.
- G. E. Hutchinson. Part 1. Geography and Physics of Lakes. In *A Treatise on Limnology*, volume 1 of *Geography, Physics, and Chemistry*, pages 334–336, 346–357, 503–512. John Wiley & Sons, 1975. ISBN 0 471 42568–0.
- J. Imberger and J.C. Patterson. A dynamic reservoir simulation model - DYRESM: 5. *Transport Models for Inland Coastal Waters*, pages 310–361, 1981.
- P.A. Jacinthe and W.A. Dick. Use of silicone tubing to sample nitrous oxide in the soil atmosphere. *Soil Biology and Biochemistry*, 28:721–726, June 1996. doi: 10.1016/j.bbr.2011.03.031.

- J. Jacquet. Simulation of the Thermal Regime of Rivers. In G.T. Orlob, editor, *Mathematical Modeling of Water Quality: Streams, Lakes, and Reservoirs*, pages 150–176. Wiley-Interscience, 1983.
- J. I. Jiménez, L. Alados-Arboledas, Y. Castro-Díez, and G. Ballester. On the Estimation of Long-Wave Radiation Flux from Clear Skies. *Theoretical and Applied Climatology*, 38:37–42, 1987. doi: 10.1007/BF00866251.
- J.A.A. Jones and I.J. van der Walt. Challenges for water sustainability in Africa. *GeoJournal*, 61(2):105–109, 2004.
- S. Katsev, S.A. Crowe, B. Mucci, A. adn Sundby, S. Nomosatryo, G. D. Haffner, and D.A. Fowle. Mixing and its effects on biogeochemistry in persistently stratified, deep, tropical Lake Matano, Indonesia. *Limnology and Oceanography*, 55:763–776, 2010.
- R. Klefoth, O. Oenema, and J.W. van Groenigen. A novel method for quantifying N₂O reduction in soil. *Vandose Zone J.*, 2011. doi: doi:10.2136/vzj2011.0107.
- G.W. Kling, S. MacIntyre, J.S. Steenfelt, and F. Hirslund. Lake Kivu gas extraction – Report on Lake stability, 2006. Report 62721–0001, World Bank.
- N. Lallemand, A. Sayre, and R. Weber. Evaluation of emissivity correlations for H₂O–CO₂–N₂/air mixtures and coupling with solution methods of the radiative transfer equation. *Progress in energy and combustion science*, 22:543–574, 1996.
- A. Lejeune and V. Frank. Distribution of *Lutra maculicollis* in Rwanda: Ecological constraints. *IUCN Otter Spec. Group Bull.*, 5:1–83, March 1990.
- A. Lorke, K. Tietze, M. Halbwachs, and Wüest. Response of Lake Kivu stratification to lava inflow and climate warming. *Limnological Oceanography*, 49:778–783, 2004.
- T. Maongo. Some characteristics of aftershock sequences of major earthquakes from 1994 to 2002 in the Kivu province, Western Rift Valley of Africa. *Tectonophysics*, 439:1–12, 2007.
- G. Marlier. Recherches hydrobiologiques dan les rivières du Congo Oriental. *Hydrobiologia*, 6(3/4):778–783, 1954.
- MundoManz. Monthly Reports. http://www.mundomanz.com/meteo_p/monthrep?1=1, 2006–2013.

- Amisi Muvundja. Riverine Nutrient Inputs to Lake Kivu. Masters Thesis, (Fisheries and Aquatic Science) in Zoology, Institut Supérieur Pédagogique de Bukavu, R.D. Congo, September 2010. Reg. No. 2007/HD13/11068X.
- F. Muvundja, N. Pasche, F.W.B. Bugenyi, M. Isumbisho, B. Müller, J.-N. Namugize, P. Rinta, M. Schmid, R. Stierli, and A. Wüest. Balancing Nutrient Inputs to Lake Kivu. *J. Great Lakes Research*, 35(3):406–418, 2009. doi: 10.1016/j.jglr.2009.06.002.
- Fred C. Newman. Temperature Steps in Lake Kivu: A Bottom Heated Saline Lake. *Journal of Physical Oceanography*, 6:157–163, March 1976. doi: 10.1175/1520--0485(1976)006<0157:TSILKA>2.0.CO;2.
- Institution of Civil Engineers. *Floods and reservoir safety*. Thomas Telford Ltd., 3rd edition, 1996. ISBN 0727725033.
- World Weather Online. Rwandan Weather Averages. <http://www.worldweatheronline.com/Gisenyi-weather-averages/Butare/RW.aspx>, October 2012.
- N. Pasche, C. Dinkel, B. Müller, M. Schmid, A. Wüest, and B. Wehrli. Physical and biogeochemical limits to internal nutrient loading of meromictic Lake Kivu. *Limnology and Oceanography*, 54(6):1863–1873, 2009.
- N. Pasche, M. Schmid, F. Vazquez, C.J. Schubert, A. Wüest, J.D. Kessler, M.A. Pack, W.S. Reeburgh, and H. Bügmann. Methane sources and sinks in Lake Kivu. *Journal of Geophysical Research*, 116, July 2011. doi: 10.1029/2011JG001690.
- N.T. Pasche, A. Mugisha, L. Rwandekwe, and A. Umutoni. Monitoring the effects of methane extraction in Lake Kivu. Technical report, Ministry of Infrastructure, Kigali, 06 July 2010.
- R. Pawlowicz. Calculating the conductivity of natural waters. *Limnology and Oceanography: Methods*, 6:489–501, 2008.
- O.P. Phillips. *The Dynamics of the Upper Ocean*. Press Syndicate of the University of Cambridge, second edition, 1977.
- P.J. Robinson and J.A. Davies. Laboratory Determinations of Water Surface Emissivity. *Journal of Applied Meteorology*, 11:1391–93, December 1972.

- E. Rosenblum, P. Garaud, A. Traxler, and S. Stellmach. Turbulent mixing and layer formation in double-diffusive convection: three-dimensional numerical simulations and theory. *The Astrophysical Journal*, 731, 2011.
- C. Rosenzweig, G. Casassa, D.J. Karoly, A. Imeson, C. Liu, A. Menzel, S. Rawlins, T.L. Root, B. Seguin, and P. Tryjanowski. Climate Change 2007: Impacts, Adaptation and Vulnerability. Contribution of Working Group II to the Fourth Assessment Report of the Intergovernmental Panel on Climate Change. Technical report, Cambridge, UK, 79-131, 2007.
- H. Sarmiento, M. Ishumbisho, and J.P. Descy. Phytoplankton ecology of Lake Kivu (Eastern Africa). *Journal of Plankton Research*, 28:815–829, June 2006.
- J. F. T. Saur and E.R. Anderson. The Heat Budget of a Body of Water of Varying Volume. *Limnology and Oceanography*, 1:247–251, October 1956. URL <http://www.jstor.org/stable/2832751>.
- M. Schmid, K. Tietze, M. Halbwachs, A. Lorke, D. McGinnis, and A. Wüest. How hazardous is the gas accumulation in Lake Kivu? Arguments for a risk assessment in light of the nyiragongo Volcano eruption of 2002. *Acta Vulcanologica*, 14/15(1–2): 115–122, 2002.
- M. Schmid, M. Halbwachs, B. Wehrli, and A. Wüest. Weak mixing in Lake Kivu: new insights indicate increasing risk of uncontrolled gas eruption. *Geochemistry, Geophysics, Geosystem*, 6:Q07009, 2005. doi: 07010.01029/02004GC000892.
- M. Schmid, M. Busbridge, and A. Wüest. Double-diffusive convection in Lake Kivu. *Limnological Oceanography*, 55:225–238, 2010. doi: 10.4319/lo.2010.55.1.0225.
- M. Schmid, K.A. Ross, and A. Wüest. Comment on *an additional challenge of lake kivu in central africa – upward movement of the chemoclines* by Finn Hirslund. *J. Limnol.*, 71(2):330–334, 2012. doi: 10.4081/jlimnol.2012.e35.
- Martin Schmid and Alfred Wüest. Stratification, Mixing and Transport Processes in Lake Kivu. In Jean-Pierre Descy, François Darchambeau, and Martin Schmid, editors, *Lake Kivu, Limnology and biogeochemistry of a tropical great lake*, volume 5 of *Aquatic Ecology Series*, pages 13–29. Springer Netherlands, 2012. ISBN 978–94–007–4242–0. doi: 10.1007/978--94--007--4243--7_2. URL http://dx.doi.org/10.1007/978--94--007--4243--7_2.

- H. Sigurdsson, J.D. Devine, F.M. Tchoua, T.S. Presser, M.K.W. Pringle, and W.C. Evans. Origin of the lethal gas burst from Lake Monoun, Cameroon. *Journal of Volcanology and Geothermal Research*, 31:1–16, 1987.
- S.H. Smith. Temperature Correction in Conductivity Measurements. *Limnology and Oceanography*, 7:330–334, 1962.
- S.A. Socolofsky and G. H. Jirka. Chapter 10: Internal Waves, 2004. Karlsruhe Institute of Technology: Lecture Notes in Environmental Fluids II.
- D.O. Staley and G.M. Jurica. Effective Atmospheric Emmissivity under Clear Skies. *Journal of Applied Meteorology*, 11:349–356, March 1972.
- R.H. Stewart. Equations of Motion with Viscosity. In *Introduction to Physical Oceanography*. Texas A&M University, 2008.
- W. C. Swinbank. Long-wave radiation from clear skies. *Q.J.R. Meteorol. Soc.*, 89: 339348, July 1963. doi: 10.1002/qj.49708938105.
- F. Tassi, O. Vaselli, D. Tedesco, G. Montegrossi, T. Darrah, E. Cuoco, M.Y. Mapendano, R. Poreda, and Huertas A Delgado. Water and gas chemistry at Lake Kivu (DRC): geochemical evidence of vertical and horizontal heterogeneities in a multi-basin structure. *Geochemistry, Geophysics, Geosystems*, 10:22 pp., 2009. doi: 02010.01029/02008GC002191.
- K. Tietze. Lake Kivu gas development and promotion-related issues: Safe and environmentally sound exploitation, 2000.
- K. Tietze. *Geophysikalische Untersuchung des Kivu sees und seiner ungewöhnlichen Methangaslagerstätte – Schichtung, Dynamik und Gasgehalt des Seewassers*. Thesis es Sciences, Christian-Albrechts-Universität, Kiel., 1978.
- K. Tietze, M. Geyh, H. Müller, L. Schröder, W. Stahl, and H. Wehner. The genesis of methane in Lake Kivu (Central Africa). *Geol. Rundsch.*, 69, 1980.
- M.L. Tuttle, J.P. Lockwood, and W.C. Evans. Natural Hazards Associated with Lake Kivu and Adjoining Areas of the Birunga Volcanic Field, Rwanda and Zaire, Central Africa. Open File Report 90–691, United States Department of the Interior Geological Survey, 1990.

- A. Venäläinen, M. Frech, M. Heikinheimo, and A. Grelle. Comparison of latent and sensible heat fluxes over boreal lakes with concurrent fluxes over a forest: implications for regional averaging. *Agricultural and Forest Meteorology*, 98–99(0):535 – 546, 1999.
- P. Verburg and R.E. Hecky. The physics of the warming Lake Tanganyika by climate change. *Limnol. Oceanography*, 54(6, part 2):2418–2430, 2009.
- M.K. Vollmer, H.A. Bootsma, R.E. Hecky, G. Patterson, J.D. Halfman, J.M. Edmond, D.H. Eccles, and R.F. Weiss. Deep-water warming trend in Lake Malawi, East Africa. *Limnology and Oceanography*, 50:727–732, 2005.
- G. Warnecke, J. Allison, L.M. McMillin, and H. Szekiolda. Remote sensing of ocean currents and sea surface temperature changes derived from the Nimbus II satellite. *J.Phys. Oceanography*, 1:45–60, 1971.
- E.W. Washburn. The equivalent conductance of electrolytes in dilute solutions. I. The water correction. *J. Am. Chem. Soc.*, 40:106–158, September 1918.
- Robert G. Wetzel and Gene E. Likens. In *Limnological Analysis*, volume 3. Springer Science and Business Media, Inc., 2000.
- A. Wüest, G. Piepke, and J.D. Halfmann. Combined Effects of Dissolved Solids and Temperature on the Density Stratification of Lake Malawi (East Africa). In Johnson and Odada, editors, *The Limnology, Climatology and Paleoclimatology of the East African Lakes*, pages 183–202. Gordon and Breach Scientific Publishers, New York, 1996.
- Lisan Yu. Global variations in oceanic evaporation (1958–2005): The role of the changing wind speed. *Journal of Climate*, 20:5376–5390, November 2007. doi: 10.1175/2007JCLI1714.1.
- H. Zhang and A. Cloud. The permeability characteristics of silicone rubber. In *Global Advances in Materials and Process Engineering*. Society for the Advancement of Material and Process Engineering, 2006.